Dissertation

SUBMITTED TO THE

Combined Faculties of the Natural Sciences and Mathematics
of the Ruperto-Carola-University of Heidelberg, Germany

AND

The National and Kapodistrian University of Athens, Greece
Nuclear and Particle Physics Section

FOR THE DEGREE OF

Doctor of Natural Sciences

Put forward by **Alexandros Konstantinos Karlis**
Born in: Athens, Greece

Oral Examination: December 14, 2012

European Union
European Social Fund
OPERATIONAL PROGRAMME
EDUCATION AND LIFELONG LEARNING
investing in knowledge society
MINISTRY OF EDUCATION, LIFELONG LEARNING AND RELIGIOUS AFFAIRS
MANAGING AUTHORITY
NSRF 2007-2013
EUROPEAN SOCIAL FUND
Co- financed by Greece and the European Union

Transport Phenomena in Time-Dependent Media

Matriculation Number:	University of Heidelberg 2805699
	University of Athens 2007513
Referees:	Prof. Dr. Fotios Diakonos
	Prof. Dr. Peter Schmelcher

I certify that I have created this Ph.D. thesis independently, using only the sources listed as aids.

Submission Date: November 5, 2012

Acknowledgements

This research has been co-financed by the European Union (European Social Fund – ESF) and Greek national funds through the Operational Program "Education and Lifelong Learning" of the National Strategic Reference Framework (NSRF) - Research Funding Program: Heracleitus II. Investing in knowledge society through the European Social Fund.

"... Probability is relative, in part to (our) ignorance, in part to our knowledge."

Pierre Simone de Laplace

Contents

Abstract

The main subject of the thesis is the study of Fermi acceleration, regarded nowadays as a fundamental acceleration mechanism, consisting in the increase of the mean energy of particles due to collisions with moving scatterers. Prior to the study of extended systems, the prototype one-dimensional dynamical system exhibiting Fermi acceleration was considered; the stochastic Fermi-Ulam model. The analysis of the dynamics in this system revealed the pitfalls of the standard, widely used, quasi-static approximation, which neglects the impact of the location of the collision events in the configuration space. In order to take this into account, a novel approximation scheme was introduced allowing both the analytical treatment of the acceleration process as well as fast numerical simulations. Furthermore, the limitations and possible inconsistencies stemming from the treatment of Fermi acceleration via the Fokker-Planck equation were brought to light. A new self-consistent methodology on the basis of the Chapman-Kolmogorov equation was put forward, capable of giving an accurate description of Fermi acceleration for all times. The understanding gained through the investigation of the Fermi-Ulam model, was then utilized for the study of Fermi acceleration in spatially extended systems, using as a prototype the two-dimensional randomized Lorentz gas. The newly introduced approximation was generalized for application to higher dimensional systems. The study revealed that the increase of the efficiency of Fermi acceleration depends only on the symmetries of the driving time-law and is insensitive to the geometrical properties of the moving scatterers and the dimensionality of the time-dependent system. Finally, the study of the driven Lorentz gas, in a channel geometry, revealed a completely new aspect of Fermi acceleration, linking it, for the first time, to the phenomenon of self-organized criticality. Particularly it was shown that Fermi acceleration permits the spontaneous synchronization of the motion of the particles with that of the moving scatterers, such that particles can travel collision-free for long times. This, in turn, gives rise to strongly intermittent dynamics, which, as it was shown, is a sufficient condition for the emergence of scale-free cross-correlations between non-interacting particles.

Zusammenfassung

Das Hauptthema der Dissertation ist die Untersuchung der Fermi-Beschleunigung, die heute als ein grundlegender Beschleunigungsmechanismus betrachtet wird, bestehend aus der Erhöhung der mittleren Energie von Teilchen durch Kollisionen mit beweglichen Streuern. Vor der Studie von ausgedehnten Systemen wurde das stochastische Fermi-Ulam-Modell untersucht, als das grundlegende, eindimensionale, dynamische System, das Fermi-Beschleunigung zeigt. Die Analyse der Dynamik in diesem System zeigte die Fallstricke der weit verbreiteten, quasi-statischen Näherung, die die Fluktuationen der Kollisionsereignisse im Konfigurationsraum vernachlässigt. Um diese Fluktuationen zu berücksichtigen wurde ein neues Approximationsschema eingeführt, das sowohl die analytische Behandlung des eschleunigungsvorgangs sowie schnelle numerische Simulationen erlaubt. Darüber hinaus wurden die Einschränkungen und möglichen Inkonsistenzen der Behandlung von Fermi-Beschleunigung über die Fokker-Planck-Gleichung ans Licht gebracht. Eine neue, selbstkonsistente Methode wurde entwickelt, die auf der Chapman-Kolmogorov-Gleichung basiert. Mit dieser Methode erreicht man eine genaue Beschreibung der Fermi-Beschleunigung für alle Zeiten. Das durch die Untersuchung des Fermi-Ulam-Modells gewonnene Verständnis wurde schließlich für das Studium der Fermi-Beschleunigung in räumlich ausgedehnten Systemen eingesetzt. Als Prototyp eines solchen Systems diente das zweidimensionale, getriebene Lorentz-Gas. Die neulich eingeführte Näherung wurde für die Anwendung auf höher dimensionale Systeme verallgemeinert. Die Studie zeigte, dass die erhöhte Effizienz der Fermi-Beschleunigung nur auf den Symmetrien des Treibgesetzes empfindlich ist. Dagegen spielen die geometrischen Eigenschaften der sich bewegenden Streuer und die Dimensionalität des zeitabhängigen Systems nur eine sekundäre Rolle. Schließlich wurde das getriebene Lorentz-Gas in einer Kanalgeometrie weitgehend untersucht. Aus dieser Studie ergab sich ein völlig neuer Aspekt der Fermi-Beschleunigung, der sie zum ersten Mal mit dem Phänomen der selbstorganisierten Kritikalität verknüpft. Insbesondere wurde gezeigt, dass die Fermi-Beschleunigung die spontane Synchronisation der Bewegung der Teilchen mit den beweglichen Streuern ermöglicht, so dass sich die Teilchen kollisionsfrei für lange Zeiten propagieren. Dies wiederum führt zu einer stark intermittenten Dynamik, die, wie bereits gezeigt, eine hinreichende Bedingung für die Entstehung von Kreuzkorrelationen zwischen nicht-wechselwirkenden Teilchen ist.

1. Introduction

1.1. Motivation and objectives

Kinetic theory and statistical mechanics are today considered one of the most brilliant moments of modern science [1–5]. The vision of the early pioneers in the 19th century, such as Maxwell and Boltzmann, was to describe macroscopic properties of matter and macroscopic phenomena starting from the microscopic dynamical laws. Research in nonequilibrium statistical mechanics is largely devoted to developing theories for the irreversible behavior of fluid and solid systems, using stochastic or probabilistic assumptions whenever necessary to obtain useful results. The use of such assumptions allows for the reduction of the implicated variables of the complex system [6]. On the basis of such assumptions an effective (kinetic) equation can be constructed, describing the evolution of the macroscopic (many-body) system, such as the famous Boltzmann equation.

Since Boltzmann, many kinetic and master equations have been derived. However, each kinetic equation necessarily involves a stochastic assumption. In fact, after so many years since the foundation of statistical mechanics, there is still no general agreement between the experts on the prerequisites for the validity of such probabilistic or statistical approaches for the description of macroscopic phenomena. Rather, the application of statistical mechanics is justified on the basis of the fact that it produces useful results. Nevertheless, acquiring the knowledge about the validity of the machinery of statistical mechanics is equally as important as the calculation of physical quantities. Even more, much less is known about the non-equilibrium phenomena. For instance, there is still no generally accepted definition of a nonequilibrium entropy, and there is also no general agreement on nonequilibrium ensembles that might replace the equilibrium ones [3, 7, 8].

In recent years, chaos theory has made an invaluable contribution towards this direction, by bridging the gap between the deterministic and time-reversible microscopic dynamical equations and the stochastic, time-irreversible macroscopic phenomena such as transport processes. Within the framework of modern theory of dynamical systems, it has been made possible to rigorously prove the existence of finite and non-zero transport

coefficients for a system of particles governed by Newton's equations of motion [9].

A paradigm for the study of the interconnection between microscopic and macroscopic dynamics is the Lorentz gas [10]. The Lorentz gas consists of circular hard scatterers, located either on the nodes of a periodic lattice or at random positions, and an ensemble of non-interacting particles traveling freely between impacts on the circular obstacles and being specularly reflected upon collision. The statistical properties of the Lorentz gas depend solely on the maximal free lengths permitted by the considered geometry, i.e. the maximum length a particle can travel between any two collisions. If the maximum free path length is bounded from above, then the Lorentz gas is said to possess a finite horizon. If this condition is not met, then the horizon is infinite. From a dynamical point of view, the finite horizon geometry leads to a fully hyperbolic system. By this virtue, the Lorentz gas with finite horizon has been one of the few and oldest systems permitting a rigorous mathematical proof for the ergodic hypothesis [11, 12, 12] and the existence of a finite diffusion coefficient directly from the microscopic equations of motion [13–16]. On the other hand, the infinite horizon Lorentz gas, due to the existence of marginally unstable fixed points in the phase space, has posed much greater difficulties in obtaining rigorous mathematical results. It was only until very recently, that the infinite horizon Lorentz gas was proven to be also ergodic [17].

Another possible research direction which has attracted much attention recently, are thermostatted variants of the Lorentz gas in the presence of an external (up to now time-independent) field. The presence of the thermostat keeps the energy of the system constant and leads to non-equilibrium steady states. Within this framework an effort is made to reconcile time-reversibility in the macroscopic scale with reversible microscopic dynamics [18–22].

Despite the rapid developments in the field, little progress has been made in understanding transport phenomena in time-dependent media [23–26]. However, given that on the microscopic scale time-independence of the medium potential is an approximation, in order to complete the task of linking microscopic dynamics with macroscopic transport phenomena the investigation of time-dependent systems is mandatory. Even more, time-dependence brings forth new fascinating phenomena, due to the breaking of the energy conservation resulting in extremely interesting and rich dynamical behavior encountered in even very simple, at least conceptually, systems [27–29], the most interesting of which, is Fermi acceleration. This acceleration mechanism was proposed in 1949 by Fermi [30] to explain the extraordinary energies of cosmic ray particles (for a review see [31]) observed experimentally. Fermi acceleration consists in the increase of the mean energy of particles propagating in a environment of time-dependent scatterers. Ever since, this has been a subject of intense study in a broad range of systems in

various areas of physics, including astrophysics [32–34], plasma physics [35, 36], atom optics [37, 38] and has even been used for the interpretation of experimental results in atomic physics [39].

Soon after his seminal paper, his co-worker Ulam introduced a simple mechanical model for testing Fermi's idea [40], known as the Fermi-Ulam model (FUM), linking for the first time Fermi acceleration with the study of time-dependent billiards (for a review see [41, 42]). The FUM consists in an ensemble of non-interacting classical point particles bouncing elastically between one fixed and one oscillating infinitely heavy wall. Many different versions of the original model have been suggested and investigated by several authors, such as variants of the FUM with dissipation [43–46] , the quantum-mechanical analog [47–51] and the, so called, bouncer model [52], where a particle performs elastic [53] or inelastic [54–59] collisions with an oscillating infinitely heavy platform under the influence of a gravitational field. Recently, a hybrid version of the FUM and the bouncer model has also been investigated [60].

Up to now, research conducted in this field is limited to a few (in large part one dimensional), spatially confined (closed) systems, with the most prominent example being the FUM and the classical or quantum kicked rotator (KR) [61–63]. Even so, the investigation of such simple systems is far from being trivial. One problem often arising in the investigation of time-dependent systems is that the equations defining the dynamics of the systems are of implicit form. This, in turn, greatly complicates numerical simulations and hinders an analytical treatment of the acceleration of particles. For example, the study of Fermi acceleration in the FUM is carried out by means of a simplification [41, 64–68], known as the *static wall approximation* (SWA) and very little is known about the possible discrepancies between the simplified FUM and the original one. These complications and the use of simplified models is even more emphasized in higher-dimensional systems, such as the time-dependent Lorentz gas. Therefore, the development of techniques and methods for the numerical and analytical treatment in time-dependent billiards constitutes state-of-the-art research topic and consists the main subject of the thesis.

Finally, the study of the time-dependent Lorentz gas in a channel geometry, revealed not only the existence of non-trivial nonequilibrium steady states, but, even more, it led us to the discovery of a new class of time-dependent billiards. Specifically, we showed that in time-dependent media, long free flights may become possible due to the self-organization of the propagating particles to these areas in phase space where the motion of the particles is synchronized with the one of the driven obstacles, in a way that particles can avoid collisions for arbitrarily long flights. Specifically, we showed that Fermi-acceleration can act as a steering force of a time-dependent extended dynamical

system towards a critical state, opening up the prospect of understanding the possible dynamical routes to criticality. In conclusion, another objective of equal importance to the ones mentioned above, is the introduction of concepts pertinent to extended time-depended systems, and the linking of them to other fundamental problems of statistical mechanics, which up to now have not be considered in this context, taking a fresh look at the possibilities opening due to the breaking of the energy shell in time-dependent media.

Part I.

The Fermi-Ulam Model

2. Pitfalls of the standard simplification

In this chapter the standard simplification employed to treat Fermi-acceleration in the FUM is reviewed in depth. We point out its shortcomings in the estimation of the efficiency of the acceleration mechanism, owing to the fact that the physical motion of the driven wall, i.e. the motion of the wall in configuration space, is neglected. A new simplified model is proposed, which succeeds in describing the dynamics of the exact model, both qualitatively and quantitatively, while it retains all the merits of the standard approach. Using this novel simplification we derive the evolution of the mean energy of particles numerically and analytically. Finally, we highlight a long-standing contradiction within the standard simplified model and provide a self-consistent method for calculating the evolution of the mean particle speed directly from the dynamical mapping.

2.1. System

We consider a dynamical system consisting of one harmonically driven and one fixed infinitely heavy wall and an ensemble of particles bouncing between them. When a particle collides with the fixed wall, a random shift of the phase of the moving wall occurs, which is uniformly distributed in the interval $[0, 2\pi)$. The stochastic component in the oscillation law of the wall simulates the influence of a thermal environment on the wall motion and leads to Fermi acceleration [60, 64–67, 69, 70]. It should be noted that although stochasticity can be introduced otherwise (for instance, via a random component in the angular frequency of oscillation) the random phase approach has become quite common as a method of randomization of the FUM and its modifications [60, 64, 71, 72]. Partially, this is because it is the only conceivable way to randomize the system without changing the energy related quantities, such as the frequency of the moving wall.

2.1.1. Exact dynamics

Without loss of generality, let us assume a FUM consisting of a moving wall on the left and a fixed wall on the right, oscillating harmonically. The specific setup of the studied system is completely determined by the oscillation frequency ω and amplitude A of the driving, as well as the distance w between the walls, when the moving wall is at equilibrium. If we further assume that the positive direction of particle velocities is towards the right, the dynamics of the billiard using as a length unit the spacing between the walls w and as a time unit $\frac{1}{\omega}$ the dynamical laws of the system can be written in a dimensionless form:

$$d_n = \epsilon \sin(\delta t_n + t_{n-1} + \eta_n) \tag{2.1a}$$

$$u_n = \epsilon \cos(\delta t_n + t_{n-1} + \eta_n) \tag{2.1b}$$

$$V_n = \pm V_{n-1} + 2u_n, \tag{2.1c}$$

where d_n stands for the position of the moving wall at the instant of the nth collision, u_n for the wall velocity, η_n for the random phase component, V_n for the particle velocity after the nth collision and $\epsilon = A/w$ the dimensionless amplitude of oscillation. The plus sign corresponds to a particle sufferring a collision with the fixed wall prior to a collision with the moving one and the minus sign to multiple collisions with the moving wall before the particle exits the interaction region. The time of free flight δt_n is obtained by solving the implicit equation

$$\begin{aligned} 2 - (V_{n-1}\delta t_n + X_{n-1}) &= X_n, \text{ (single collision event)}, \\ V_{n-1}\delta t_n + X_{n-1} &= X_n \text{ (multiple successive collisions)}, \end{aligned} \tag{2.2}$$

where X_n denotes the position of the particle in the instant of the nth collision. The equation can be solved numerically, keeping the smallest positive solution. Obviously, Eq. (2.2) links the time of the nth collision $t_n = \delta t_n + t_{n-1}$ to the position X_{n-1} of the particle on the $(n-1)$th collision.

2.1.2. The simplified Fermi-Ulam model: SWA

The most interesting and physically relevant driving function of the moving wall is the harmonic one, in which case the equations defining the dynamics of the FUM are of implicit form with respect to the collision time. The implicit form of the equations hinders an analytical treatment and greatly complicates numerical simulations. A simplification [41, 64, 65], known as the *static wall approximation* (SWA), has become over

the time the standard approximation for studying the FUM [66–68, 73] and its variants [44–46, 53–55, 57, 74]. The simplification consists in treating the oscillating wall as fixed in space, yet transfer of momentum is allowed as if the wall were oscillating. With the use of this approximation, the equation defining the time of the next impact with the "*moving*" wall ("*moving*" wall denotes the static wall providing momentum transfer on the particle within the SWA) is rendered explicit, which permits an analytical treatment of Fermi acceleration and greatly speeds-up numerical simulations, while it retains the main features of the complete model. Moreover, this simplification has been generalized for application in higher-dimensional billiards with time-dependent boundaries, such as the time-dependent Lorentz Gas [71, 72] and the stadium like billiard [75].

The static wall approximation (SWA) simplifies the process on the basis of the assumption that the time of free flight, δt_n, depends only on particle velocity, i.e. $\delta t_n = \frac{2}{V_{n-1}}$. Thus, Eqs. (2.1) and (2.2) are simplified to

$$t_n = t_{n-1} + \frac{2}{V_{n-1}} \tag{2.3a}$$

$$V_n = |V_{n-1} + 2\epsilon \cos(t_n + \eta_n)|. \tag{2.3b}$$

The absolute value function has the physical interpretation that a particle must always move away from the "moving" wall after a collision. This assumption is necessary, since multiple collisions cannot be taken into account within the SWA.

2.2. Underestimation of Fermi acceleration's efficiency

If we apply the SWA to the system, then it is possible to extract analytically the ensemble averaged change of the square particle velocity $\langle \delta V_n^2 \rangle = \langle V_n^2 - V_{n-1}^2 \rangle$ after integration over the random phase η_n. It should be noted that the ensemble trajectories are characterized by the same initial velocity V_0. From Eq. (2.1) follows that the square of the modulus of particle velocity is $V_n^2 = V_{n-1}^2 + 4u_n V_{n-1} + 4u_n^2$. Thus,

$$\delta V_n^2 = V_n^2 - V_{n-1}^2 = 4u_n V_{n-1} + 4u_n^2 \tag{2.4}$$

After averaging Eq. (2.4) over the random phase component we obtain:

$$\langle \langle \delta V_n^2 \rangle \rangle = 2\epsilon^2. \tag{2.5}$$

In Eq. (2.5) the notation $\langle\langle \quad \rangle\rangle$ is used for phase averaging. To extract the ensemble average one should also integrate over the velocity distribution $\rho(|V|, n)$, which in this case is trivial, since the result of Eq. (2.5) is independent of the particle velocity. Given that $\langle V_n^2 \rangle = \sum_{i=1}^{n} \langle \delta V_i^2 \rangle + V_0^2$, the root mean square particle velocity $\bar{V}$ is:

$$\bar{V}_{\mathrm{SWA}}(n) = \sqrt{2\epsilon^2 \cdot n + {V_0}^2}. \tag{2.6}$$

Independently, the rms velocity can be obtained numerically, by the iteration of the set of Eqs. (2.3). Results, yielded by the numerical simulation of an ensemble of 10^4 particles, for $n = 5 \times 10^5$ collisions, with $\epsilon = \frac{1}{15}$ and $V_0 = \frac{100}{15}$ are presented in Fig. 2.1 along with numerical results using the exact Eqs. (2.1) and (2.2). Clearly, and despite the external randomization [64] the SWA fails to provide an accurate description of the acceleration process; more specifically, the energy gain of the particles is substantially underestimated. The inadequacy of the SWA must be attributed to the fact that it does not take into account the displacement of the scatterer upon collision. Thus, it is crucial, in order to correctly describe the evolution of the root mean square particle velocity, to incorporate the oscillation of the walls in configuration space.

2.2.1. A novel approximation: HWA

As mentioned above, one of the advantages of the SWA is the explicit form of Eqs. (2.3), which facilitates the analytical treatment of the acceleration problem as well as substantially simplifies and speeds up numerical simulations. Therefore, a promising candidate as an alternative to this approximation should also have these merits but at the same time being capable of providing an accurate description of the acceleration process.

For this reason we introduce the so-called *hopping* wall approximation (HWA), which takes into account the effect of the wall displacement. Using this approximation we clarify how the oscillation of the wall in configuration space affects the acceleration law of an ensemble of particles. Furthermore, the corresponding map allows an analytical treatment and is as computationally efficient as the SWA, enabling us to calculate the evolution of the velocity distribution of the particles for long time periods.

The key simplifying assumption of the HWA is that the wall position on the nth collision can be approximated with its position at the previous, $(n-1)$th, collision. This approximation is based on the observation that with increasing particle velocity, the time of free flight decreases, becoming much smaller compared to the oscillation period of the walls and consequently the relative displacement of the wall between two successive collisions becomes very small, i.e. negligible. So, according to the HWA, the

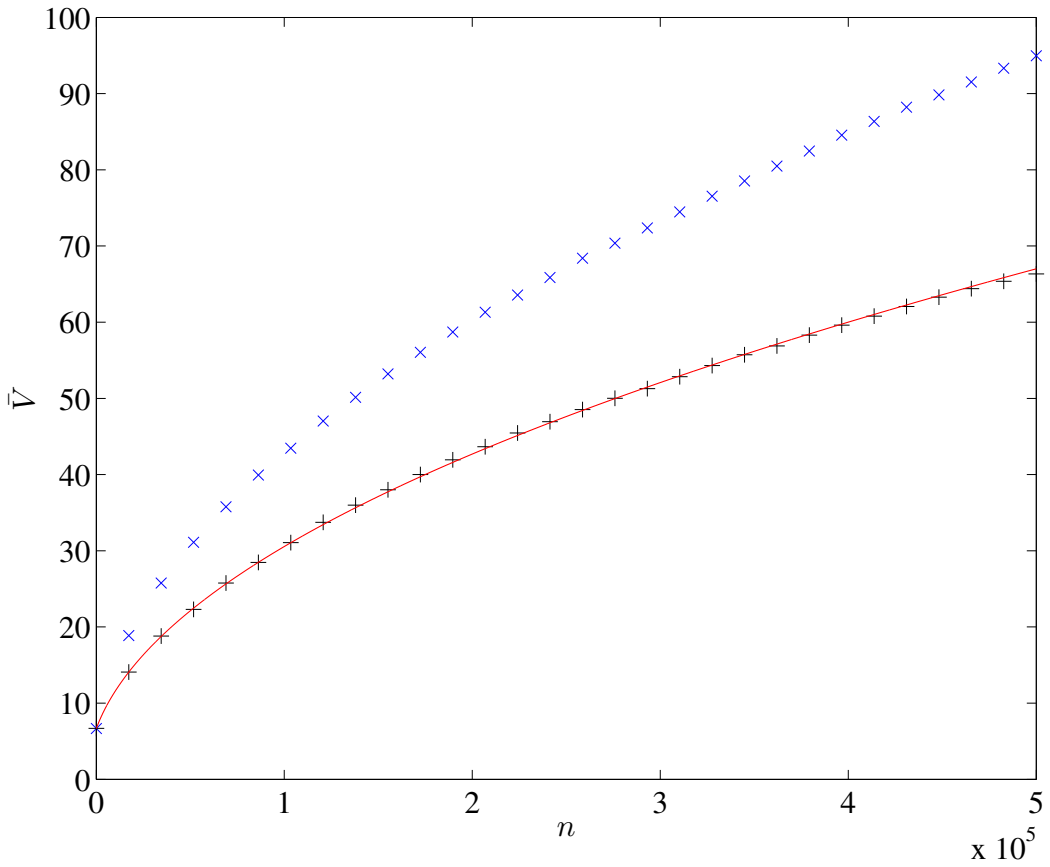

Figure 2.1.: Numerical results for $\bar{V}$ of an ensemble of 10^4 particles evolving in a stochastic FUM as a function of the number of collisions. Results were obtained by iterating the exact ($\times$) as well as the corresponding *static* ($+$) approximate map, with $\epsilon = \frac{1}{15}$ and $V_0 = \frac{100}{15}$. $\bar{V}$ is measured in units of ωw. The analytical result according to the SWA, obtained by averaging over the random phase, (solid line) is also shown.

oscillating wall moves only when a particle collides with the fixed wall. Thus, when a particle collides with the static wall, the moving "hops" (is instantly moved) to its new position (as defined by the deterministic component one collision earlier with the addition of its current random phase component) and remains fixed until the particle collides with it again. However, the velocity of the moving wall is allowed to oscillate continuously. The equations defining the HWA read:

$$d_n = \epsilon \sin\left(t_{n-1} + \eta_n\right) \tag{2.7a}$$

$$u_n = \epsilon \cos\left(t_n + \eta_n\right) \tag{2.7b}$$

$$V_n = \left|V_{n-1} + 2u_n\right| \tag{2.7c}$$

The time t_n when the nth collision occurs is determined by Eq. (2.2), which within the framework of HWA can be solved analytically to obtain

$$t_n = t_{n-1} + \underbrace{2/V_{n-1}}_{\text{SWA}} + \delta t_n^* \tag{2.8a}$$

$$\delta t_n^* = -\frac{\epsilon\left[\sin(t_{n-1}+\eta_n) + \sin(t_{n-2}+\eta_{n-1})\right]}{V_{n-1}}, \tag{2.8b}$$

where δt_n^* is the correction term to the time of free flight predicted by SWA, due to wall displacement.

In order to obtain the rms particle velocity within the framework of HWA, the mean energy gain per collision $\langle \delta V_n^2 \rangle$ must be calculated. Let us first calculate the average energy gain over the phase of oscillation, $\langle\langle \delta V_n^2 \rangle\rangle$. This is done by averaging Eq. (2.4) over the random phase component η_n, using the set of Eqs. (2.8), which leads to the following integrals:

$$I_j = \int_0^{2\pi} \frac{1}{2\pi}\left[\epsilon \cos\Big(t_n + \eta_n\Big)\right]^j d\eta_n, \tag{2.9}$$

where $j = 1, 2$ and t_n is given by Eq. (2.8a). An exact analytical calculation of the integrals I_1, I_2 is not possible. However, for the set of parameters considered here, δt_n^* is much smaller compared to the other phase components. Therefore, we expand the r.h.s. of Eq. (2.9) to the leading order of δt_n^*, to obtain:

$$I_1 = \frac{1}{2\pi}\int_0^{2\pi}\left[\epsilon\cos\left(\frac{1}{V_{n-1}} + t_{n-1} + \eta_n\right) - \epsilon\sin\left(\frac{1}{V_{n-1}} + t_{n-1} + \eta_n\right)\delta t_n^*\right] d\eta_n \tag{2.10}$$

and

$$\begin{aligned} I_2 = \frac{1}{2\pi}\int_0^{2\pi}\Bigg[&\epsilon^2\cos^2\left(\frac{1}{V_{n-1}} + t_{n-1} + \eta_n\right) - 2\epsilon^2\cos\left(\frac{1}{V_{n-1}} + t_{n-1} + \eta_n\right) \\ &\times \sin\left(\frac{1}{V_{n-1}} + t_{n-1} + \eta_n\right)\delta t_n^*\Bigg] d\eta_n. \end{aligned} \tag{2.11}$$

After the substitution of Eq. (2.8b) into Eqs. (2.10) and (2.11) the calculation of the integrals yields:

$$I_1 \approx \frac{\epsilon^2 \cos\left(\frac{1}{V_{n-1}}\right)}{2V_{n-1}} \quad ; \quad I_2 \approx \frac{\epsilon^2}{2}$$

Therefore, we find

$$\langle\langle \delta V_n^2 \rangle\rangle \approx 2\epsilon^2 \cos\left(\frac{1}{V_{n-1}}\right) + 2\epsilon^2 \tag{2.12}$$

In the limit of high particle velocities $V_{n-1} \gg 1$, Eq. (2.12) is simplified to, $\langle\langle \delta V_n^2 \rangle\rangle \simeq 4\epsilon^2$.

Since the result is independent of the particle velocity, the ensemble mean energy gain is

$$\langle \delta V_n^2 \rangle \simeq 4\epsilon^2 \tag{2.13}$$

which is exactly two times the result obtained by neglecting wall displacement. Consequently the root mean square velocity as a function of the number of collisions is:

$$\bar{V}_{\mathrm{HWA}} = \sqrt{4\epsilon^2 \cdot n + \langle V_0^2 \rangle}. \tag{2.14}$$

The analytical result of Eq. (2.14) together with the numerical results obtained by the simulation of 10^4 particles utilizing the HWA map, are shown in Fig. 2.2. For the sake of comparison, numerical results using the exact map are also presented.

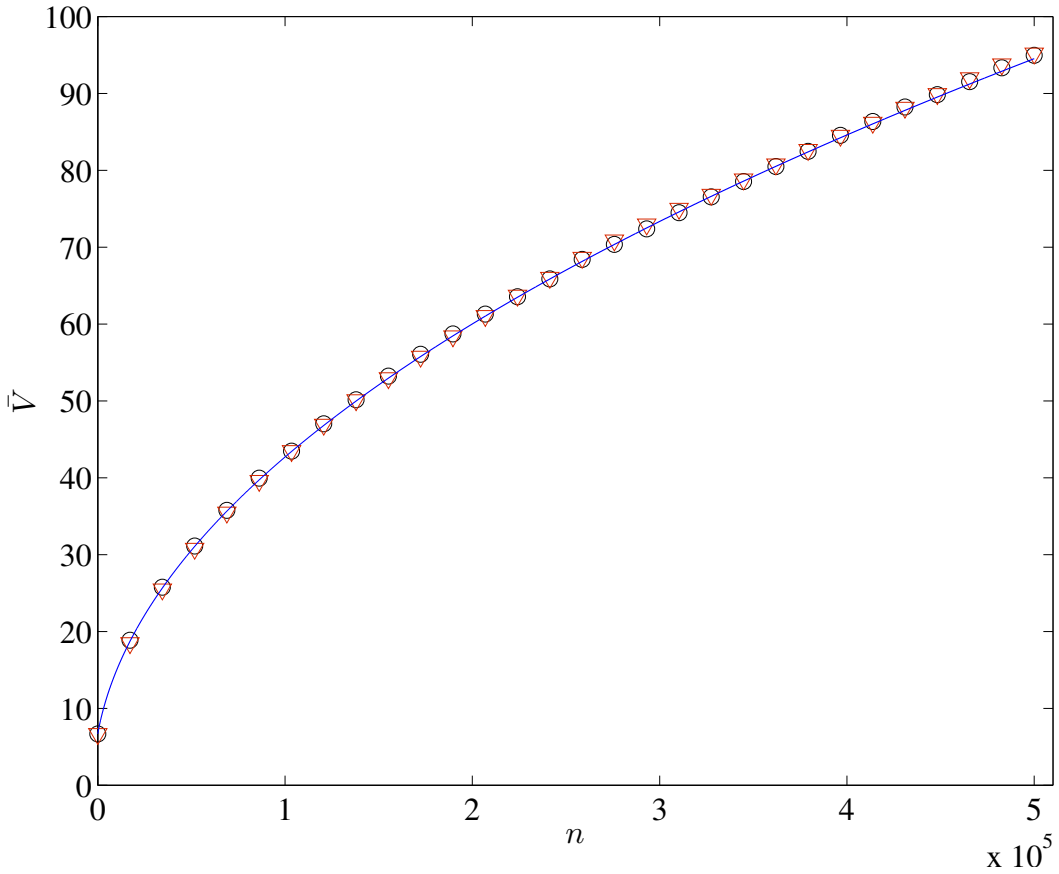

Figure 2.2.: Numerical results for $\bar{V}$ of an ensemble of 10^4 particles evolving in a stochastic FUM with two oscillating walls as a function of the number of collisions. Results were obtained by iterating the exact ($\circ$) as well as the corresponding HWA map ($\triangledown$), with $\epsilon = \frac{1}{15}$ and $V_0 = \frac{100}{15}$. It is noted that $\bar{V}$ is measured in units of ωw. The analytical result according to the HWA, Eq. (2.14), obtained by averaging over the random phase, (solid line) is also shown.

As seen in Fig. 2.2 the numerical results given by the iteration of the exact and the hopping approximative map virtually coincide. Furthermore, the analytical result of Eq. (2.14) is also in agreement with the numerical results obtained using the exact map. Obviously, the HWA succeeds in describing particle acceleration, in clear contrast with the SWA which leads to a substantial underestimation. This indicates that the increased particle acceleration is due to the impact of the dynamically induced correlation between the position and velocity of the oscillating wall in the collision process.

2.2.2. Physical interpretation

The previous analysis reveals the role of the fluctuations in the time of flight δt_n between successive collisions caused by the displacement of the scatterer. Despite the existence of an external stochastic component in the phase of the oscillating wall these fluctuations lead to a *systematic* increase of the acceleration of the particles. A simple explanation of the physical mechanism leading to the increased acceleration becomes possible by considering the various configurations of the collision processes between the walls and the particles.

Let us assume for a given velocity of the incident particle that the wall is moving in the same direction as the particle after passing the equilibrium position, as shown in Fig. 2.3. The collision time, as given by the exact map, Eq. (2.2) –corresponding to the intersection of the particle trajectory with the curve representing the position of the scatterer as a function of time– denoted by t', is increased compared to the time t on the assumption of a wall fixed in space. In Figure (2.3) this is shown as the intersection of the particle trajectory with the line corresponding to the equilibrium position. In this case, the velocity of the harmonically oscillating wall is a decreasing function of time and therefore an increase of the collision time leads to a decrease of the wall velocity on the actual instant of the collision when compared to the *static wall* approximation. This in turn leads to a reduced energy loss in the course of the collision. This reasoning holds equally for all other types of collisional events, leading to the general picture of reduced energy loss or enhanced energy gain when the wall displacement is taken into account.

It should be stressed that although the additional fluctuations in the time of free flight due to wall displacement lead always to an increased acceleration compared to the acceleration predicted by the SWA, the specific amount of the increase in the energy gain *per collision* due to the wall displacement, depends on the characteristics of the

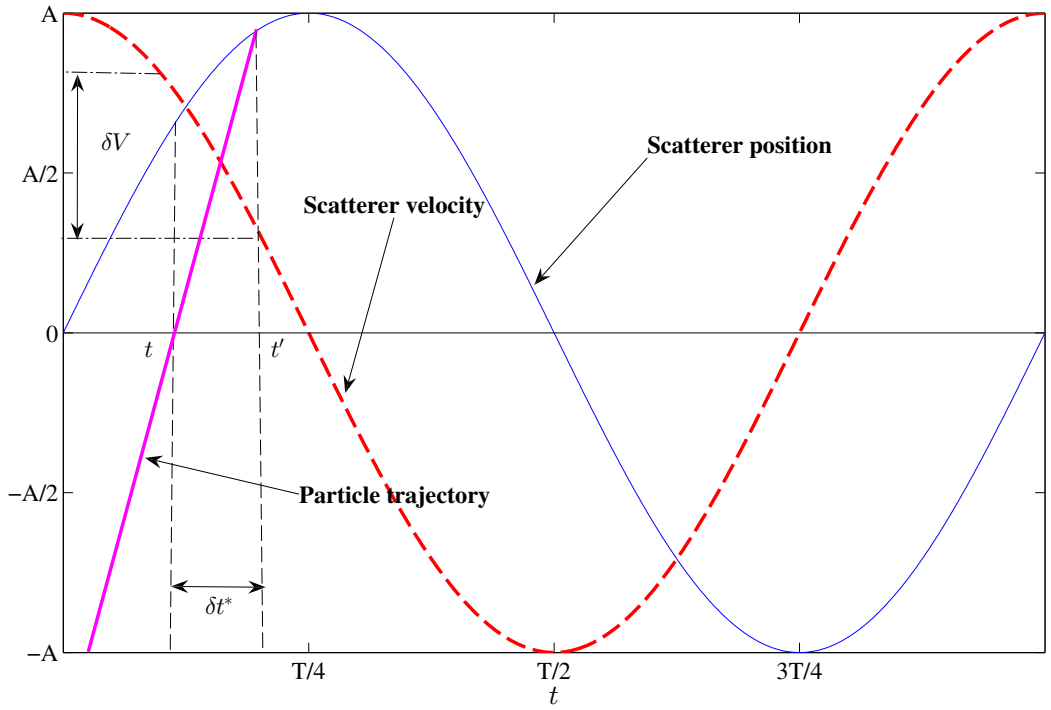

Figure 2.3.: The position and the velocity of one of the oscillating walls as a function of time. The straight line represents the trajectory of an incident particle.

oscillation law. For this reason the ratio

$$R_h\left(n\right) = \frac{\left(\langle V_n^2\rangle - \langle V_0^2\rangle\right)_{\text{exact}}}{\left(\langle V_n^2\rangle - \langle V_0^2\rangle\right)_{\text{SWA}}} = \frac{\sum_{i=1}^{n}\langle \delta V_i^2\rangle_{\text{exact}}}{\sum_{i=1}^{n}\langle \delta V_i^2\rangle_{\text{SWA}}} \tag{2.15}$$

is introduced, which enables us to compare the relative efficiency of the mechanism leading to the increased acceleration between setups with different driving force laws. The specific definition of $R_h(n)$, compared to that given in Ref. [76], is more convenient for numerical calculations as it converges much more rapidly, while at the same itme provides us with the same information about the increase in acceleration due to the wall displacement and shares the same asymptotic behavior. For the harmonically driven FUM (with randomized phase of oscillation) the correction factor $R_h(n)$ can readily be calculated using Eqs. (2.5) and (2.12), to obtain:

$$R_h(n) = \frac{1}{n}\sum_{i=1}^{n}\left\langle \cos\left(\frac{1}{V_{i-1}}\right)\right\rangle + 1 \tag{2.16}$$

Due to the Fermi acceleration mechanism developed in the FUM particle velocities

quickly acquire large values, i.e. $\frac{1}{V} \ll 1$. The expansion of the right-hand side of Eq. (2.16) in powers of $\frac{1}{V}$ yields

$$R_h(n) = 2 + O\left(\left\langle \frac{1}{V^2} \right\rangle\right) \tag{2.17}$$

Consequently, in the case of the two-moving wall variant of the FUM driven by a harmonic driving force and randomized phase of oscillation, the function $R_h(n)$ is (within the leading order of $\left\langle \frac{1}{V} \right\rangle$ approximation) independent of n and equals 2. It should be stressed that this result applies also to the original FUM, with one fixed and moving wall. Indeed, due to the randomization of the phase of oscillation and the symmetry $u\left(m\frac{T}{2} + \frac{T}{4} - t\right) = -u\left(m\frac{T}{2} + \frac{T}{4} + t\right), \quad (m = 0, 1, 2, \ldots)$ of the oscillation time-law, the two-wall variant of the FUM becomes fully equivalent to the original FUM, because collisions of the particles with either side of the moving wall(s), on the average, result to the same energy transfer. However, we will show that this is not the case when this particular symmetry of the oscillation law is broken.

2.2.3. The effect of dynamical symmetries

In order to demonstrate the variability of the factor R_h and its dependence on the characteristics of the oscillation law, we perform an analysis of the case of a sawtooth driving law, in the context of the original –consisting of one moving and one fixed wall– as well as the two-moving wall FUM variant. In all occasions the phase of the oscillating wall(s) is\are shifted randomly (according to a uniform distribution) after each collision with a particle. The following class of time-periodic laws for the moving wall(s) are considered:

$$x_i(t) = x_{0,i} + \begin{cases} \frac{1}{a}\frac{(t+\eta)A}{T} & \left| \begin{array}{l} \frac{(t+\eta)}{T} \in [0, a) \\ \frac{(t+\eta)}{T} \in [a, b] \\ \frac{(t+\eta)}{T} \in (b, 1] \end{array} \right. \\ -\frac{2}{b-a}\frac{(t+\eta)A}{T} & \\ \frac{1}{1-b}\frac{(t+\eta)A}{T} & \end{cases} \tag{2.18}$$

$$u(t) = \begin{cases} \frac{1}{a}\frac{A}{T} & \left| \begin{array}{l} \frac{(t+\eta)}{T} \in [0, a) \\ \frac{(t+\eta)}{T} \in [a, b] \\ \frac{(t+\eta)}{T} \in (b, 1] \end{array} \right. \\ -\frac{2}{b-a}\frac{A}{T} & \\ \frac{1}{1-b}\frac{A}{T} & \end{cases} \tag{2.19}$$

where T is the period of the oscillation, A the amplitude, $x_{0,(L,R)}$ the equilibrium position of the left or right moving wall and η a random number uniformly distributed in $[0, 2\pi)$. Despite the randomization of the phase of oscillation, due to the breaking of the symmetry $u\left(m\frac{T}{2} + \frac{T}{4} - t\right) = -u\left(m\frac{T}{2} + \frac{T}{4} + t\right), \quad (m = 0, 1, 2, \ldots)$, the acceleration rate in a FUM with one oscillating and one fixed wall and in a two-moving wall FUM is not

identical. To clarify this, let us calculate the factor $R_{h,i}(n)$, $(i = L, R)$ in each setup, beginning from the FUM with one vibrating wall at $x = 0$ and a fixed wall at $x = w$.

The change of the particle square velocity on the nth collision is given by the expression:

$$\delta V_n^2 = V_n^2 - V_{n-1}^2 = -4V_n u_n + 4u_n^2 \tag{2.20}$$

where u_n is the wall velocity upon the nth collision and V_{n-1} is the particle velocity before this collision. The parameters a, b control the asymmetry of $x(t)$. In order to calculate the average over the phase $\langle\langle \delta V_n^2 \rangle\rangle$ within the framework of the SWA we need to separate the ensemble of particle trajectories in two sets. The first set consists of trajectories for which the acceleration process is identical to that of the exact model. The second set consists of trajectories for which the acceleration in the SWA is underestimated. Each

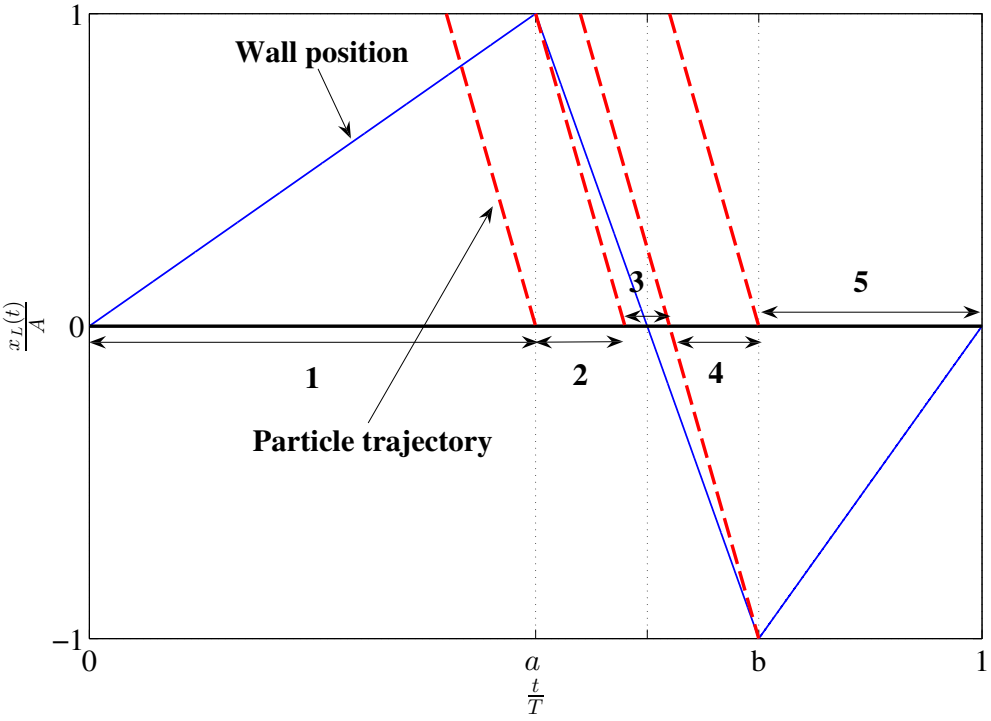

Figure 2.4.: The oscillation law for the FUM (with one oscillating wall). The borderlines of the zones discussed in the text are delimited by the dashed lines of slope $\lambda = \frac{|V_n|T}{A}$. The zones are also marked by double arrows.

zone is characterized by a fixed value of: $\langle\langle \delta V_n^2 \rangle\rangle$. The zones in question can easily be determined graphically, given that the collision time predicted by the exact dynamics corresponds to the intersection of the particle trajectory and the piecewise linear curve representing the wall position as a function of time $x(t)$ –see Fig. 2.4. The instant of

collision as given by the SWA corresponds to the intersection of the particle trajectory and the t-axis. This treatment requires the division of the interval $[0, T]$ in 5 zones –for the oscillation law of Eq. (2.18), as shown in Fig. 2.4. It is clear that, within some of the aforementioned zones the intersection of the particle trajectory with $x_L(t)$ and the t axis corresponds to instants characterized by different wall velocities, which, consequently, leads to different predictions for the energy gain of the particle by the SWA compared to the exact model. It is noted that the difference in the wall velocity due to the different predictions for the instant of collision between the two models is such that it always leads to an increased acceleration for the exact case, in accordance with the discussion of the previous section. Since the phase is uniformly distributed the size of the zones determines also the statistical weight of each zone. If we denote $\lambda = \frac{|V_n|T}{A}$ then the location and the size of the zones p_i is:

- Zone 1: $\frac{t}{T} \in [0, a] \Rightarrow p_1 = a$
- Zone 2: $\frac{t}{T} \in [a, a + \frac{1}{\lambda}] \Rightarrow p_2 = \frac{1}{\lambda}$
- Zone 3: $\frac{t}{T} \in [a + \frac{1}{\lambda}, b - \frac{1}{\lambda}] \Rightarrow p_3 = b - a - \frac{2}{\lambda}$
- Zone 4: $\frac{t}{T} \in [b - \frac{1}{\lambda}, b] \Rightarrow p_4 = \frac{1}{\lambda}$
- Zone 5: $\frac{t}{T} \in [b, 1] \Rightarrow p_5 = 1 - b$

Therefore the average over the phase is given by:

$$\langle\langle \delta V_n^2 \rangle\rangle = \sum_{i=1}^{5} p_i \delta V_{n,i}^2$$

For the exact model using $u_0 = \frac{A}{T}$ we obtain:

$$\begin{aligned} \langle\langle \delta V_n^2 \rangle\rangle_{exact} =& 4u_0^2 \left[2 \left(\frac{1}{a} + \frac{4}{b-a} + \frac{1}{1-b} \right) \right. \\ &\left. + \frac{1}{\lambda} \left(\frac{1}{a^2} - \frac{8}{(b-a)^2} + \frac{1}{(1-b)^2} \right), \right] \end{aligned} \tag{2.21}$$

while using the SWA we get:

$$\langle\langle \delta V_n^2 \rangle\rangle_{SWA} = 4u_0^2 \left(\frac{1}{a} + \frac{4}{b-a} + \frac{1}{1-b} \right). \tag{2.22}$$

Thus, the function $R_h(n)$ is:

$$R_{h,L}(n) = 2 + \frac{F(a,b)}{n} \sum_{i=1}^{n} \frac{1}{\lambda} \tag{2.23}$$

with

$$F(a,b) = \frac{\frac{1}{a^2} - \frac{8}{(b-a)^2} + \frac{1}{(1-b)^2}}{\frac{1}{a} + \frac{4}{b-a} + \frac{1}{1-b}}$$

Now we can perform also the averaging over the velocity distribution of the particles and obtain the final expression:

$$R_{h,L}(n) = 2 + \frac{u_0 F(a,b)}{n} \sum_{i=1}^{n} \left\langle \frac{1}{|V_{i-1}|} \right\rangle \tag{2.24}$$

To derive a formula featuring explicitly the dependence on n it is necessary to determine $\langle \frac{1}{|V_{n-1}|} \rangle$ as a function of n. Since the FUM under discussion is randomized, the acceleration of the particles can be described as a diffusion process in momentum space, i.e. by the Fokker-Planck equation. The solution of the Fokker-Planck equation [see Appendix A] assuming a perfectly reflective barrier at $V = 0$ leads to the following asymptotic ($n \gg 1$) expression for $\left\langle \frac{1}{V_{n-1}} \right\rangle$:

$$\begin{aligned} \left\langle \frac{1}{|V_{n-1}|} \right\rangle &\simeq \sqrt{\frac{\pi}{2}} \frac{1}{\sigma} \\ \sigma &= \sqrt{g(a,b)(n-1) + \frac{V_0^2}{2}} \\ g(a,b) &= 4u_0^2 \left(\frac{1}{a} + \frac{4}{b-a} + \frac{1}{1-b} \right). \end{aligned} \tag{2.25}$$

The summation after the substitution of Eqs. (2.25) into Eq. (2.24) yields

$$R_{h,L}(n) = 2 + \frac{u_0 F(a,b)}{n} \sqrt{\frac{\pi}{2g(a,b)}} \left[\zeta\left(\frac{1}{2}, \frac{V_0^2}{2g(a,b)} \right) - \zeta\left(\frac{1}{2}, n + \frac{V_0^2}{2g(a,b)} \right) \right], \tag{2.26}$$

where ζ stands for the generalized Riemann (Hurwitz) zeta function. For $n \gg 1$, $R_{h,L}(n) - 2 \propto \frac{1}{\sqrt{n}} + O\left(\frac{1}{n}\right)$. Consequently, $R_{h,L}(n)$ for $n \to \infty$ approaches asymptotically the value 2 with a rate controlled by the parameters a, b. This is illustrated in Fig. 2.5, where numerical results for $R_{h,L}(n)$ obtained for $a = 5 \times 10^{-3}$ and $b = 0.67$ are shown along with the analytical result of Eq. (2.26). As demonstrated in this figure, for the particular choice of the parameter values, the function $R_{h,L}(n)$ deviates from the value 2 even for relatively large n.

Let us now discuss the case of a FUM consisting of one fixed wall at $x = 0$ and one moving at $x = w$. As already mentioned, the two symmetrical FUM setups (moving wall on the right and fixed wall on the left and vice versa) do not lead to the same acceleration rate if the wall displacement on collision is taken into account, provided that

the $u\left(m\frac{T}{2}+\frac{T}{4}-t\right)=-u\left(m\frac{T}{2}+\frac{T}{4}+t\right),\quad (m=0,1,2,\ldots)$ symmetry of the oscillation law is broken. This is so because, on the average, more energy is gained by a particle if it collides only with the right side of the wall than if it collides with its left side. Indeed, if we follow the steps outlined above then we obtain the following expression for $R_{h,R}(n)$ for a FUM with one moving wall on the right:

$$R_{h,R}(n)=2-\frac{u_0F(a,b)}{n}\sqrt{\frac{\pi}{2g(a,b)}}\left[\zeta\left(\frac{1}{2},\frac{V_0^2}{2g(a,b)}\right)-\zeta\left(\frac{1}{2},n+\frac{V_0^2}{2g(a,b)}\right)\right], \quad (2.27)$$

which implies that a FUM with a moving wall on the right leads to a slower acceleration rate compared to its counterpart. Obviously, for the case of a two-moving wall FUM the factor R_h is given by:

$$R_h(n)=\frac{R_{h,L}(n)+R_{h,R}(n)}{2}=2 \quad (2.28)$$

Thus, for a two-moving wall FUM the correction factor for the increased acceleration due to the wall displacement on collision, considering that both walls follow the dynamics of Eq. (2.18), is independent of n and equal to that obtained for the case of harmonic driving (Eq. (2.17)). In conclusion, $R_h(n)$ for the FUM setups with one moving wall depends on the number of collisions n and tends to the value $R_h(\infty)=2$, in a manner specified by the particular oscillation law, which is characterized here by the parameters a, b. On the other hand, when both walls of the FUM are allowed to move, then unless a specific choice for the dynamics of each of the walls is made, $R_h(n)$ is rendered independent of n and equals that obtained when a harmonic driving is considered.

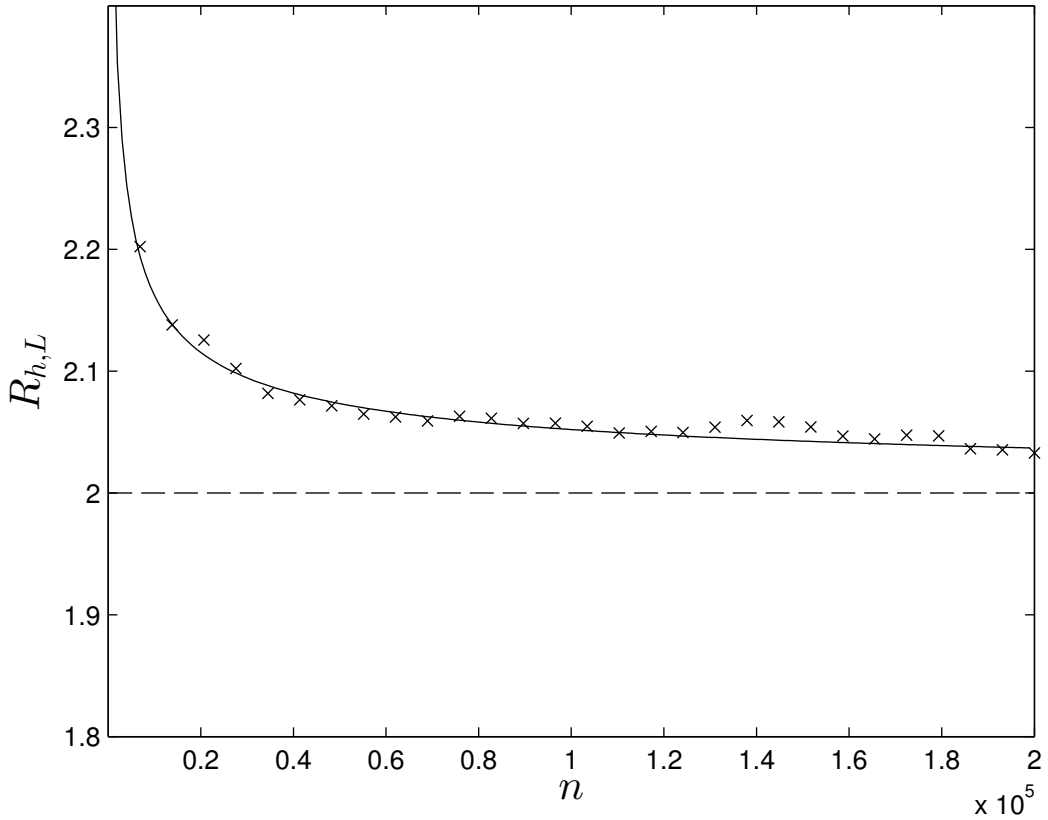

Figure 2.5.: Numerical results (×) as well as analytical results (see Eq. (2.26)), for $R_{h,L}(n)$ in the original FUM, employing sawtooth driving for $u_0 = 0.01$, $a = 5 \times 10^{-3}$ and $b = 0.67$.

2.3. The impact of rare events

Despite the fact that the application of the SWA in the FUM leads to a considerable underestimation of the acceleration of the particles as we saw in §2.2, the qualitative description of the velocity diffusion process at the level of the fluctuations of the particle velocity is described successfully. A characteristic property of the SWA is that, since the spatial location of the "*moving*" scatterer is held fixed, multiple consecutive collisions between the wall and the particles cannot occur. However, there is a correspondence between multiple collision events taking place in the exact model and collisions occurring in the SWA after which particles continue moving towards the "*moving*" wall. To avoid the passing of a particle through the hard wall after such a collision, one has in this case to reverse factitiously the velocity of the particle. These events are very rare, occurring only in the low velocity regime (particle velocities comparable with the maximum wall velocity) and in order to ease the analytical treatment of the acceleration problem, it has become a standard practice to neglect them. This approximation appears very

reasonable, especially after a sufficiently large number of collisions with the "*moving*" wall has been reached and Fermi acceleration is fully developed, irrespective of the initial velocity distribution of the particles. Moreover, neglecting these rare events allows the simplified map of the FUM or its variants, after a proper transformation, to be locally approximated by the standard map [53, 65–68].

Nevertheless, this further simplification of the SWA (neglecting the events which lead to an artificial velocity reversal of the particles), gives rise to a fundamental inconsistency: the ensemble mean of the absolute velocity does not change through collisions with the "*moving*" wall [41, 71, 72], despite the well-established numerical result that Fermi acceleration does take place in the phase randomized FUM. It follows that a direct computation of the mean absolute velocity of the particles from the difference equations defining the dynamics of the system, if the collisions leading to an artificial reversal are not taken into account, is not feasible.

In the following we continue to consider a stochastic simplified FUM, with the phase of the velocity of the "*moving*" wall randomly shifted upon each collision with the fixed wall. For the sake of convenience we write again the simplified mapping [§ 2.2, Eqs. (2.3)].

$$t_n = t_{n-1} + \frac{2}{|V_{n-1}|} \tag{2.29a}$$

$$V_n = |V_{n-1} + 2u_n| \tag{2.29b}$$

$$u_n = \epsilon \cos(t_n + \eta_n) \tag{2.29c}$$

where u_n is the velocity of the "*moving*" wall, V_n is the algebraic value of the particle velocity immediately *after* the nth collision with the "*moving*" wall measured in units of ωw (w denoting the spacing between the walls), t_n the time when the nth collision occurs measured in units of $1/\omega$, η_n a random variable uniformly distributed in the interval $[0, 2\pi)$ updated immediately after each collision between a particle and the fixed wall, and ϵ the dimensionless ratio of the amplitude of oscillation to the spacing between the moving and the fixed wall.

It is noted that in all numerical results presented in the following, ϵ was fixed at $1/15$ and that the initial absolute velocities of the ensemble of particles were chosen randomly according to the probability density function (PDF)

$$\rho(|V|, 0) = \frac{1}{\sigma}\sqrt{\frac{2}{\pi}} e^{-|V|^2/(2\sigma^2)},$$

$\sigma^2 = \frac{100}{225}$, unless stated otherwise.

As was briefly mentioned in § 2.1.2, the absolute value in Eq. (2.29b) is introduced

because particle velocities cannot be allowed to take negative values after a collision with the "*moving*" wall, since a negative sign of the particle velocity corresponds to a particle escaping from the area between the walls. It should be mentioned, that such a collision, within the framework of the exact model, corresponds to a particle experiencing multiple collisions with the moving wall. Therefore, if $V_{n-1} < 2|u_n|$ and $u_n < 0$, in order to prevent the particle from escaping the region between the walls the velocity is reversed "by hand". The presence of the absolute value function in Eq. (2.29b), nevertheless, complicates the analytical treatment of the acceleration problem. For this reason, it has become a standard practice in the treatment of the FUM to remove the absolute function, thereby neglecting the collision events upon which the particle direction is not reversed after its collision with the "*moving*" wall. However, as will be demonstrated in the following, neglecting this type of collision events, leads to a glaring inconsistency.

2.3.1. Formulation of the Inconsistency

Let us study the increase of the particle absolute velocity in the course of one collision, $\delta|V_n| = |V_n| - |V_{n-1}|$. This is a key quantity for the estimation of the mean absolute velocity. Furthermore, the calculation of $\delta|V_n|$ is mandatory for a complete statistical description of the evolution of absolute velocities of the particles through a kinetic equation, such as the Fokker-Planck equation [41, 64, 65]. As we notice by inspecting Eq. (2.29b), obtaining $\delta|V_n|$ as a function of the phase of the wall upon collision is impeded because of the absolute value taken on the right-hand side (RHS). Due to Fermi acceleration after a sufficiently large number of collisions, $n \gg 1$, the mean absolute velocity of the particles becomes much larger than the maximum wall velocity, irrespective of the initial distribution of particle velocities. Thus, one can intuitively assume that the vast majority of particles evolving in the FUM also possesses absolute velocities much larger compared to the maximum wall velocity. Following this reasoning, the absolute value in Eq. (6.1) is usually dropped [41, 53, 64, 65]. Doing so and further by introducing in Eq. (2.29b) the absolute velocity, in order to determine the mean increase of the magnitude of particle velocities, Eqs. (2.29) yield

$$t_n = t_{n-1} + \frac{2}{|V_{n-1}|} \tag{2.30a}$$

$$|V_n| = |V_{n-1}| - 2\epsilon\cos(t_n + \eta_n). \tag{2.30b}$$

Consequently,

$$\delta|V_n| = -2\epsilon\cos(t_n + \eta_n) \tag{2.31}$$

The mean increase of particle absolute velocities over the phase of oscillation can

be calculated by integrating Eq. (2.31) over the random phase component η_n. Since the random variable η_n is uniformly distributed in the interval $[0, 2\pi)$ it follows that [41, 64, 65]

$$\langle\langle \delta|V_n| \rangle\rangle = 0 \tag{2.32}$$

In Eq. (2.32) $\langle\langle \ \ \rangle\rangle$ denotes phase averaging. Formally, in order to obtain the ensemble average one has to integrate Eq. (2.32) over the PDF of particle absolute velocities. However, this step is trivial since the RHS of Eq. (2.32) does not depend on the particle velocity. Consequently, $\langle\langle \delta|V_n| \rangle\rangle \equiv \langle \delta|V_n| \rangle$, where $\langle \delta|V_n| \rangle$ stands for the ensemble mean change of particle absolute velocities. Moreover,

$$\langle |V_n| \rangle = \sum_{i=1}^{n} \langle \delta|V_i| \rangle + \langle |V_0| \rangle = const. \tag{2.33}$$

The analytical result provided by Eq. (2.33) is in apparent contradiction with the development of Fermi acceleration, i.e. unbounded growth of the mean absolute particle velocity, in the phase randomized FUM [45, 60, 67].

The increase of the mean of the magnitude of the particle velocity can be also calculated using the "exact" set of Eqs. (6.1) numerically. However, this specific quantity is characterized by large statistical uncertainties –of the order of $\pm 100\%$ for an ensemble of 5×10^4 particles. In order to smooth out the results we compute instead the cumulative mean $\langle \delta|\tilde{V}_n| \rangle = \frac{1}{n} \sum_{i=1}^{n} \langle \delta|V_i| \rangle$ [46, 60]. It is worth mentioning, that if the mean velocity over the ensemble is a power law as a function of the number of collisions, the cumulative mean is also a power law with the same exponent. In Fig. 2.6 numerical results for $\langle \delta|\tilde{V}_n| \rangle$ are shown, obtained by the iteration of the "exact" set of Eqs. (2.30a), as a function of the number of collisions n. As can be seen in Fig 2.6, $\langle \delta|\tilde{V}_n| \rangle$ does not equal zero for any finite number of collisions with the moving wall n. More specifically, perfoming a fit with a power-law, $\langle \delta|\tilde{V}_n| \rangle \propto n^k$, for $n > 10^5$ yields $k = 0.492 \pm 10^{-3}$, which shows that $\langle \delta|\tilde{V}_n| \rangle \to 0$ only for $n \to \infty$.

Given the inconsistency between the numerical results for the "exact" SWA mapping defined by Eqs. (6.1), which takes into account the artificial reversal of the particle velocity occurring in the low velocity regime, and the analytical estimation which is obtained using Eq. (2.30) (without the modulus function), we conclude that when this rare class of events is neglected –on which the particle velocity is artificially reversed– the acceleration problem cannot be treated successfully, leading to the false prediction that Fermi acceleration is not feasible in the stochastic FUM [71, 72].

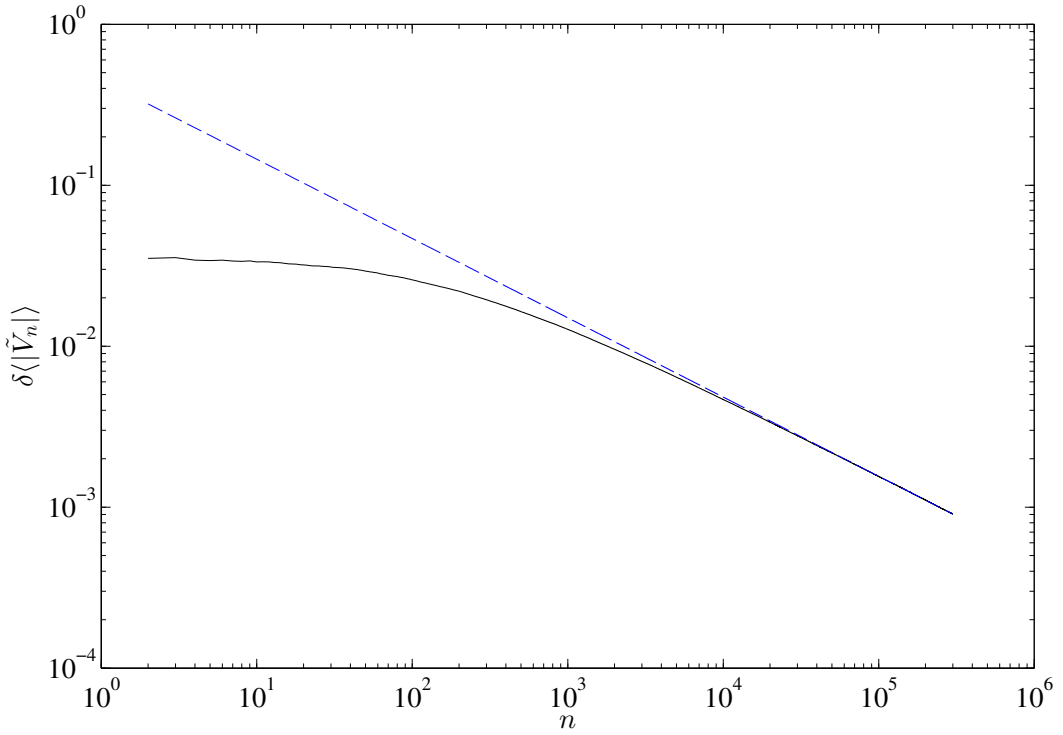

Figure 2.6.: Numerical results (solid line) for $\langle\delta|\tilde{V}_n|\rangle = \frac{1}{n}\sum_{i=1}^{n}\langle\delta|V_i|\rangle$ on the basis of an ensemble of 5×10^4 particles evolving in a phase randomized FUM as a function of the number of collisions. Results were obtained by iterating the exact map given by Eqs. (6.1) for 3×10^5 number of collisions, with $\epsilon = \frac{1}{15}$. It is noted that $\langle\delta|\tilde{V}_n|\rangle$ is measured in units of ωw. The numerical results were fitted with a power-law model, $\langle\delta|\tilde{V}_n|\rangle \propto n^k$, for $n > 10^5$ yielding $k = 0.492 \pm 10^{-3}$ (dashed line).

2.3.2. Remedy for the Problem

In order to obtain correctly the increase of the mean absolute velocity upon a collision, let us separate the collision events into two sets, C_1 and C_2. The set of events C_1 contains all collisions on which particle velocity is "naturally" reversed (without the use of the absolute value function in Eq. (6.1)), whereas the set C_2 is its complement, containing the class of rare events discussed above. The increase of the ensemble mean velocity $\langle \delta |V_n| \rangle$ is then given as the sum of the corresponding quantities $\langle \delta |V_n| \rangle_i$, calculated within each set of events C_i, multiplied by the respective statistical weights $w_i(n)$ of each collision type ($i = 1, 2$).

$$\langle \delta |V_n| \rangle = w_1(n) \langle \delta |V_n| \rangle_1 + w_2(n) \langle \delta |V_n| \rangle_2 \tag{2.34}$$

The magnitude of the particle velocity after the nth collision is determined for each of these sets of events by the equation:

$$|V_n| = \pm \left(|V_{n-1}| + 2u_n \right) \tag{2.35}$$

where the positive sign corresponds to collision events which are elements of the set C_1 and the minus sign to those which belong to the set C_2. From Eq. (2.35) one can determine the change in the magnitude of the particle absolute velocity $\delta |V_n|_i$ in a collision event, which belong to the set C_i ($i = 1, 2$) as:

$$\delta |V_n|_1 = 2u_n \tag{2.36a}$$

$$\delta |V_n|_2 = -2(|V_{n-1}| + u_n) \tag{2.36b}$$

As has already been mentioned, in order for the particle velocity to be artificially reversed, the necessary condition $|V_{n-1}| \leq 2u_n$, or equivalently, $V_{n-1} < 2\epsilon$ and $u_n < 0$, must be fulfilled. In other words, the occurrence of collisions belonging to the set C_2, depends only on the particle absolute velocity immediately before such a collision and the phase upon collision of the "*moving*" wall, which needs to lie in the interval $(\pi/2, 3\pi/2)$, independently of the number of collisions n. Since all phases upon collision with the "*moving*" wall are equally probable with respect to the total ensemble of particles $C \equiv C_1 \cup C_2$ –owing to the random shift of the phase upon collision of a particle with the fixed wall– the fraction of particles which undergo artificial velocity reversal depends only on their absolute velocities. Therefore, $w_2(n) \propto \int_0^{2\epsilon} \rho\left(|V|, n\right) d|V|$, where $\rho(|V|, n)$ stands for the PDF of particle absolute velocities, after n collisions with the "*moving*" wall. Let us for a moment turn our attention to the corresponding PDF of the algebraic value

V of particle velocities instead of the magnitude $|V|$. Obviously, the algebraic value on the nth collision is the sum $V_n = \sum_{i=1}^{n} \delta V_i$, where δV_i is the change of the algebraic value of the particle velocity on the ith collision. Since V_n is the sum of independent random quantities, employing the Central Limit Theorem we conclude that for $n \gg 1$, V_n follows a Gaussian distribution, with a mean value $\sum_{i=1}^{n} \langle \delta V_i \rangle$ and variance $\sum_{i=1}^{n} (\langle (\delta V_i)^2 \rangle - \langle \delta V_i \rangle^2)$. Since the particles are confined between the walls, no flow (drift) of the particles can take place. Therefore, $\langle \delta V_i \rangle = 0$. Furthermore, it can be shown (see Appendix B) that to the leading order:

$$(\delta V_n)^2 = 2\epsilon^2 \tag{2.37}$$

Hence, the PDF of the algebraic value of particle velocities for $n \gg 1$ is expected to be described by $\rho(V, n) = \frac{1}{2\epsilon\sqrt{\pi n}} e^{-V^2/(4\epsilon^2 n)}$. Due to the symmetry of the Gaussian density function, the corresponding PDF of the absolute particle velocities defined in the semi-infinite interval $[0, \infty)$ is $\rho(|V|, n) = 2\rho(V, n)$. Thus,

$$\rho(|V|, n) = \frac{1}{\epsilon\sqrt{\pi n}} e^{-|V|^2/(4\epsilon^2 n)} \tag{2.38}$$

Let us determine the statistical weight $w_2(n)$ of the set of collision events on which the particle velocity needs to be reversed "by hand", i.e. by applying the absolute value function on the right-hand side (RHS) of (6.1). By mere inspection of (6.1) we conclude that the particle will continue travelling towards the same direction it was prior to the collision with the "moving" wall, if and only if, $|V| < 2u$ and $u > 0$. Therefore,

$$w_2(n) = \int_{\pi}^{3\pi/2} d\xi \int_{0}^{2u} dV \rho(V) \underbrace{\int_{0}^{\epsilon} du p(u) \left\{ \frac{1}{2}\delta\left[\xi - g(u)\right] + \frac{1}{2}\delta\left[\xi + g(u)\right] \right\}}_{I}, \tag{2.39}$$

where $\rho(V)$ stands for the PDF of the algebraic value of particle velocities and $p(u)$ for the corresponding PDF of the velocity of the "moving" wall and $g(u) = \cos^{-1}(u/\epsilon)$ [see (6.1)]. Given that, $u < 0$ the function $g(u)$ takes values in the interval $(\pi/2, 3\pi/2)$. The last term on the RHS of (2.39) compensates for the missing set of possible phases leading to $u \in (0, \epsilon]$, namely $\xi \in (\pi, 3\pi/2$, due to the branch cut of the inverse cosine function in $g(u)$.

The corresponding PDF of the wall velocity $p(u)$ can easily be derived, considering that the phase of oscillation of the wall upon collision follows a uniform distribution due to the random phase-shift performed before each collision, through the addition of a random number uniformally distributed in the interval $(0, 2\pi]$. Applying the fundamental

transformation law of probabilities one obtains,

$$p(u) = \frac{1}{\pi\sqrt{\epsilon^2 - u^2}} \tag{2.40}$$

Using the property of the Dirac delta function $\delta\left(f(x)\right) = \sum_i \frac{\delta(f(x_i))}{|f'(x_i)|}$, where x_i are the real roots of the equation $f(x) = 0$, we can rewrite the integral I in (C.1) as,

$$\begin{aligned} I \;\equiv\; & \int_0^{\epsilon} du \frac{1}{\pi\sqrt{\epsilon^2 - u^2}} \left\{ \frac{1}{2}\delta\left[\xi - g(u)\right] + \frac{1}{2}\delta\left[\xi + g(u)\right] \right\} = \\ & = \int_0^{\epsilon} \frac{1}{2} \left[\sum_i \frac{\delta\left(u - u_i\right)}{\left| -\frac{1}{\sqrt{\epsilon^2 - {u_i}^2}} \right|} + \sum_i \frac{\delta\left(u - {u_i}'\right)}{\left| -\frac{1}{\sqrt{\epsilon^2 - {u_i}'^2}} \right|} \right] \frac{1}{\pi\sqrt{\epsilon^2 - u^2}} du \end{aligned} \tag{2.41}$$

where, $u_i = \epsilon\cos(\xi)$ and ${u_i}' = \epsilon\cos(\xi + \pi/2)$. The integration over u and then V of (C.1) gives,

$$w_2(n) = \int_{\pi/2}^{3\pi/2} \frac{1}{2\pi} \left\{ \frac{1}{2} \left[\mathrm{Erf}\left(\frac{u_i}{\sqrt{n}\epsilon} \right) + \mathrm{Erf}\left(\frac{{u_i}'}{\sqrt{n}\epsilon} \right) \right] \right\} d\xi. \tag{2.42}$$

The expansion of (2.42) at $n \to \infty$ followed by integration over ξ yields,

$$w_2(n) = \frac{2}{\sqrt{n}\pi^{3/2}} + \mathcal{O}\left(\frac{1}{n^{3/2}} \right). \tag{2.43}$$

It is worth noticing, that for the SFUM and in contrast to the exact model, within which the displacement of the scatterer is taken into account, the most probable, i.e. maximum of $\rho(|V|, n)$, occurs for $n \gg 1$ at $|V| = 0^+$, despite the increase of the mean absolute velocity as can be seen in Fig 2.7. Therefore, the fraction of particles with absolute velocities within the interval $|V| < 2\epsilon$, which is a necessary condition for the factitious reversal of the particle velocity, remains always finite for finite n, despite the fact that $\langle |V_n| \rangle \gg \epsilon$.

The statistical weight $w_2(n)$ of the set of collision events C_2 can also be determined numerically. Fig. 2.8 shows numerical results for $w_2(n)$ as a function of the number of collisions n, obtained on the basis of an ensemble of 1.6×10^5 particles. The data series of $w_2(n)$ shown in Fig. 2.8 has been processed with a 2×10^3 point moving average filter in order to reduce the statistical fluctuations.

The specific minimum number of collisions which need to be reached in order for

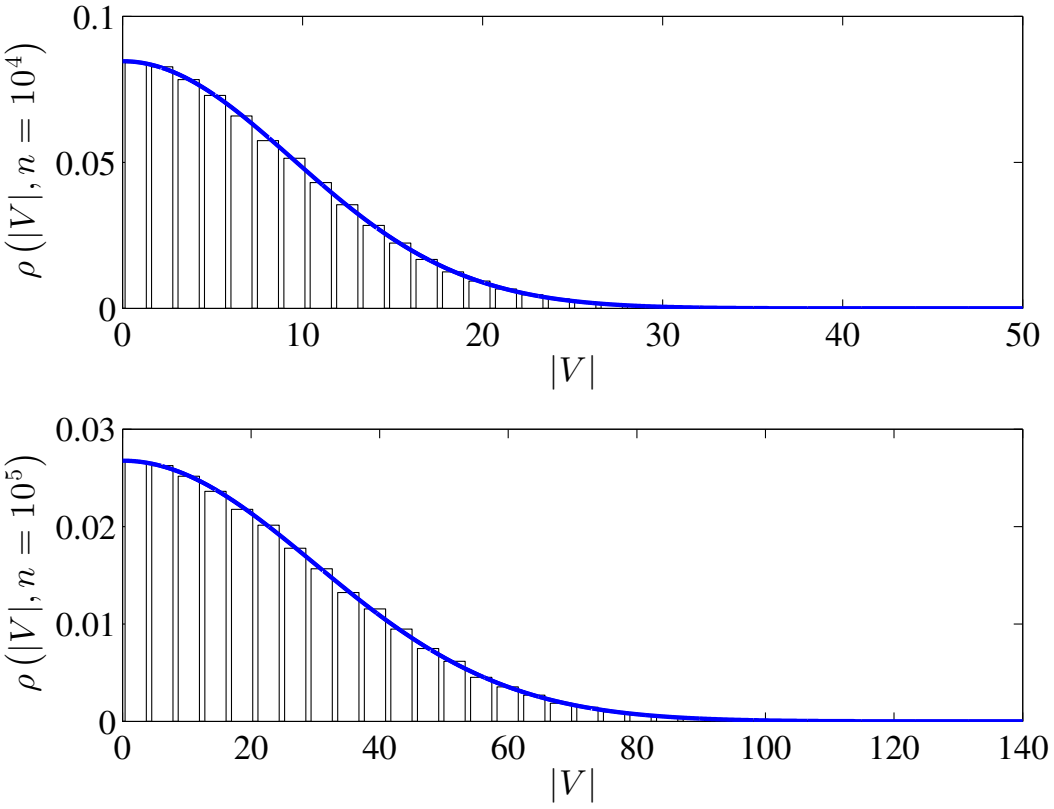

Figure 2.7.: Histograms (bars) of the particle absolute velocities for 10^4 and 10^5 collisions. Numerical results were obtained on the basis of an ensemble of 1.6×10^5 trajectories. The analytical solution given by Eq. (2.38) (black line) is also shown. $|V|$ is measured in units of ωw.

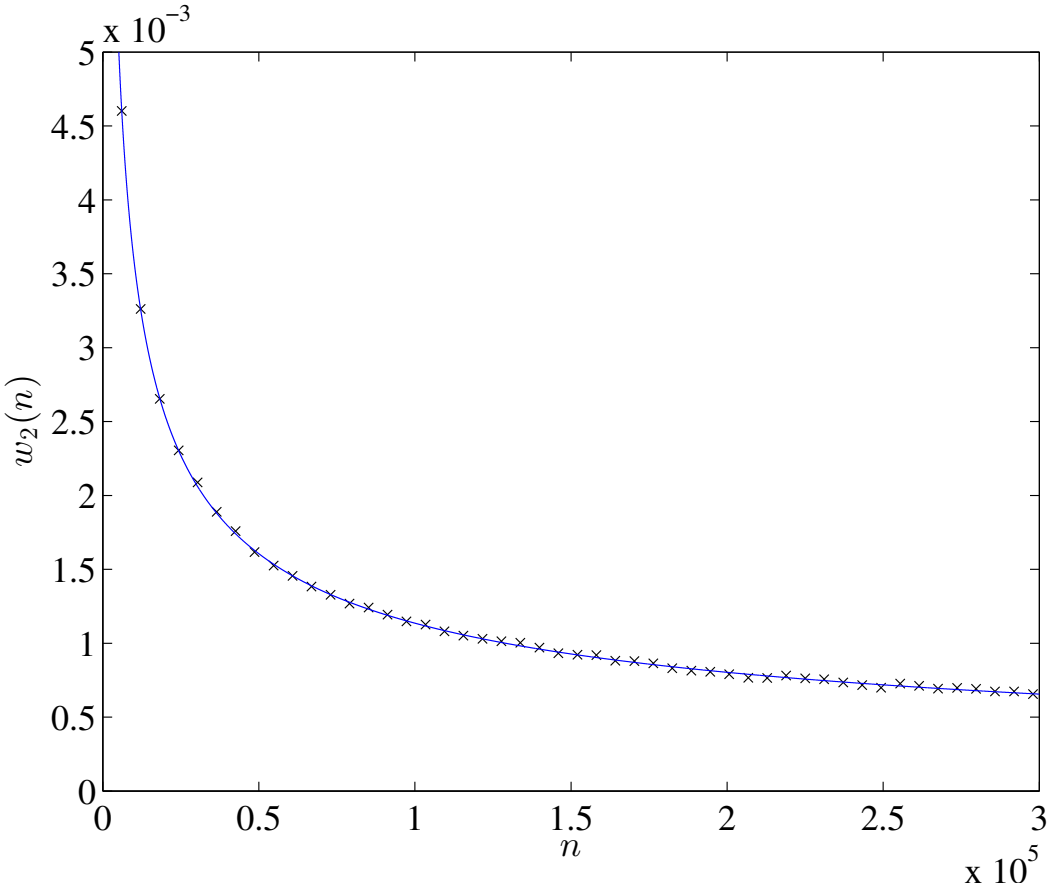

Figure 2.8.: Numerical results ($\times$) for the statistical weight of the set of collision events C_2 obtained on the basis of an ensemble of 1.6×10^5 trajectories propagated for 3×10^5 collisions. Results were smoothed using a 2×10^3 point moving average filter to reduce statistical fluctuations. The analytical result of Eq. (2.43) is also shown (solid line).

the PDF of particle absolute velocities to converge to Eq. (2.38) and thus Eq. (2.43) to describe the evolution of $w_2(n)$, bears a strong dependence on the initial PDF of particle velocities. Numerical results obtained with a Gaussian initial distribution of particle absolute velocities, centered at $|V| = 4.5$ with variance $\sigma^2 = \frac{100}{225}$, and smoothed using a moving average filter with a 2×10^4 span, are presented in Fig. 2.9. As can be seen, $w_2(n)$ demonstrates a very different behavior as opposed to that observed in Fig. 2.8. Specifically, in Fig. 2.8 it is seen that $w_2(n)$ is a monotonically decreasing function of the number of collisions n, whereas in Fig. 2.9 the function is not monotonic. On the contrary, we see that for $n \lessapprox 10^5$, $w_2(n)$ is increasing, and only for larger number of collisions becomes a decreasing function of n.

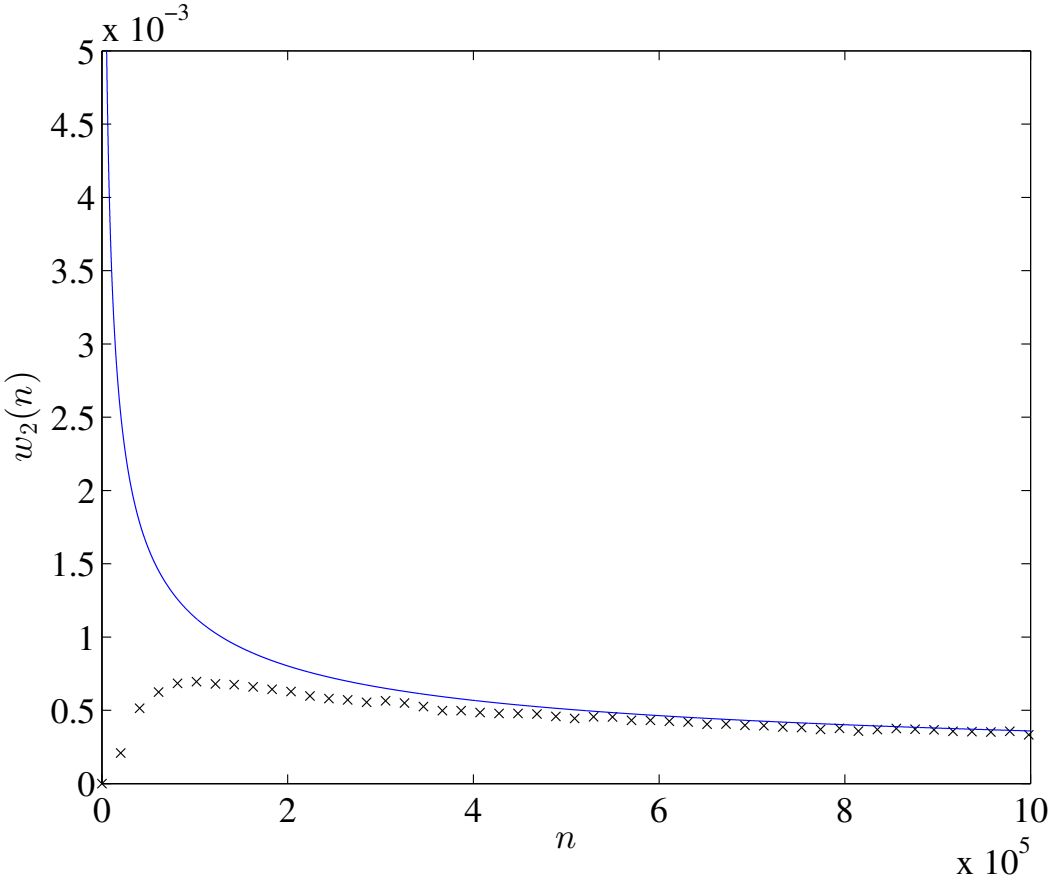

Figure 2.9.: Numerical results –(×)– for the statistical weight of the set of collision events C_2. Numerical results were obtained on the basis of an ensemble of 4×10^4 trajectories propagated for 10^6 collisions and with a Gaussian initial distribution of particle absolute velocities centered at $|V| = 4.5$, with variance $\sigma^2 = \frac{100}{225}$. Results were smoothed using a 2×10^4 point moving average filter. The analytical expression given by Eq. (2.43) is also plotted for the sake of comparison.

To obtain the mean of the magnitude of the particle velocity within each of the sets C_1 and C_2, the average of the particle velocity with respect to the phase upon collision $\xi = t + \eta$ for each set needs to be determined. Obviously, if $p_1(\xi, n)$, $p_2(\xi, n)$ and $p(\xi, n)$ are the PDFs of the phase upon the nth collision for the set of collision events C_1, C_2 and $C = C_1 \cup C_2$, respectively, then

$$p(\xi, n) = w_1(n)p_1(\xi, n) + w_2(n)p_2(\xi, n). \tag{2.44}$$

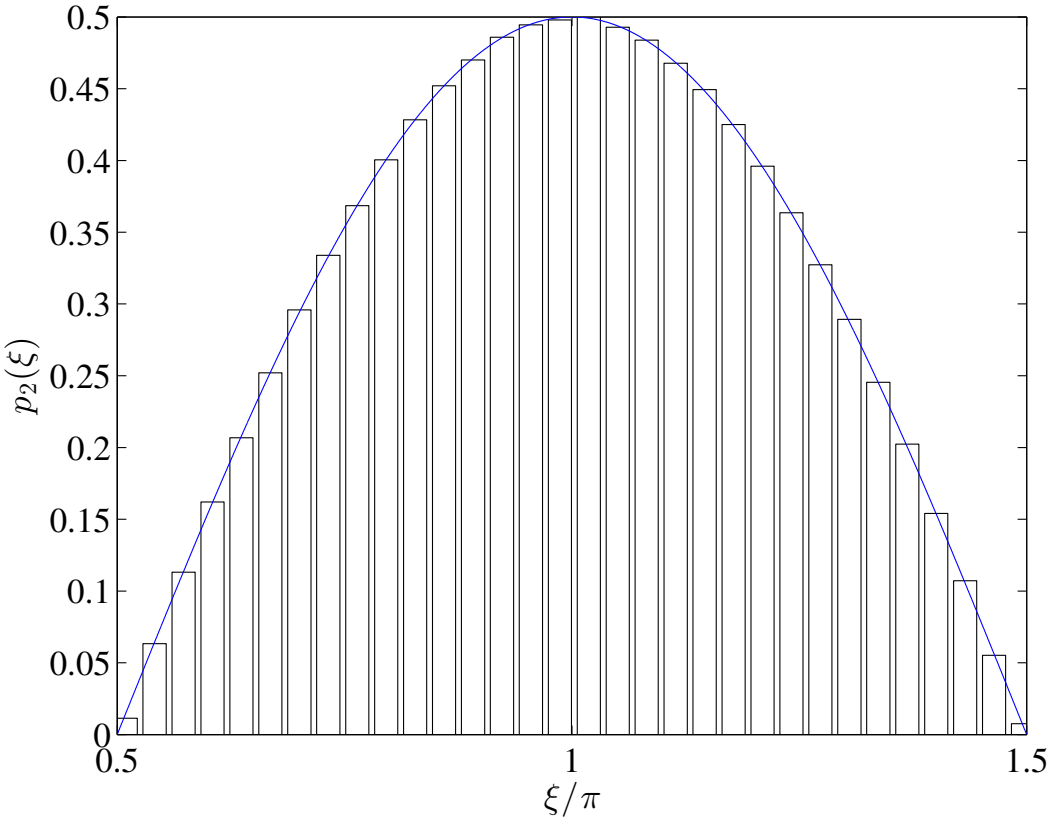

Figure 2.10.: Numerical results (bars) for the PDF of the phase upon collisions for events which are elements of the set C_2. Numerical results were obtained on the basis of an ensemble of 3×10^4 collision events, on which the particle velocity was "artificially" reversed. The analytical estimation of the PDF is also shown (solid line). The phase is given in units of π.

In Fig. 2.10 numerical results for the PDF of the phase of the "*moving*" wall upon collision for the set of collisions C_2, computed on the basis of an ensemble of 3×10^4 such events, are presented. As can be seen, the probability of a particle experiencing a collision upon which its velocity direction is artificially reversed, is higher the greater the wall velocity is, with a maximum at 0 and 2π where the wall velocity is also maximum. It should be noted that the numerical results, regardless of the specific choice of initial

conditions for the ensemble of trajectories, converge after a short transient period ($n < 10^3$) to the steady state PDF shown in Fig. 2.10. Consequently, $p_2(\xi, n)$ for $n \gg 1$ becomes independent of the number of collisions, i.e. $p_2(\xi, n) \approx p_2(\xi)$. The function $\frac{1}{2}\cos(\xi)$ is also plotted which fits very accurately the numerical data. Therefore,

$$p_2(\xi) = \begin{cases} \frac{1}{2}\cos(\xi) & \xi \in [0, \frac{\pi}{2}) \vee (\frac{3\pi}{2}, 2\pi) \\ 0 & \xi \in [\frac{\pi}{2}, \frac{3\pi}{2}] \end{cases} \tag{2.45}$$

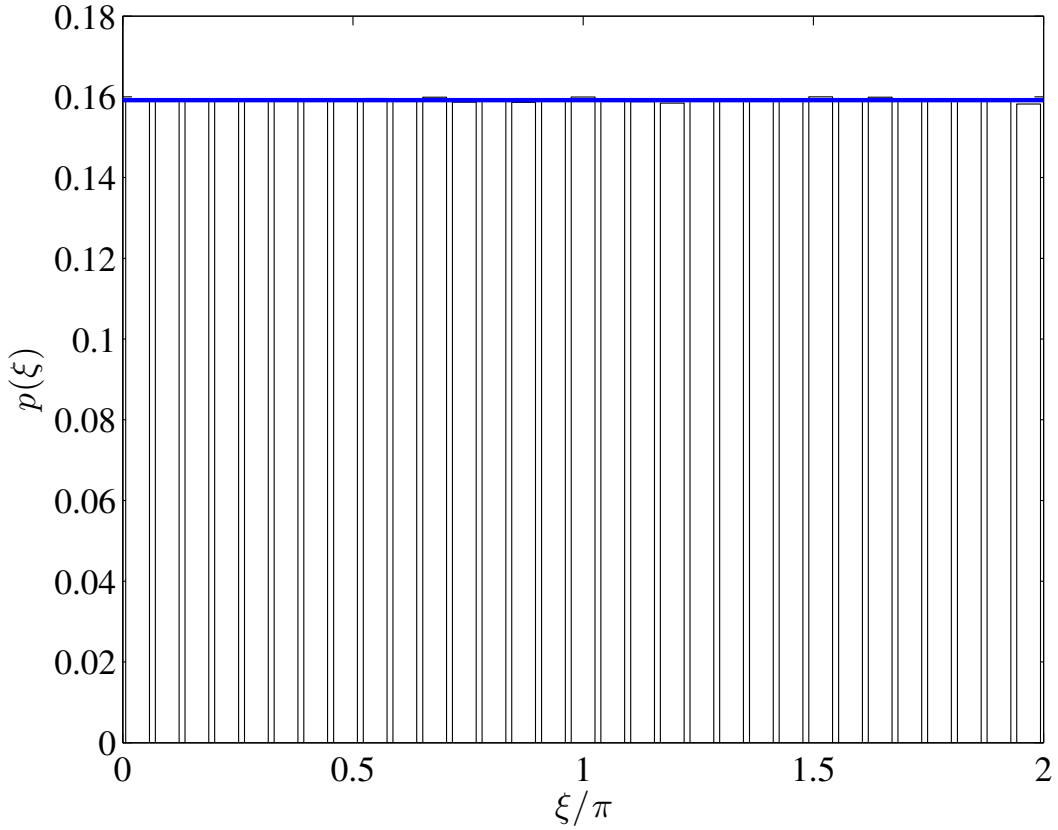

Figure 2.11.: Numerical results (bars) for the PDF of the phase upon all types of collisions. Numerical results were obtained on the basis of an ensemble of 10^6 collision events. The uniform distribution is also plotted for the sake of comparison –solid line. The phase axis is normalized by division with π.

In Fig. 2.11 numerical results for the PDF of the phase of the oscillating wall upon *all* collisions are plotted. Given that the phase of the moving wall is randomized after each collision by the addition of η, which is uniformly distributed in the interval $[0, 2\pi)$, and further given that the deterministic component t is also distributed uniformly in the same interval [41], ξ is expected to follow the same distribution for any number of collisions n. Therefore, $p(\xi, n)$ is independent of the number of collisions n. The uniform

distribution $p(\xi) = \frac{1}{2\pi}$ is also plotted in Fig. 2.11 for the sake of comparison, revealing that the prediction of a uniform distribution of phases upon all collisions is accurate.

Given that $p(\xi)$ and $p_2(\xi)$ are independent of the number of collisions, and further that for $n \gg 1$, $w_2(n) \propto 1/\sqrt{n} + \mathcal{O}(1/n)$, it follows from Eq. (2.44) that within the leading order of $1/n$ the PDF of the phase upon collision for the type of collision events without artificial reversal is given by:

$$p_1(\xi, n) = \frac{1}{2\pi}\left[1 + w_2(n)\right] - w_2(n)p_2(\xi) + \mathcal{O}\left(\frac{1}{n}\right) \tag{2.46}$$

Integrating Eqs. (2.36) over the phase upon collision utilizing Eqs. (2.45) and (2.46) we obtain the average of the change of particle absolute velocities in one mapping period over the phase for each set of collisions events, i.e. C_1 and C_2.

$$\langle\langle \delta|V_n|\rangle\rangle_1 = -2\int_0^{2\pi} p_1(\xi, n)u_n d\xi = w_2(n)\frac{\pi}{2}\epsilon \tag{2.47a}$$

$$\begin{aligned}\langle\langle \delta|V_n|\rangle\rangle_2 &= -2\int_0^{2\pi} p_2(\xi)\left(|V_{n-1}|_2 - u_n\right) d\xi \\ &= -2\langle\langle |V_{n-1}|\rangle\rangle_2 + \frac{\pi}{2}\epsilon\end{aligned} \tag{2.47b}$$

To obtain the ensemble average $\langle|V_n|\rangle_i$, $(i = 1, 2)$ within each set of collision events C_i, $(i = 1, 2)$ we need further to integrate over the corresponding distribution of particle velocities, $\rho_i(|V|, n)$, $(i = 1, 2)$. Therefore,

$$\langle \delta|V_n|\rangle_1 = \int_0^{\infty} w_2(n)\frac{\pi\epsilon}{2}\rho_1(|V|, n)d|V| = w_2(n)\frac{\pi\epsilon}{2} \tag{2.48a}$$

$$\begin{aligned}\langle \delta|V_n|\rangle_2 &= \int_0^{2\epsilon}\left(-2\langle\langle |V_{n-1}|\rangle\rangle_2 + \frac{\pi\epsilon}{2}\right)\rho_2(|V|, n)d|V| \\ &= -2\langle|V_{n-1}|\rangle_2 + \frac{\pi\epsilon}{2},\end{aligned} \tag{2.48b}$$

where $\langle|V_{n-1}|\rangle_2$ is the ensemble mean absolute velocity of the particles which experience a collision leading to an artificial reversal of their velocity. Numerical results for the cumulative mean of $\langle|V_{n-1}|\rangle_2$ are presented in Fig. 2.12. As shown, after a short transient period the cumulative mean $\langle|\tilde{V}_{n-1}|\rangle_2$ becomes independent of the number of collisions n and reaches a constant value. Consequently, $\langle|V_{n-1}|\rangle_2$ shares the same behavior. The best linear fit yields:

$$\langle|V_{n-1}|\rangle_2 \approx \frac{\pi}{4}\epsilon. \tag{2.49}$$

The substitution of Eq. (2.49) into Eqs. (2.48) and then of the result in Eq. (2.34)

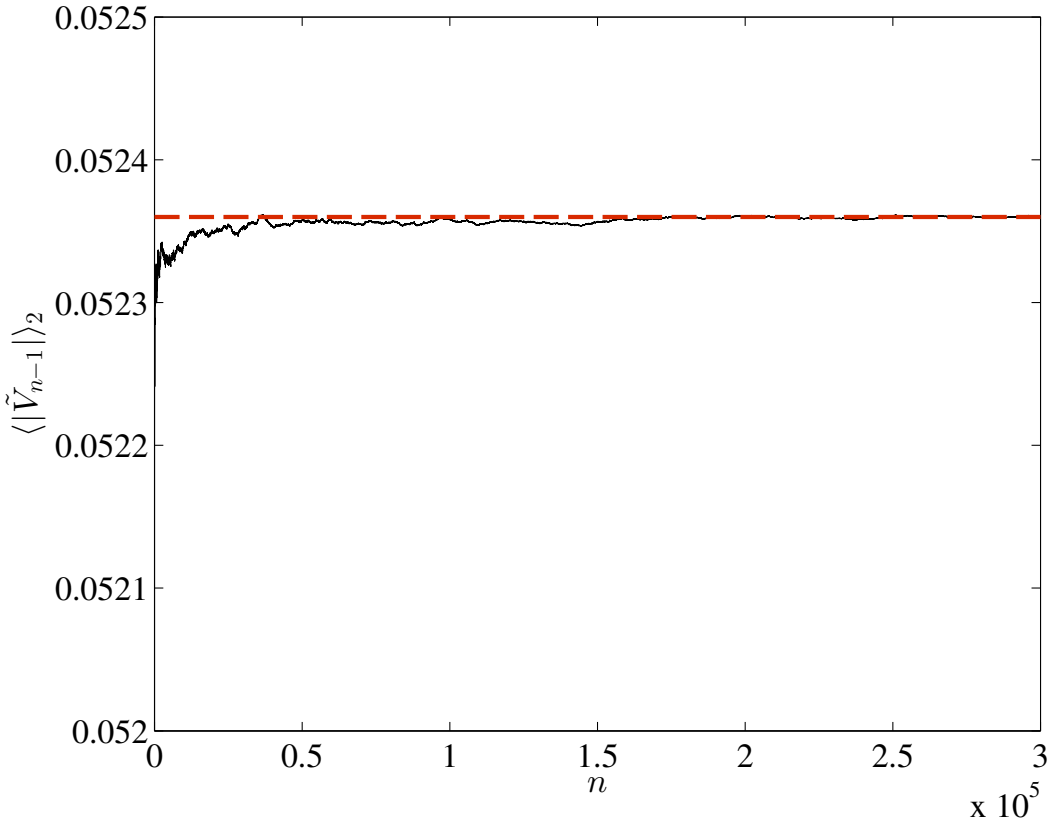

Figure 2.12.: Numerical results (solid line) for the cumulative ensemble mean absolute velocity of the particles undergoing collisions which lead to an artificial velocity reversal. Numerical results were obtained on the basis of an ensemble of 1.6×10^5 trajectories propagated for 3×10^5 collisions. The best linear fit is also shown (dashed line). It is noted that $\langle|\tilde{V}_{n-1}|\rangle_2$ is measured in units of ωw.

(neglecting terms of the order $1/n$) yields

$$\langle \delta |V_n| \rangle = w_2(n) \frac{\pi}{2} \epsilon. \tag{2.50}$$

Therefore, for $n \gg 1$ the ensemble mean of particle velocities is

$$\langle |V_n| \rangle = \sum_{i=1}^{n} \delta |V_i| + \langle |V_0| \rangle = \frac{H_n^{\left(\frac{1}{2}\right)}}{\sqrt{\pi}} + \langle |V_0| \rangle, \tag{2.51}$$

where $H_n^{\left(\frac{1}{2}\right)}$ is the nth harmonic number of order $1/2$.

Obviously, Eq. (2.51) are valid for the assumption $w_2(n) \propto 1/\sqrt{n}$.

The semi-analytical estimation given by Eq. (2.51) is presented in Fig. 2.13, along with numerical results obtained by the iteration of the SWA map defined by Eqs. (6.1). Particle initial velocities were randomly chosen, following a half-Gaussian distribution centered at $|V| = 0$. For this specific choice of the initial distribution of particles velocities, the statistical weight of the collisions leading to an artificial reversal of the particle velocity $w_2(n) \propto \mathrm{Erf}\left(\frac{1}{\sqrt{n}}\right)$, as shown in Fig. 2.8. Clearly, the numerical results and the semi-analytical result of Eq. (2.51) are in agreement.

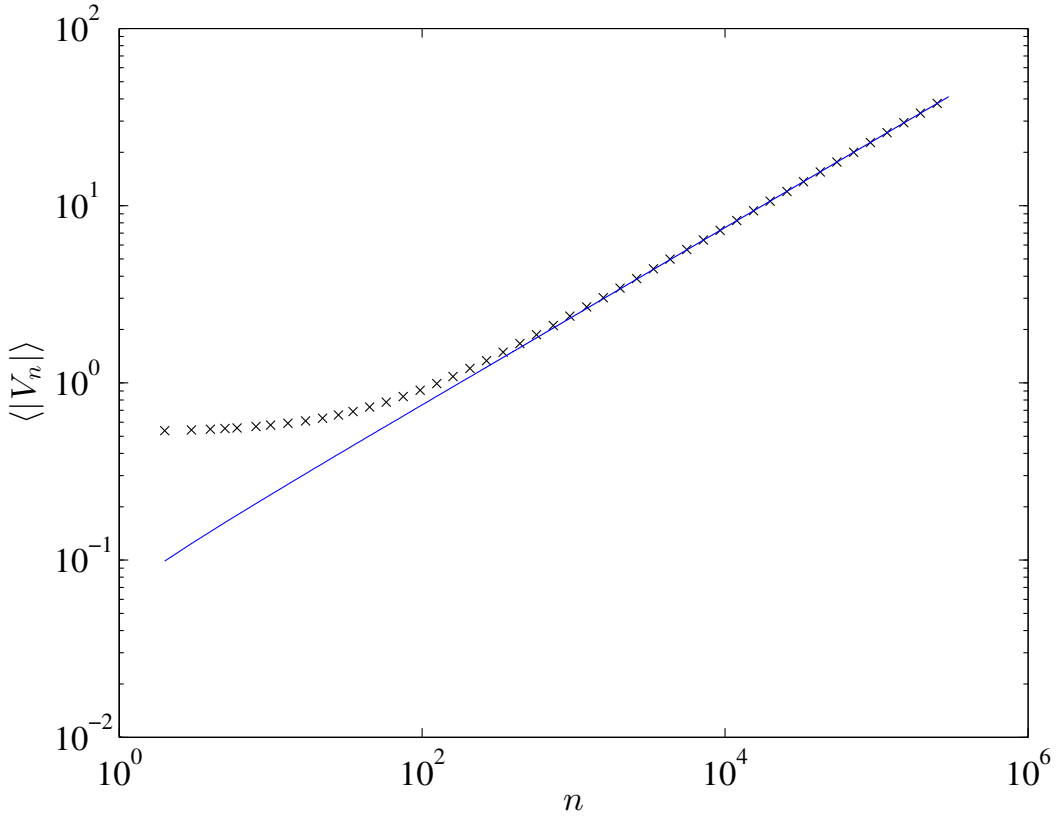

Figure 2.13.: Numerical results ($\times$) for the ensemble mean absolute velocity as a function of the number of collisions n. Numerical results were obtained on the basis of an ensemble of 1.6×10^5 trajectories propagated for 3×10^5 collisions. The semi-analytical estimation of Eq. (2.51) is also plotted (solid line). It is noted that $\langle |V_n| \rangle$ is measured in units of ωw.

3. Fermi acceleration as a stochastic process

Fermi acceleration developing in a time-dependent billiard can be described in terms of a stochastic process taking place in the momentum space. For the sake of simplicity, Fermi acceleration in the context of dynamical systems [41, 64, 65, 71, 72] and Astrophysics [77–81] is described in the literature as a continuous stochastic process. This allows the description of the evolution of the PDF of particle velocities via a differential equation, i.e. the Fokker-Planck equation (FPE). Despite the extensive use of the FPE, in this chapter we show the limitations and conceptual problems stemming from treating Fermi acceleration as a continuous random process. Finally, we show how a consistent and complete statistical description of the stochastic acceleration can be achieved on the basis of the Chapman-Kolmogorov equation.

3.1. Fundamentals

Let $W(v, z)$ denote the probability of a particle being at the velocity z to perform a jump to velocity v in the course of a single collision and $\rho(v, n|v', n')$ the probability of a particle to possess velocity v after n collisions given that at the n'th collision it had velocity v'. This jump process can be described by the following equation:

$$\rho\left(v, n|v', n'\right) = \int dz \rho\left(z, n-1|v', n'\right) W\left(v, z\right) \tag{3.1}$$

Eq. (3.1) is exact, on the condition that the process is Markovian. From a physical point of view, this means that the probability of a particle to experience a velocity jump equal to Δv upon the nth collision depends only on the velocity it had at the previous step, i.e at the nth-1 collision.

3.1.1. The Fokker-Planck approximation

The standard approach in the literature for the determination of the asymptotic behaviour of the PDF of particle velocities, is the approximation of the jump process with a diffusion process, described by the FPE [41, 64, 65]. This approximation has also been used for the analytical treatment of Fermi acceleration developing in higher-dimensional billiards, like the simplified periodic Lorentz gas [71, 72], i.e. the oscillating hard circular scatterers oscillate only in the velocity space. An equation of the form of the FPE can be derived from Eq. (3.1) as follows [82]:

If we introduce $\Delta v \equiv v - z$, then the integrand in Eq. (3.1) can be rewritten as,

$$\begin{aligned} \rho\left(v, n|v', n'\right) = \int d(\Delta v) \rho\left(v - \Delta v, n-1|v', n'\right) \\ \times W\left(v - \Delta v + \Delta v, v - \Delta v\right). \end{aligned} \tag{3.2}$$

Expanding the distribution function $\rho\left(v, \Delta v, v', n'\right)$ and the transition probability function (TPF) $W(v; \Delta v)$ in a Taylor series yields,

$$\begin{aligned} \rho\left(v, n|v', n'\right) = \int d(\Delta v) \sum_{m=0}^{\infty} \frac{(-1)^m}{m!} (\Delta v)^m \\ \times \frac{\partial^m}{\partial v^m} \rho\left(v, n-1|v', n'\right) W\left(v + \Delta v, v\right) \end{aligned} \tag{3.3}$$

Integrating now Eq. (3.3) over Δv we obtain,

$$\rho\left(v, n|v', n'\right) = \sum_{m=0}^{\infty} \frac{(-1)^m}{m!} \frac{\partial^m}{\partial v^m} M_m(v) \rho\left(v, n-1|v', n'\right), \tag{3.4}$$

where $M_m(v)$ stands for the mth moment of the TPF, i.e.

$$M_m(v) = \int (\Delta v)^m W(v + \Delta v, z) d(\Delta v).$$

Therefore,

$$\rho\left(v, n|v', n'\right) - \rho\left(v, n-1|v', n'\right) = \sum_{m=1}^{\infty} \frac{(-1)^m}{m!} \frac{\partial^m}{\partial v^m} M_m(v) \rho\left(v, n|v', n'\right) \tag{3.5}$$

By truncating the above series to the second order, and further by approximating the

discrete derivative

$$\Delta_k \rho(v, n|v', n') = \left[\rho(v, n+k|v', n') - \rho(v, n|v', n')\right]/k,$$

$(k = 1)$ with the continuous derivative $\partial\rho(v, n|v', n')/\partial n$, for $n \gg 1$ one obtains an equation resembling the FPE.

$$\begin{aligned}\frac{\partial}{\partial n}\rho\left(v, n|v', n'\right) = &-\frac{\partial}{\partial v}\left[B\rho\left(v, n|v', n'\right)\right] \\ &+\frac{1}{2}\frac{\partial^2}{\partial v^2}\left[D\rho\left(v, n|v', n'\right)\right],\end{aligned} \tag{3.6}$$

where the coefficient B and D is the ensemble average of the change of particle velocities and its square, respectively, in one mapping period.

The approximations applied above for the construction of the FPE are valid on the condition that only very small jumps are probable and further that the solution $\rho\left(v, n|v', n'\right)$ varies slowly with v so that one can perform the expansion in a Taylor series. More formally [83], we demand that there exists a $\delta > 0$,

$$W(z + \Delta z, z) \approx 0, \qquad \text{for } |\Delta z| > \delta \tag{3.7a}$$

$$\rho(v + \Delta v, n|v', n') \approx \rho(v, n|v', n'), \qquad \text{for } |\Delta v| < \delta. \tag{3.7b}$$

In the literature [41] the derivation of an FPE from Eq. (3.1) for the statistical description of Fermi acceleration is carried out on an *ad hoc* basis. As a consequence, as shown in the following, it has produced contradictory results. Moreover, by construction, the description of Fermi acceleration with a continuous stochastic process, can at best describe the statistics only for $n \gg 1$. Hence, a full description of FA in a time-dependent billiard can only be given in the context of a jump process and consequently by Eq. (3.1).

In the context of this approximation, the transport coefficients B, D are,

$$B(V) = \left(\frac{1}{\Delta n}\right)\int \Delta|V| P \; d(\Delta|V|) \tag{3.8a}$$

$$D(V) = \left(\frac{1}{\Delta n}\right)\int (\Delta|V|)^2 P \; d(\Delta|V|) \tag{3.8b}$$

In Eqs. (3.8) P is the probability of a particle possessing the velocity $|V|$ if it had the velocity $|V| - \Delta|V|$, Δn collisions earlier. Assuming that $\Delta n = 1$, Eqs. (3.8) become $B(V) = \langle\delta|V|\rangle$ and $D(V) = \langle(\delta|V|)^2\rangle$, where $\langle\delta|V|\rangle$ is the mean increment of the magnitude of the particle velocity during one mapping period, i.e. in the course of one

collision.

3.1.2. A complete description: The Chapman-Kolmogorov equation

The study of the transient statistics can only be accomplished by means of the Chapman-Kolmogorov equation, i.e. Eq. (3.1). Assuming that initially particle velocities are distributed according to $\rho(v,0)=\delta(v-z)$, Eq. (3.1) can be rewritten in respect with the one-step TPF. $W(v,v')$ as,

$$\rho(v_n,n|z,0)=\int\cdots\int W(v_n,v_{n-1})\cdots W(v_1,z)\mathbf{dv}, \tag{3.9}$$

where $\mathbf{dv}=\prod_{i=1}^{n-1}dv_i$. The derivation of the one-step TPF can be achieved by determining the PDF $p(\mathbf{q})$ of the variables $\mathbf{q}\equiv\{x_i\}$ appearing in the dynamical equation defining the velocity of a particle after a collision with the moving boundary of the time-dependent billiard, $v_n=f(v_{n-1},\mathbf{q})$. Then, the TPF is

$$W(v_n,v_{n-1})=\int p(\mathbf{q})\delta\left[v_n-f(\mathbf{q},v_{n-1})\right]\mathbf{dq}. \tag{3.10}$$

If the resulting TPF is a function of the difference of velocities at successive steps $W(v_n,v_{n-1})=W(v_n-v_{n-1})$, Eq. (3.9) can be easily solved in the Fourier space. Specifically, if this condition is met, then by taking the Fourier transform of Eq. (3.9) we find,

$$\mathcal{F}\left[\tilde{\rho}(v,n|z,0)\right]=(2\pi)^{\frac{n-1}{2}}e^{-ikz}\left\{\mathcal{F}\left[W(v)\right]\right\}^n, \tag{3.11}$$

where $\mathcal{F}=1/(\sqrt{2\pi})\int_{-\infty}^{\infty}\exp[-ikv]dv$.

Moreover, in this case an approximate solution can be obtained directly in the velocity space, using the saddlepoint approximation technique [84]. Specifically, from Eq. (3.9), one can derive the moment generating function

$$\begin{aligned}\phi(t,n)&=\int_{-\infty}^{\infty}e^{tx}\rho(v,n|z,0)dv\\&=\left(\int_{-\infty}^{\infty}e^{tv}W(v)dv\right)^n e^{tz}\end{aligned} \tag{3.12}$$

of the velocity PDF. To find the saddlepoint $\hat{t}(v,n)$, we solve the equation $\kappa'(t,n)=v$,

where $\kappa(t.n) = \log(\phi(t, n))$. Then, the PDF is approximately,

$$\rho(v, n|z, 0) \approx \sqrt{\frac{1}{2\pi\kappa''(\hat{t}(v, n))}} \times \exp\left[\kappa(\hat{t}(v, n)) - \hat{t}(v, n)v\right]. \tag{3.13}$$

3.2. Fermi acceleration in the stochastic simplified FUM

In the following, we present a complete statistical description of the Fermi acceleration mechanism exhibited in the FUM. We study the simplified FUM, as well as, the full dynamics. We choose the FUM as it has been established over the time as the prototype dynamical system exhibiting Fermi acceleration. We show that in the full model of the FUM a quilitative change in the functional form of the PDF is brought upon due to the fluctuations of the time of free flight between collisions due to the wall displacement [see §2.2.2].

3.2.1. Time asymptotics of the PDF of particle velocities

Application of the central limit theorem

In this section we will discuss the asymptotic behaviour of the PDF of particle velocities in the SFUM. Evidently, after n collisions the velocity of a particle evolving in the SFUM is the sum of the velocity jumps it has experienced up to this point, i.e. $v_n = \sum_{m=1}^{n} \Delta v_n + v_0$. Furthermore, due to Fermi-acceleration developing in the SFUM, after $n \gg 1$ collisions, the vast majority of the particles has acquired velocities much greater than the maximum wall velocity, irrespective of the initial distribution. Therefore, most of the collisions, after a sufficiently large "time", take place in the high velocity regime. In this limit, the absolute value function can be neglected and we immediately obtain [64] $\langle \Delta v \rangle = 0$ and $\langle (\Delta v)^2 \rangle = 2\epsilon^2$. Therefore, the velocity jumps are completely uncorrelated, i.e. do not depend on the velocity the particle had at the previous step. Thus, for $n \gg 1$ and $v \gg \epsilon$ the central limit theorem (CLT) dictates that the PDF of particle velocities tends to a Gaussian distribution, with a mean value equal to $\sum_{i=1}^{n} \langle \Delta v_i \rangle$ and variance $\sigma^2 = \sum_{i=1}^{n} \left[\left\langle (\Delta v_i)^2 \right\rangle - \langle \Delta v_i \rangle^2 \right]$.

Hence, the PDF of particle velocities for $n \gg 1$ is

$$\rho(v, n) = \frac{1}{\epsilon \sqrt{\pi n}} \exp\left[-\frac{v^2}{4\epsilon^2 n} \right]. \tag{3.14}$$

In Fig. 3.1, Eq. (3.14) is plotted along with the histogram of particle velocities obtained from the simulation of 1.2×10^6 trajectories for $n = 10^5$ collisions. The ensemble was initially distributed according to the delta function $\delta(v - \epsilon)$. The analytical result obtained from the application of the CLT is in perfect agreement with the numerically

computed PDF.

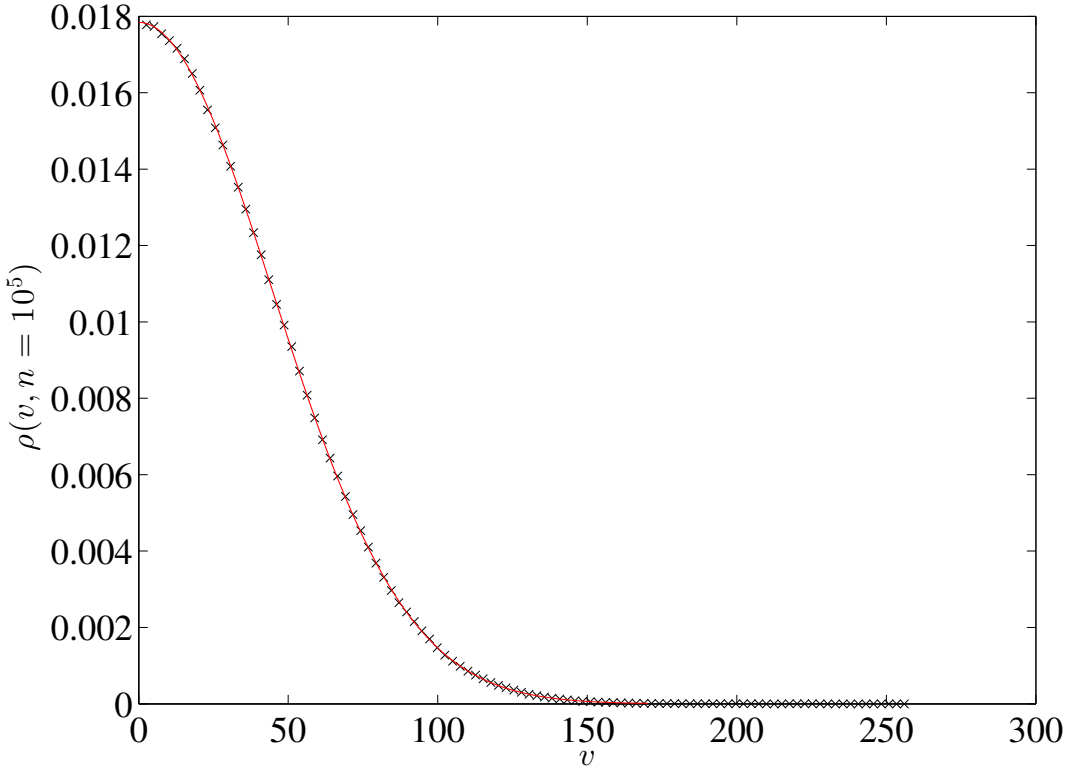

Figure 3.1.: Histogram —diagonal crosses— of particle velocities after $n = 10^5$ collisions, obtained by the iteration of Eqs. (2.3), on the basis of an ensemble of 1.2×10^6 particles initially distributed as $\rho(v, 0) = \delta(v - \epsilon)$. The analytical result derived through the application of the CLT [Eq. (3.14)] is also plotted — solid (red) line.

FPE equation in the SFUM

As mentioned in the §3.2.1, assuming that for $n \gg 1$ the probability measure of the events occurring in the low-velocity regime is negligible, $B \equiv \langle \Delta v \rangle \backsimeq 0$, $D \equiv \langle (\Delta v)^2 \rangle \backsimeq 2\epsilon^2$. In this limit Eq. (3.6) obtains the form of a standard diffusion equation. which for a delta initial distribution of velocities $v = z$ together with reflecting conditions at $v = 0$ has as a solution the sum of two spreading Gaussians

$$\rho\,(v, n|z, 0) = \frac{1}{2\sqrt{\pi n\epsilon^2}}\left\{ \exp\left[-\frac{(v-z)^2}{4n\epsilon^2}\right] + \exp\left[-\frac{(v+z)^2}{4n\epsilon^2}\right]\right\}, \tag{3.15}$$

which for $n \geq z^2/(4\epsilon^2 \ln 2)$ transforms to Eq. (3.14).

Remarks

Although the solution derived by means of the FPE is in agreement with the one obtained from the application of the CLT, the methodology used for the derivation of Eq. (3.6) stands on very shaky ground, since the termination of the series at the second term in Eq. (3.5) is completely arbitrary [83]. In general, a jump process can be approximated by a diffusion process, on the condition that a scaling assumption for the transition probability holds. Namely, in the limit of infinitely small time intervals, the jumps should become smaller and more frequent, such that the random process can be viewed as a continuous one [85]. An intuitive way to examine this is to consider the average square of the jump size $\langle(\Delta v)^2\rangle$ a particle makes having a velocity v prior to the collision.

Given that the SWA treats the moving wall as fixed in the configuration space, all phases upon collision are possible, independently of the velocity v of particles before a collision. As a result, the average jump size is not reduced as $v \to 0$. In contrast, within the exact model, as the velocity of the particle prior to a collision decreases, it becomes increasingly probable to collide with the wall at the turning points, where its velocity is close to zero. Moreover, if the velocity of the particle before a collision is small, then successive collisions are likely to occur, the exact dynamics result to higher exit velocities. Consequently, successive collisions render small particle velocities improbable, as opposed to the SFUM, where as shown in §3.2.1, $v = 0$ is the most probable velocity.

Summarizing, the application of the CLT for the determination of the long-time statistics is much more straightforward and renders the solution of a differential equation redundant. More importantly, the assumption of continuity of the stochastic process describing Fermi acceleration, which is essential for the construction of an FPE, is not required.

3.2.2. Short-time statistics in the SFUM

From Eqs. (2.3) the particle velocity after the nth collision given that it had velocity z is,

$$v = -z - 2u - 2\,(z + 2u)\,\Theta\,(2u + z)\,, \tag{3.16}$$

where $\Theta(x)$ is the Heaviside unit-step function.

According to Eq. (6.1) the wall velocity u_n is determined by the phase $\xi_n \equiv t_n + \eta_n$ of oscillation at the instant of the nth collision. Due to the fact that in the stochastic SFUM the phase is randomly shifted through the addition of a random number η_n — distributed uniformly in the interval $(0, 2\pi)$— after each collision, the oscillation phase ξ_n is completely uncorrelated between collisions, following a uniform distribution. Further-

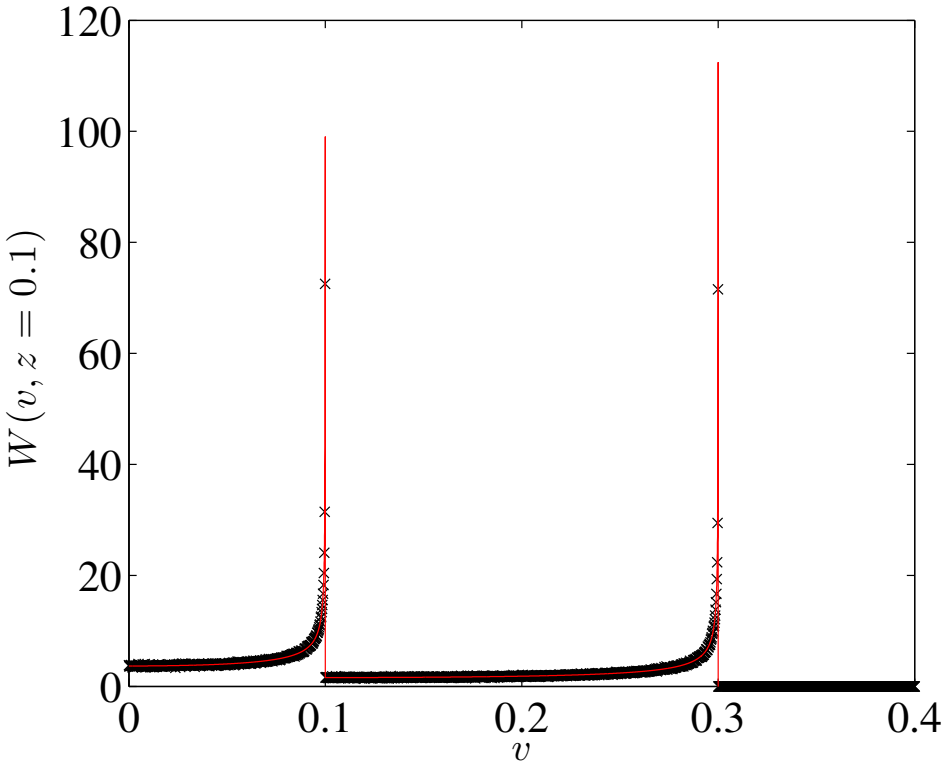

Figure 3.2.: Histogram —diagonal crosses— of particle velocities after a single collision with the "moving" wall, obtained using Eqs. (2.3) and an ensemble of 1.2×10^6 particles with initial velocity $z = 0.1$. The analytical result [Eq. (3.19)] for the one-step transition probability is also plotted for the sake of comparison —solid line

more, given that in the context of the SFUM the wall remains fixed in the configuration space, the wall velocity upon collision does not depend on the velocity of the particle, therefore, u_n and v_{n-1} are also uncorrelated. From the fundamental transformation law of probabilities the PDF of the wall velocity upon collision is,

$$p(u) = \frac{1}{\pi\sqrt{\epsilon^2 - u^2}}. \tag{3.17}$$

For the single-step TPF $W(v, z)$ we can write,

$$W(v, z) = \int_{-\epsilon}^{\epsilon} p(u)\delta\left[v - v(u, z)\right] du. \tag{3.18}$$

Substituting Eqs. (3.17) and (3.16) into Eq. (3.18) we obtain after integrating over u,

$$W(v,z) = \frac{1}{\pi}\Bigg[\frac{\Theta(2\epsilon - v - z, 2\epsilon - z)}{\sqrt{4\epsilon^2 - (v+z)^2}} + \frac{\Theta(2\epsilon - v + z, 2\epsilon + v - z)}{\sqrt{4\epsilon^2 - (v-z)^2}}\Bigg] \tag{3.19}$$

In Fig. 3.2 the analytical result of Eq. (3.19) is compared with the histogram of particle velocities after a single collision, obtained numerically using Eqs. (2.3) and an ensemble of 1.2×10^6 particles, with initial velocity $z = 0.1$. Clearly, the numerical and analytical results are in agreement.

The analytical result of Eq. (3.19) reveals that the TPF depends only on the most immediate history of a particle, that is on the velocity it had at the previous step. Consequently, the stochastic process is indeed Markovian. Even more, if the particle before a collision has velocity $z > 2\epsilon$, then the velocity jump $\Delta v = v - z$ it undergoes is completely independent on its history. Therefore, changes in velocity in the high-velocity regime are completely uncorrelated.

In more detail, Eq. (3.19), consists of two parts, one of which does indeed depend only on the jump size. However, the other branch of the TPF, taking effect for $v < 2\epsilon$ —relating to the set of rare events [see §2.3— depends also on the velocity at the last step. Nevertheless, the action of both branches of W allows of a simple geometrical interpretation: At each step, the second branch of the TPF stretches the PDF $\rho(v, n|z, 0)$, resulting to a probability flux towards negative values of velocity. This unphysical result caused by the stretching is negated by the first branch, which folds the part of the ρ density over the vertical line at $v = 0$. Therefore, the solution of Eq. (3.9) can be obtained by extending the domain of $\rho(v, n|z, 0)$ to the whole real line and applying the method of images. Thus, for any number of collisions, we have

$$\rho(v, n|z, 0) = \tilde{\rho}(v, n|z, 0) + \tilde{\rho}(v, n| - z, 0), \tag{3.20}$$

where $\tilde{\rho}$ is the solution of the unrestricted problem. Substituting Eq. (3.19) into Eq. (3.11) we obtain,

$$\tilde{\rho}(k, n|z, 0) = \frac{1}{\sqrt{2\pi}} \exp(-ikz) J_0(2\epsilon|k|)^n \tag{3.21}$$

Eq. (3.21) cannot be inverted analytically. To obtain an analytical result into the velocity space, we use the saddlepoint approximation [Eq. (3.13)]. The moment generating

function of $\rho(v,n|z,0)$ is,

$$\phi(t,n) = (I_0(2t\epsilon))^n\, e^{tz}, \tag{3.22}$$

where I_0 is the modified Bessel function of the first kind. Consequently, the characteristic function is $\kappa(t,n) = \log\phi(t,n) = n\log(I_0(2t\epsilon)) + tz$. The saddlepoint is the point $\hat{t}(v,n)$ that satisfies

$$\kappa'(t,n) = v \Rightarrow \frac{2n\epsilon I_1(2t\epsilon)}{I_0(2t\epsilon)} + z = v. \tag{3.23}$$

Eq. (3.23) is implicit and cannot be solved analytically. To derive an explicit equation we expand $\kappa'(t,n)$ in powers of ϵ to second order. Doing so we get,

$$\hat{t}(v,n) = \frac{v-z}{2n\epsilon^2}. \tag{3.24}$$

Substituting Eq. (3.24) into Eq. (3.13) we have,

$$\begin{aligned}\rho(v,n|z,0) \approx & \frac{1}{2\epsilon} e^{-\frac{(v-z)^2}{2n\epsilon^2}} I_0\left(\frac{v-z}{n\epsilon}\right)^n \\ & \times \left[\frac{I_0\left(\frac{v-z}{n\epsilon}\right)^2}{\pi n I_0\left(\frac{v-z}{n\epsilon}\right)^2 + \pi n I_2\left(\frac{v-z}{n\epsilon}\right) I_0\left(\frac{v-z}{n\epsilon}\right) - 2\pi n I_1\left(\frac{v-z}{n\epsilon}\right)^2}\right]^{1/2}.\end{aligned} \tag{3.25}$$

In Fig. 3.3 we present the exact numerical solution of Eq. (3.9) [red solid line] as well as the approximate one given by Eq. (3.25) [blue solid line] for $n = \{3, 5, 10, 31\}$, using only the second branch of the one-step TPF [Eq. (3.19)], followed by the application of the method of images [Eq. (3.20)]. The numerical solution is in total agreement with the histogram of particle velocities obtained by the iteration of the dynamical equations (2.3) [upright crosses], for all times. Even more, we see that the saddlepoint approximative solution describes very accurately the evolution of the PDF for $n \geq 5$. As can be observed, the PDF of particle velocities quickly approaches to a Gaussian distribution, in accordance with the prediction of the CLT. This is attributed to the fact that the TPF can be reduced to a difference kernel. Consequently, the additional assumption we made for the application of the CLT in § 3.2.1, namely that the statistical weight of the rare events [§2.3] is negligible, is redundant. This can be circumvented, as aforementioned, by extending the domain of particle velocities. Thus, if one applies the CLT on the whole real line, then all the conditions for its applications are met exactly. As a final remark, we would like to stress that the success of the Fokker-Planck type of equation reported in the literature for even short times is attributed to the validity of the CLT, guaranteeing that the PDF will converge to a normal distribution, allowing for the use of a diffusion equation. If however, the reduction of the TPF to a difference

kernel is not feasible, then the transient can be arbitrarily long, a point demonstrated via an example in the following section.

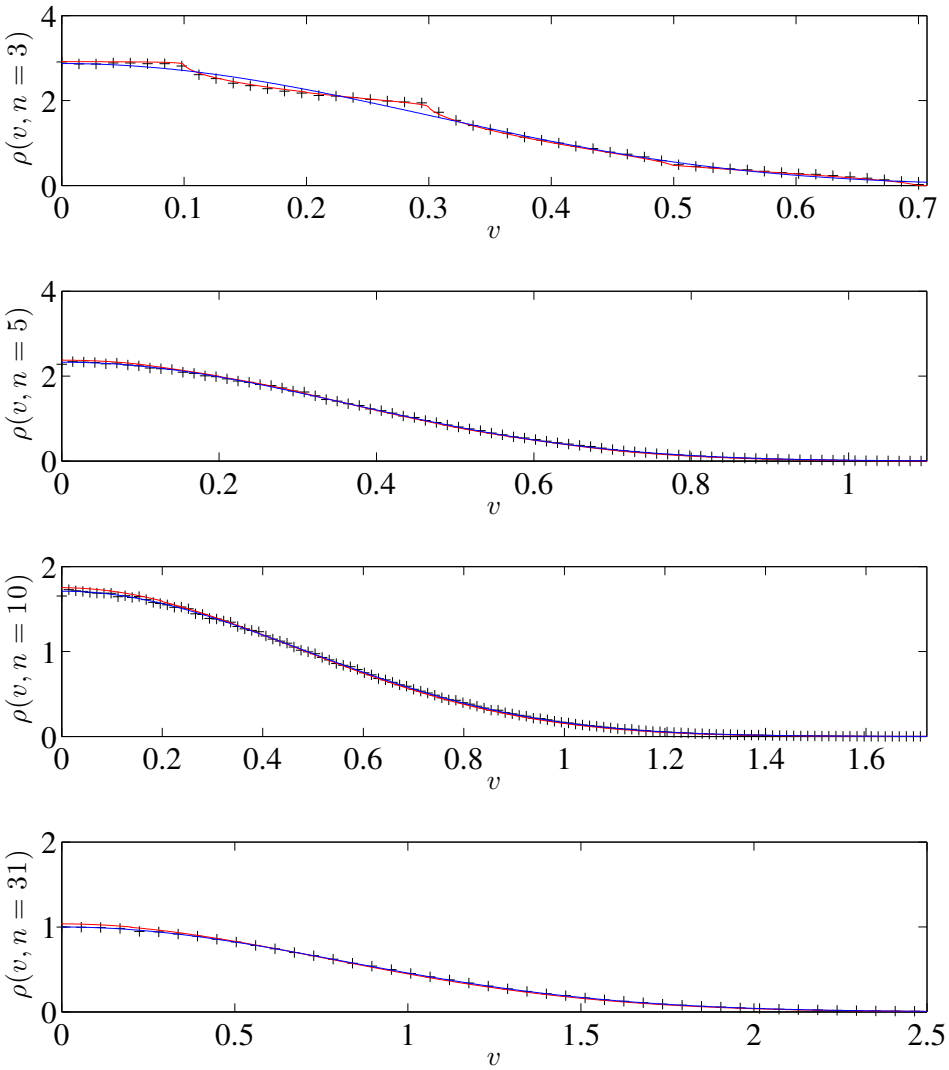

Figure 3.3.: Histogram —upright crosses— of particle velocities after $n = \{3, 5, 10, 31\}$ collisions, obtained by the iteration of Eqs. (2.3), on the basis of an ensemble of 1.2×10^6 particles initially distributed as $\rho(v, 0) = \delta(v - \epsilon)$. The exact numerical solution of Eq. (3.9) [red solid line] as well as the approximate one given by Eq. (3.25) [blue solid line] for $n = \{3, 5, 10, 31\}$, using only the second branch of the one-step TPF [Eq. (3.19)], followed by the application of the method of images [Eq. (3.20)] are also plotted for the sake of comparison. line.

3.2.3. Long Transients

In the last section we showed that the specific choice made for treating negative velocities after a collision, i.e. reflection with respect to the $v = 0$, reduces the TPF to an even function of the jump size. As a consequence, the PDF of particle velocities approaches rapidly to a sum of two spreading Gaussians. Clearly, after a number of collisions the system will "forget" its initial distribution, and the sum will converge to a single half-Gaussian centered at $v = 0^+$. Therefore, the most probable velocity for a particle evolving in the phase-randomized SFUM will eventually be $v_p = 0^+$, in clear contrast with the results given by the numerical simulation and analytical results derived using the exact dynamical mapping as we will see in §3.3.1, according to which as $v \to 0$, $\rho(v, n) \to 0$. From a physical point of view this happens because if the motion of the wall in the configuration space is taken into account, as $v \to 0$ collisions resulting in an energy loss can occur only in a small neighborhood around the wall's extreme positions, where its velocity is zero, resulting to a minimal energy loss. Furthermore, if the particle velocity is comparable to the wall velocity, consecutive collisions can take place, resulting in a higher exit velocity from the interaction region within the exact model.

On account of these properties of the collision process in the exact model, the reflection of negative velocities is not realistic. To gap the difference between the results of the simplified and the exact FUM, we propose instead of the inversion of negative particle velocities, the inversion of the direction of the wall's velocity, if the collision would lead to a negative particle velocity. This would lead in a greater energy gain in comparison with the reflection, as $|v + u| \leq |v| + |u|$. Therefore, Eqs (2.3) change to,

$$t_n = t_{n-1} + \frac{2}{V_{n-1}} \tag{3.26a}$$

$$V_n = V_{n-1} + 2|u_n| \tag{3.26b}$$

$$u_n = \epsilon \cos(t_n + \eta_n). \tag{3.26c}$$

Let us now derive the TPF. From Eqs. (3.17), (3.18) and (3.26b) we obtain,

$$\begin{aligned} W(v, z) = &\frac{\Theta(2\epsilon + z - v)}{\pi\sqrt{4\epsilon^2 - (v - z)^2}} \Big\{ \Theta(2\epsilon + z - v) \\ &+ \Theta(\epsilon - z/2) \left[\Theta(z - v - 2\epsilon) + \Theta(v - 2z) \right] \Big\} \end{aligned} \tag{3.27}$$

A comparison of the analytical result given by Eq. (3.27) and the histogram of velocities obtained on the basis of an ensemble of 1.2×10^6 particles after 1 iteration of Eqs. (2.1) is presented in Fig .3.4, proving the validity of the derived result.

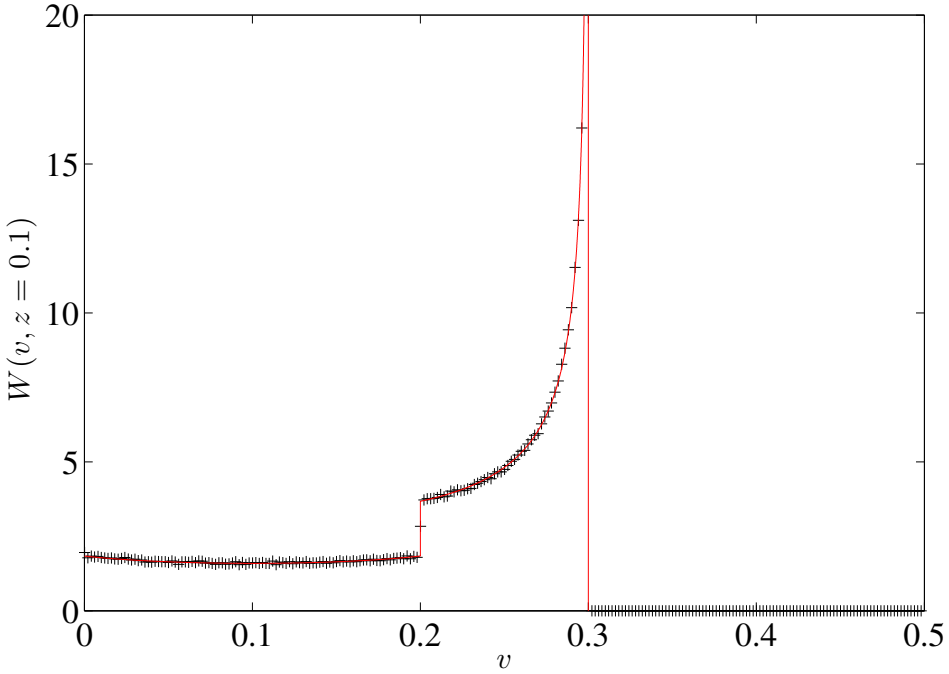

Figure 3.4.: Histogram —diagonal crosses— of particle velocities after a single collision with the "moving" wall, obtained using Eqs. (2.1) and an ensemble of 1.2×10^6 particles with initial velocity $z = 0.1$. The analytical result [Eq. (3.27)] for the one-step transition probability is also plotted for the sake of comparison —solid line

As expected, the TPF has two branches, one taking effect only in the low velocity regime, i.e. $z < 2\epsilon$ and another which is nonzero for any velocity z prior to a collision. As was also the case in the SFUM with reflection of negative velocities, the part of the TPF that is relevant to the low-velocity regime, depends on the jump size, as well as, on the velocity of a particle prior to a collision. However, due to the fact that this branch of W does not have a simple geometrical interpretation, the single-step transition function cannot be reduced to a difference propagator by an extension of the domain of W to the whole real line. Thus, the conditions for the application of the CLT are not met exactly. However, due to the acceleration of the particles, as $n \to \infty$, the probability measure of particles having velocity $z < 2\epsilon$ becomes negligible. Therefore, for $n \gg 1$ and $v \gg \epsilon$ the PDF of particle velocities tends to a Gaussian distribution [Eq. (3.14)].

The study of the transient behaviour of the PDF requires the solution of the CKE [Eq. (3.9)]. The numerical solution of Eq. (3.9) at times $n = \{3, 5, 17, 316\}$ is presented in Fig. 3.5. The histograms of particle velocities for the same times, calculated by iterating an ensemble of 1.2×10^6 particles for up to $n = 10^5$ collisions, are also plotted for the sake of comparison. It can be seen, that the solution of the CKE is in agreement with the results of the simulation for all times presented. In Fig. 3.6 the histogram of

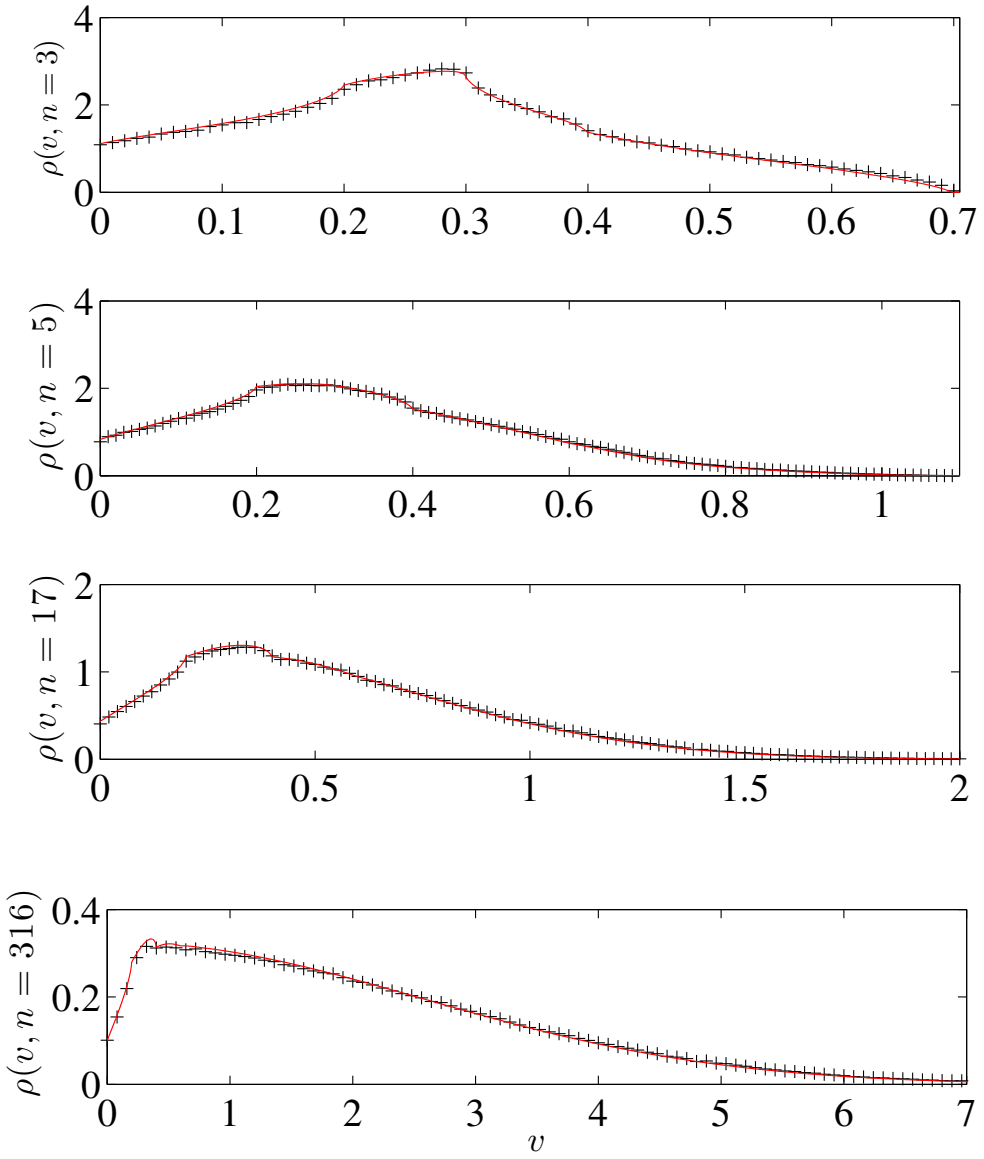

Figure 3.5.: Histogram —upright crosses— of particle velocities after $n = \{3, 5, 17, 316\}$ collisions, obtained by the iteration of Eqs. (2.1), on the basis of an ensemble of 1.2×10^6 particles initially distributed as $\rho(v, 0) = \delta(v - \epsilon)$. The solution obtained by numerically solving the forward CKE [Eq.3.9] using as the TPF of the modified version of the SFUM [Eq. 3.27] is also plotted —solid (red) line.

velocities for $n = 10^5$ collisions is plotted. The solution obtained from the application of the CLT —on the assumption that the statistical weight of collisions happening in the region $v < 2\epsilon$ is negligible, is also plotted, and is full agreement with the PDF in this velocity region. However, a blow-up of the low-velocity region shows that even after 10^5 collisions, the PDF diverges from the Gaussian profile. This is clear evidence that even after a very large number of collisions, the PDF in the whole velocity domain cannot be described by an FPE, in contrast to the standard version of the SFUM [Eqs. (2.3)] even though the argumentation used in both cases was the same, i.e. the particles are accelerated. This exemplifies the potential pitfalls of a diffusion approximation of Fermi-acceleration in time-dependent billiards.

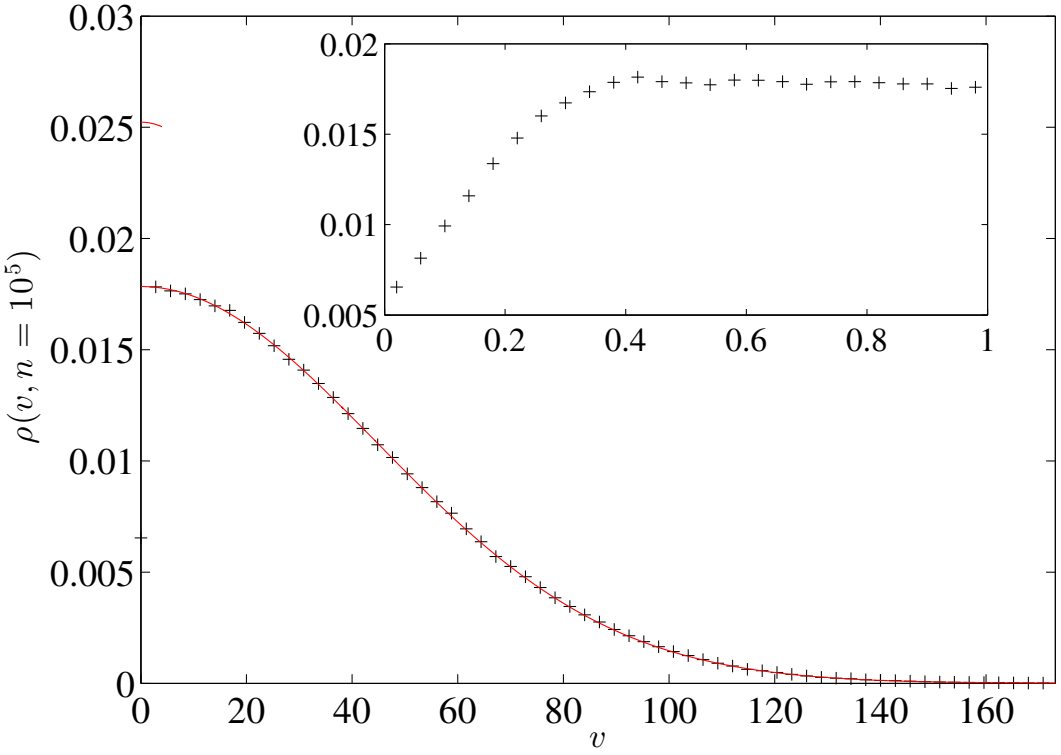

Figure 3.6.: Histogram —upright crosses— of particle velocities after $n = 10^5$ collisions, obtained by the iteration of Eqs. (2.1), on the basis of an ensemble of 1.2×10^6 particles initially distributed as $\rho(v, 0) = \delta(v-\epsilon)$. The asymptotic Gaussian distribution [Eq. (3.14)] predicted by the CLT is also plotted –solid (red) line. A blow-up of the numerically obtained histogram at the low-velocity region is illustrated in the inset.

3.3. Fermi acceleration in the exact FUM

The development of dynamical correlations between impact velocity and position in the configuration space, causes the CLT to break down and the asymptotic PDF cannot be predicted by its application. This also indicates that the PDF needs not be a normal distribution, as is the case in the simplified FUM. Thus, the application of the FPE is mandatory of the investigation of the PDF for $n \gg 1$.

3.3.1. Application of the FPE in the FUM

In order to study the asymptotic behavior of the PDF of particle speeds in the FUM we will use the HWA presented in Chapter 2, §2.2.1, since the map describing the HWA is explicit in regard with the time of the next collision and analytical approximations are possible. We point out that the exact dynamics cannot be used for the construction of the FPE. Therefore, except for the accurracy of HWA in the description of the first and second moments of the PDF, it can also be used for obtaining the PDF of particle velocities in the asymptotic time-limit, rendering thus possible the full statistical description of the Fermi acceleration taking place in the FUM.

If we neglect low energy collision events, then from Eq. (2.7c) it follows that $|V_{n+1}| = |V_n| + 2u_n$. Thus,

$$\Delta|V_n| = 2u_n \tag{3.28}$$

In order to obtain $B(V)$, the average of Eq. (3.28) over the random phase component η_n must be calculated using the set of Eqs. (2.8) [§2.2.1], leading to $B(V) = 2|I_1|$ where I_1 is given by Eq. (2.11). Therefore, $B(V) = \epsilon^2 \frac{\cos(\frac{1}{V})}{V}$. Due to the Fermi-acceleration mechanism, the majority of the particles of the ensemble for $n \gg 1$, possesses velocities with a magnitude much larger than the corresponding initial value, i.e. $|V_n| \gg |V_0| > 0$. Thus, we can expand $B(V)$ to the leading order of $\frac{1}{V}$ to obtain $B(V) = \frac{\epsilon^2}{V}$. The diffusion coefficient $D(V)$ can be derived in a similar way. By raising Eq. (3.28) to the square we obtain, $D(V) = (\Delta|V|)^2 = 4u^2$. The integration over η_n leads to $D(V) = 4I_2$, where I_2 is given by Eq. (2.11). Therefore, $D(V) = 2\epsilon^2$.

Substituting the values of the transport coefficients into Eq. (3.6) and assuming a perfectly reflecting barrier at $|V| = 0$ the following analytical expression for the PDF is obtained, which describes the magnitude of the particle velocity for $n \gg 1$:

$$\rho(|V|, n) = \frac{1}{\sigma^2}|V|e^{-V^2/(2\sigma^2)} \tag{3.29}$$

where $\sigma = \sqrt{\frac{4\epsilon^2 n + V_0^2}{2}}$. In Figs. 3.7(a) and 3.7(b) it is clearly seen that this analytical

result predicted by the HWA accurately reproduces the exact behavior of the system.

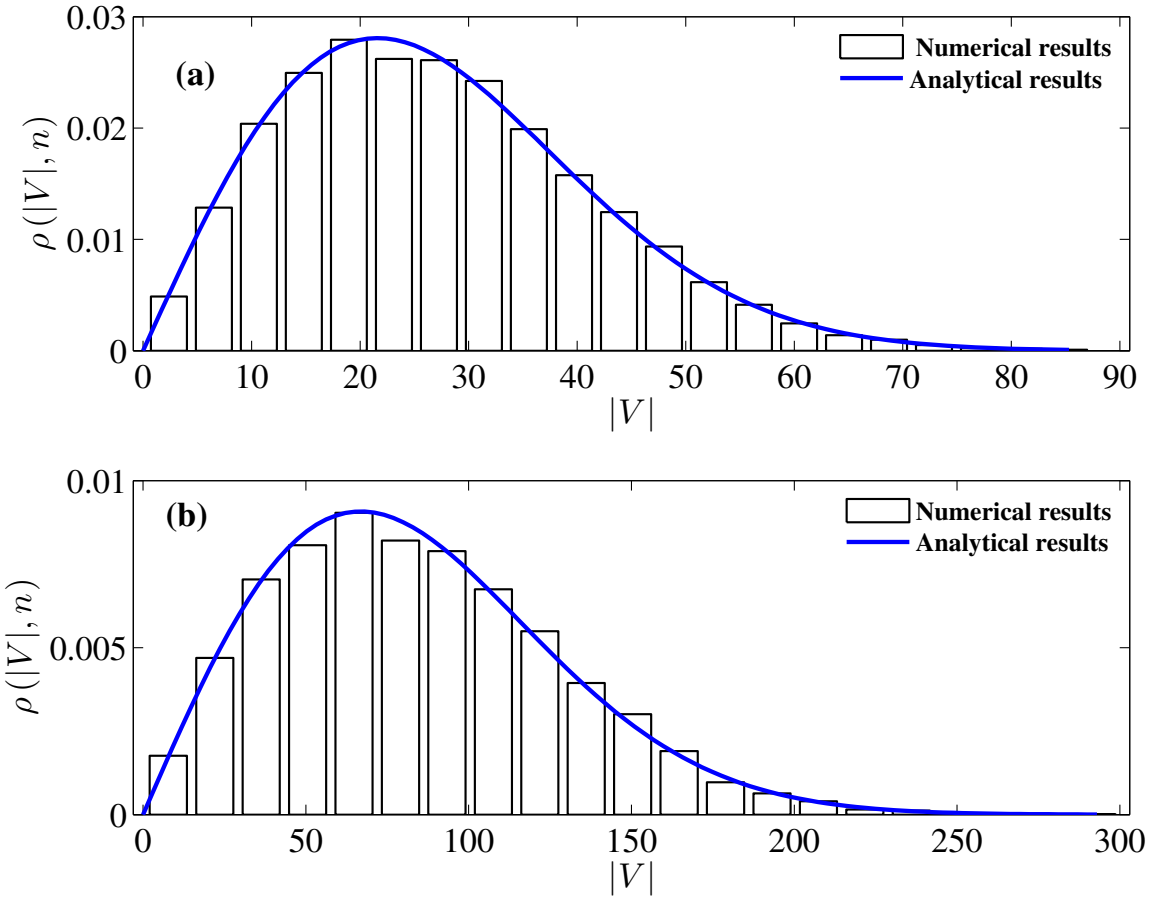

Figure 3.7.: Numerically computed PDF for the magnitude of the particle velocity using an ensemble of 10^4 trajectories and following the exact dynamics of Eq. (2.1) for: (a) $n = 5 \times 10^4$ and (b) $n = 5 \times 10^5$. In each case the analytical result given by Eq. (3.29) using the HWA is also shown (solid line).

Furthermore, Fig. 3.8 shows the evolution of the mean value of the magnitude of the particle velocity $\langle |V| \rangle$ as a function of the number of collisions n obtained numerically for the exact dynamics. An analytical expression for $\langle |V| \rangle$ can easily be derived employing Eq. (3.29):

$$\langle |V| \rangle = \frac{\sqrt{\pi(4\epsilon^2 n + V_0^2)}}{2} \tag{3.30}$$

For the sake of comparison this analytical result is also presented in Fig. 3.8. Once again, results yielded by the exact and the HWA map are in excellent agreement.

Therefore,the attractor of the PDF of velocities in the function space is a Maxwell-Boltzman like distribution, i.e. independently of the initial distribution of velocities, the PDF converges to a Maxwell-Boltzman like distribution. Therefore, in the case of the exact FUM for $v \to 0^+$, $\rho(v, n|z, 0) \to 0$, in contrast to the SFUM where $\rho(v, n|z, 0)$

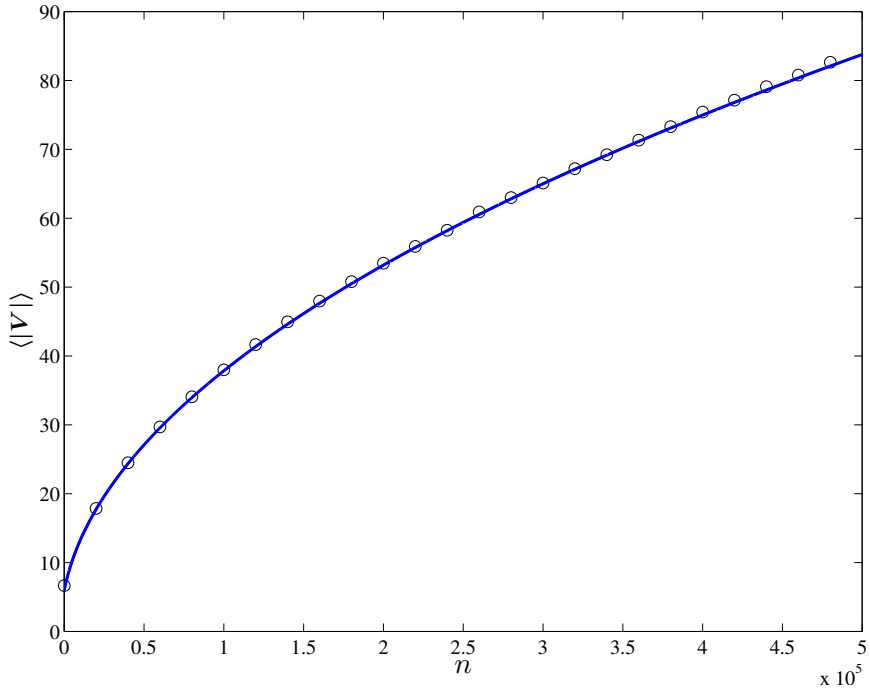

Figure 3.8.: Numerical results obtained by the iteration of the exact ($\circ$) map for the evolution of the ensemble mean magnitude of particle velocity $\langle |V| \rangle$ versus the number of collisions, n for $\epsilon = \frac{1}{15}$ and $|V_0| = \frac{100}{15}$. It is noted that $\langle |V| \rangle$ is measured in units of ωw. The analytical result according to the HWA, Eq. (3.30) (solid line) is also shown.

attains its maximum value for $v \to 0^+$. This difference between the simplified and the exact FUM can be understood as follows: If the velocity of a particle after a collision with the moving wall is small, then multiple successive collisions are likely to occur within the exact FUM, resulting into higher exit velocities, as opposed to the simplified model, within which successive collisions cannot be realized.

Another subtle difference between the simplified and the exact FUM [see § 3.2.1] is that within the exact FUM particles with low velocity are more likely to collide with the oscillating wall near its turning points, where the wall velocity is close to 0. Hence, the velocity jump performed by a particle due to a collision with the wall $\Delta v \to 0$ as $v \to 0$. As a result, Fermi acceleration, when using the exact dynamics, can be better approximated by a continuous stochastic process, or equivalently, by the FPE. Still, the transient statistics in the system can only be studied by means of the CKE.

3.3.2. Short-time statistics

As aforementioned, the movement of the wall in the configuration space described by the exact dynamics results into a more efficient energy transfer from the moving wall to the particles upon collision, when compared to the SFUM. In mathematical terms, this causes the PDF of the oscillation phase on collisions to deviate from the uniform distribution, reflecting the fact that head-on collisions are more preferable than head-tail collisions. However, the phase of oscillation of the moving wall when a particles collides with the fixed wall —or when it passes through any fixed point within the area between the two walls comprising the FUM— is uniformly distributed.

If we denote the phase of oscillation of the moving wall when a particle collides with the fixed wall with ψ, then

$$\psi_n = \cos^{-1}\left(\frac{u_n}{\epsilon}\right) + \frac{1}{z}\left(1 + \sqrt{\epsilon^2 - u_n^2}\right) \tag{3.31}$$

For Eq. (3.31) we obtain for the distribution of the wall velocity upon collision,

$$p_e(u) = \frac{u + z}{\pi z \sqrt{\epsilon^2 - u^2}}. \tag{3.32}$$

Installing Eq. (3.32) into Eq. (3.18) we obtain the one-step TPF for the exact model

$$W_e(v, z) = \frac{\Theta(2\epsilon - |v - z|)(v + z)}{2\pi z \sqrt{4\epsilon^2 - (v - z)^2}}. \tag{3.33}$$

Inserting Eq. (3.33) into the CKE we can numerically compute the evolution of the PDF

of particle velocities. In Fig. 3.9, the numerical solution of the CKE is compared with the histogram of particle velocities, obtained by simulating 1.2×10^6 trajectories using Eqs. (2.1). The particles were initially distributed according to $\rho(v, 0) = \delta(v - 10)$. Once more, the solution of the CKE is in complete agreement with the results of the simulation, proving that the method can also be successfully employed when the exact dynamics are taken into account.

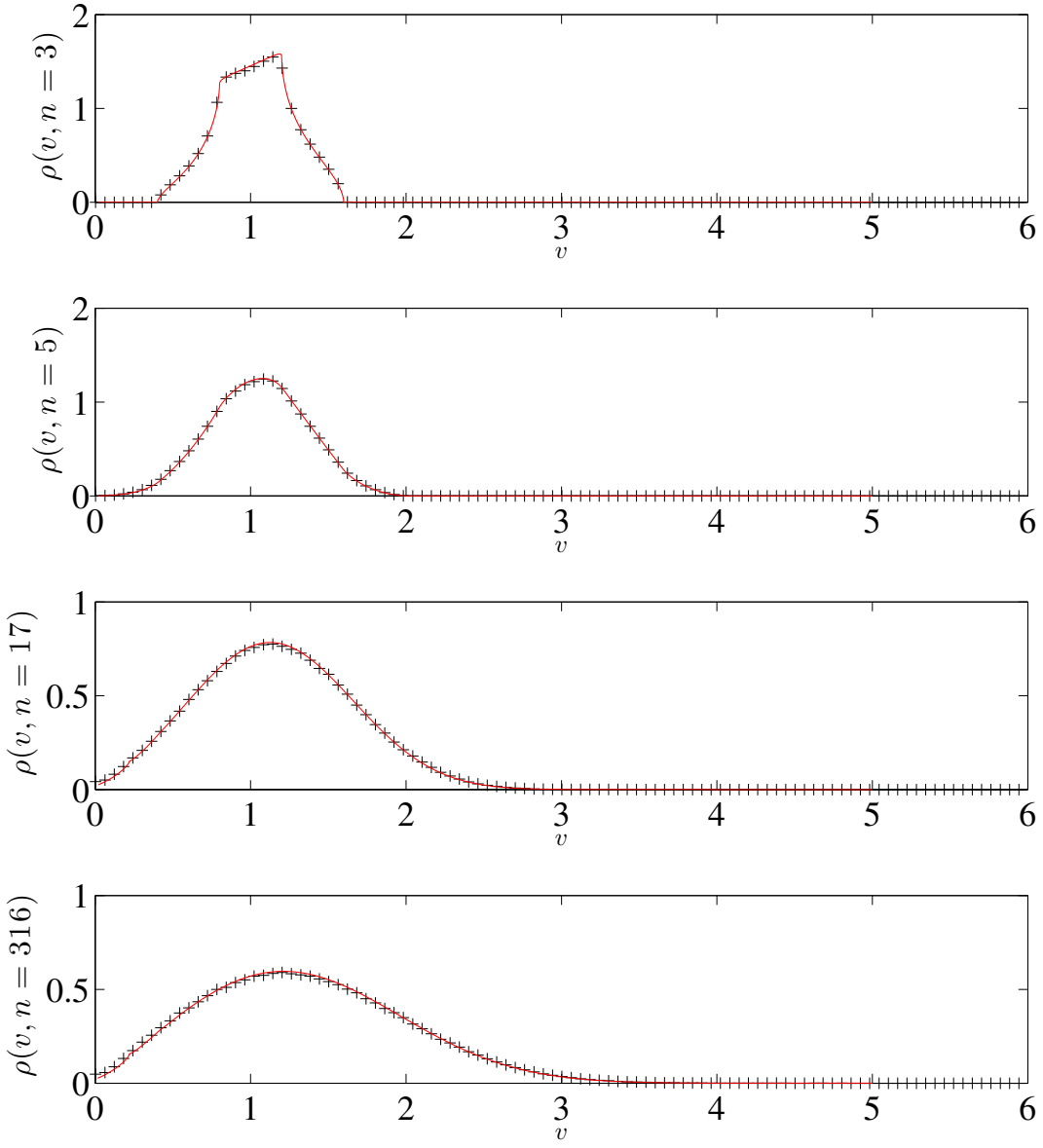

Figure 3.9.: Histogram —upright crosses— of particle velocities after $n = \{3, 5, 17, 316\}$ collisions, obtained by the iteration of Eqs. (2.1), on the basis of an ensemble of 1.2×10^6 particles initially distributed as $\rho(v, 0) = \delta(v - 10)$. The solution obtained by numerically solving the forward CKE [Eq.3.9] using as the TPF of the exact model [Eq. 3.33] is also plotted —solid (red) line.

Part II.

The Lorentz gas

4. Fermi acceleration in the Lorentz gas

In this chapter we introduce the driven Lorentz gas. Due to the breaking of the energy shell and the strong chaotic properties of the static counterpart, Fermi acceleration becomes possible. The four-dimensional discrete mapping is derived. We further extend the HWA presented in §2.2.1. Using the HWA, we show that Fermi acceleration is augmented if the motion of the scatterers is taken into account, doubling the mean energy increase of the particles per collision. The latter points to the direction that the phenomenon of Fermi hyperacceleration is generic, indepedent of the dimensionality of the dynamical system.

4.1. Dynamics

4.1.1. Full model

The dynamics of a point particle suffering elastic collisions with a circular infinitely heavy harmonically driven scatterer are described by the following set of equations [27]:

$$\begin{aligned} 0 &= c_1 \left(t_n - t_{n-1}\right)^2 + c_2 \sin^2(\omega t_n + \eta_n) + c_3 (t_n - t_{n-1}) \\ &\quad + \sin(\omega t_n + \eta_n) + c_4 \left(t_n - t_{n-1}\right) + c_5 \sin(\omega t_n + \eta_n) + c_6 \qquad (4.1a) \\ \mathbf{r}_n &= \mathbf{r}_{n-1} + \mathbf{V}_{n-1} \left(t_n - t_{n-1}\right) \qquad (4.1b) \\ \mathbf{u}_{n,i} &= \mathbf{A}_i \omega \cos\left(\omega t_n + \eta_n\right) \qquad (4.1c) \\ \mathbf{V}_n &= \mathbf{V}_{n-1} - 2\left[\hat{\mathbf{n}} \left(\mathbf{V}_{n-1} - \mathbf{u}_n\right)\right] \hat{\mathbf{n}}, \qquad (4.1d) \end{aligned}$$

where $\mathbf{A}_i$ is a vector directed along the randomly chosen axis of oscillation with magnitude equal to the amplitude of the oscillation of the ith scatterer, ω is the angular frequency of oscillation, η_n is a random number uniformly distributed in the interval $[0, 2\pi)$, t_n is the instant when the nth collision occurs, $\mathbf{r}_\mathrm{n}$ the position vector of the

particle at the instant t_n, $\mathbf{V}_{\rm n}$ the particle velocity vector immediately after the collision, $\mathbf{u}_{\rm n}$ the velocity of the scatterer, and finally $\hat{\mathbf{n}}$ the inward normal vector at the point of collision on the scatterer's boundary where collision occurs. Parameters $c_1, \ldots, c_6$ are given by

$$\begin{aligned} c_1 &= \mathbf{V}_{n-1}^2 \\ c_2 &= (\mathbf{A}_i)^2 \\ c_3 &= -2\mathbf{V}_{n-1} \cdot \mathbf{A}_i \\ c_4 &= 2\left(\mathbf{r}_{n-1} - \mathbf{d}_{0,i}\right) \cdot \mathbf{V}_{n-1} \\ c_5 &= 2\left(\mathbf{r}_{n-1} - \mathbf{d}_{0,i}\right) \cdot \mathbf{V}_{n-1} \\ c_6 &= \left(\mathbf{r}_{n-1} - \mathbf{d}_{0,i}\right)^2 - \left(R_i\right)^2, \end{aligned}$$

where $\mathbf{d}_{0,i}$ is the position vector of the center of the ith scatterer at equilibrium and R_i its radius. For the sake of simplicity in the present analysis we assume that all the scatterers have the same amplitude of oscillation and radii. In order to eliminate the non-relevant parameters, the dimensionless quantity $\epsilon = \frac{|\mathbf{A}|}{w}$ is introduced, where w denotes the spacing between the disk centers. Using as a length unit w and as a time unit $\frac{1}{\omega}$ the map given by Eqs. (4.1) can be rewritten in a dimensionless form

$$\begin{aligned} 0 &= c_1\left(t_n - t_{n-1}\right)^2 + c_2 \sin^2(t_n + \eta_n) + c_3(t_n - t_{n-1})\sin(t_n + \eta_n) \\ &\quad + c_4\left(t_n - t_{n-1}\right) + c_5 \sin(t_n + \eta_n) + c_6 \qquad (4.2a) \\ \mathbf{r}_n &= \mathbf{r}_{n-1} + \mathbf{V}_{n-1}\left(t_n - t_{n-1}\right) \qquad (4.2b) \\ \mathbf{u}_n &= \epsilon[\cos(\theta)\hat{\boldsymbol{\imath}} + \sin(\theta)\hat{\boldsymbol{\jmath}}]\cos\left(t_n + \eta_n\right) \qquad (4.2c) \\ \mathbf{V}_n &= \mathbf{V}_{n-1} - 2\left[\hat{\mathbf{n}}\left(\mathbf{V}_{n-1} - \mathbf{u}_n\right)\right]\hat{\mathbf{n}}, \qquad (4.2d) \end{aligned}$$

where θ is the angle between the oscillation and the x-axis and $\hat{\boldsymbol{\imath}}$, $\hat{\boldsymbol{\jmath}}$ are the unitary vectors along the x and y axis, respectively. The parameters $c_1, \ldots, c_6$ become

$$\begin{aligned} c_1 &= \mathbf{V}_{n-1}^2 \\ c_2 &= \epsilon^2 \\ c_3 &= -2\ \mathbf{V}_{n-1} \cdot \epsilon[\cos(\theta)\hat{\boldsymbol{\imath}} + \sin(\theta)\hat{\boldsymbol{\jmath}}] \\ c_4 &= 2(\mathbf{r}_{n-1} - \mathbf{d}_{0,i}) \cdot \mathbf{V}_{n-1} \\ c_5 &= 2\left(\mathbf{r}_{n-1} - \mathbf{d}_{0,i}\right) \cdot \mathbf{V}_{n-1} \\ c_6 &= \left(\mathbf{r}_{n-1} - \mathbf{d}_{0,i}\right)^2 - R^2. \end{aligned}$$

4.1.2. Static approximation

As already mentioned above, the exact map describing the system dynamics is implicit with respect to the collision time, see Eq. (4.2a), rendering an analytical treatment of the acceleration process practically impossible. Moreover, the numerical solution of this implicit transcendental equation greatly complicates numerical simulations, making the long-term prediction of the particle acceleration a difficult task. In order to overcome these difficulties one usually resorts to the *static* approximation, according to which –as in the case of the FUM– the scatterer is considered to be fixed in configuration space, and yet when the particle suffers a collision with it the particle exchanges momentum as if the scatterer were oscillating. Thus, the exact map is simplified to the following set of equations, which can now be solved explicitly for the collision time t_n

$$\begin{aligned} 0 &= c_1 \left(t_n - t_{n-1}\right)^2 + c_2 \left(t_n - t_{n-1}\right) + c_3 && \text{(4.3a)} \\ \mathbf{r}_n &= \mathbf{r}_{n-1} + \mathbf{V}_{n-1} \left(t_n - t_{n-1}\right) && \text{(4.3b)} \\ \mathbf{u}_n &= \left[\cos(\theta)\hat{\boldsymbol{\imath}} + \sin(\theta)\hat{\boldsymbol{\jmath}}\right] \epsilon \cos\left(t_n + \eta_n\right) && \text{(4.3c)} \\ \mathbf{V}_n &= \mathbf{V}_{n-1} - 2\left[\hat{\mathbf{n}} \left(\mathbf{V}_{n-1} - \mathbf{u}_n\right)\right] \hat{\mathbf{n}}, && \text{(4.3d)} \end{aligned}$$

where the parameters $c_1, \ldots, c_3$ are given by

$$\begin{aligned} c_1 &= \mathbf{V}_{n-1}^2 \\ c_2 &= 2\left(\mathbf{r}_{n-1} - \mathbf{d}_{0,i}\right) \cdot \mathbf{V}_{n-1} \\ c_3 &= \left(\mathbf{r}_{n-1} - \mathbf{d}_{0,i}\right)^2 - R^2. \end{aligned} \qquad (4.4)$$

It should be noted that if the combination of particle and disk velocity along the normal direction to the boundary at the point of collision is such that the normal particle velocity is not reversed after a collision, then it is done so factitiously, in order to prohibit the particle from traveling through the scatterer.

4.1.3. Hopping approximation

As explained in §2.2.1, instead of being treated as spatially static, scatterers within the *hopping* approximation are allowed to oscillate not only in velocity space but also in configuration space. Provided that the time of free flight between two successive collisions is small compared to the period of oscillation, i.e. high particle velocities, one can assume that a scatterer on the instant of the nth collision occupies the position it held on the $(n-1)$th collision, since the displacement of a disk between successive collisions is negligible. Thus, within the framework of this approximation, the deterministic com-

ponent of the phase of the scatterer's position at the nth collision is taken to be equal to the deterministic phase component of the scatterer's velocity at the $(n-1)$th collision. This leads to an explicit mapping with regard to the instant of collision, t_n, which greatly speeds up numerical simulations, as the solution of transcendental equations is no longer necessary. The dynamics of this approximation, is described by the following set of equations:

$$\begin{aligned}
\mathbf{d}_{n,i} &= \mathbf{d}_{0,i} + [\cos(\theta)\hat{\boldsymbol{\imath}} + \sin(\theta)\hat{\boldsymbol{\jmath}}]\epsilon \sin\left(t_{n-1} + \eta_n\right) && \text{(4.5a)}\\
0 &= c_1\left(t_n - t_{n-1}\right)^2 + c_2\left(t_n - t_{n-1}\right) + c_3 && \text{(4.5b)}\\
\mathbf{r}_n &= \mathbf{r}_{n-1} + \mathbf{V}_{n-1}\left(t_n - t_{n-1}\right) && \text{(4.5c)}\\
\mathbf{u}_n &= [\cos(\theta)\hat{\boldsymbol{\imath}} + \sin(\theta)\hat{\boldsymbol{\jmath}}]\epsilon \cos\left(t_n + \eta_n\right) && \text{(4.5d)}\\
\mathbf{V}_n &= \mathbf{V}_{n-1} - 2\left[\hat{\mathbf{n}}\left(\mathbf{V}_{n-1} - \mathbf{u}_n\right)\right]\hat{\mathbf{n}}, && \text{(4.5e)}
\end{aligned}$$

where $\mathbf{d}_{n,i}$ stands for the position vector of the ith scatterer's center on the nth collision.

4.2. Numerical results

It is convenient to express the dynamics of hard disk billiards in terms of canonical variables, which for the static Lorentz gas are the azimuthal angle $\phi \in [0, 2\pi)$ and the incidence angle $a \in [-\frac{\pi}{2}, \frac{\pi}{2}]$ between the inward normal vector to the surface $\hat{\mathbf{n}}$ and the particle velocity $\mathbf{V}$ before the collision. In the case of a billiard with oscillating scatterers, one has to introduce three more variables, namely the magnitude of the particle velocity $|\mathbf{V}|$, the angle between the axis of oscillation and the x-axis $\theta \in [0, \pi)$ and the collision time t. The different variables involved in the description of a collisional event are illustrated in Fig. 4.1.

Moreover, due to the fact that multiple collisions with the same disk are feasible, the incidence angle a no longer lies in the interval $[-\frac{\pi}{2}, \frac{\pi}{2}]$, but rather $a \in [-\pi, \pi]$. Given that only the normal component of the velocity changes in the process of scattering, and that the tangential component remains unchanged, the particle velocity vector after the collision is given by Eq. (4.2d). Assuming harmonic oscillation for the centers of the circular scatterers the boundary velocity at the moment of collision is, $\mathbf{u}_n = \epsilon[\cos(\theta)\hat{\boldsymbol{\imath}} + \sin(\theta)\hat{\boldsymbol{\jmath}}]\cos\left(t_n + \eta_n\right)$, Therefore, the normal component of the boundary velocity vector at the time and point of collision is

$$u_{\perp,n} = \epsilon \cos(t_n + \eta_n) \cdot \cos(\pi - \phi_n + \theta_n). \tag{4.6}$$

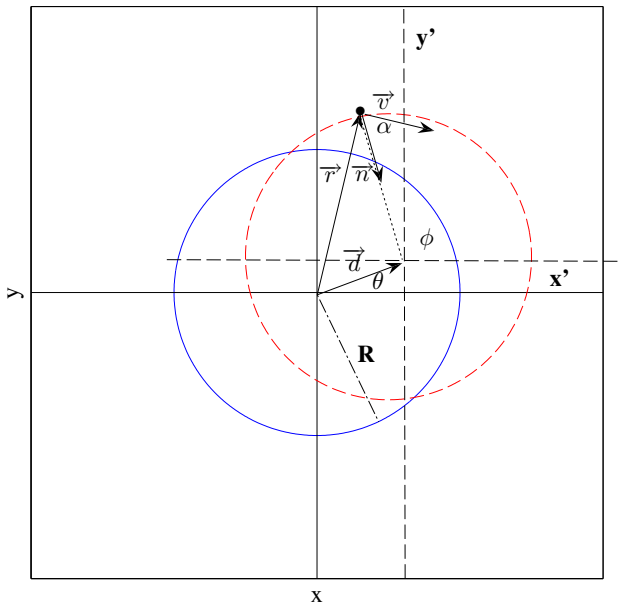

Figure 4.1.: The canonical variables associated with an elementary collision process.

Thus, the square of the modulus of the particle velocity after the nth collision is

$$V_n^2 = V_{n-1}^2 - 4u_{\perp,n}V_{n-1}\cos(a_n) + 4(u_{\perp,n})^2. \tag{4.7}$$

Consequently, the change of the magnitude square of the particle velocity $\delta|V_n|^2 = |V_n|^2 - |V_{n-1}|^2$ is given by the equation

$$\delta|V|^2 = -4u_{\perp,n}V_{n-1}\cos(a_n) + 4(u_{\perp,n})^2. \tag{4.8}$$

In the static Lorentz gas, due to the mixing properties of the system, the probability distribution function (PDF) of a is given by [71]:

$$\rho(a) = \frac{1}{2}\cos(a), \tag{4.9}$$

while the angle ϕ, follows a uniform distribution

$$\rho(\phi) = \frac{1}{2\pi}. \tag{4.10}$$

Generally, this does not apply for a billiard with time-dependent boundaries. In the present analysis we exclusively consider ensembles of trajectories with initial velocities larger than the maximum velocity of the scatterers, rendering multiple collisions with the

same wall highly improbable and therefore negligible. It follows that the PDF of a can accurately be approximated by Eq. (4.9). These assumptions are validated numerically to a high accuracy, using an ensemble of 10^5 particle trajectories each one investigated for up to 10^4 collisions. Particles were randomly positioned close to the boundary of the scatterer, at a distance equal to $1.03R$ –R denoting the radii of the scatterers– with a velocity vector, $\mathbf{V} = (|\mathrm{V}|\cos \mathrm{z}, |\mathrm{V}|\sin \mathrm{z})$, of magnitude $|\mathbf{V}| = \mathrm{V} = \frac{100}{215}$, with the angle z being a random variable uniformly distributed in the interval $[0, 2\pi)$ and $\epsilon = \frac{1}{215}$. Results for the case of using phase randomization are shown in Fig. 4.2. It should be noted that all studied setups yield identical results for these distributions, regardless of the map type (exact or simplified), implemented in the numerical simulations.

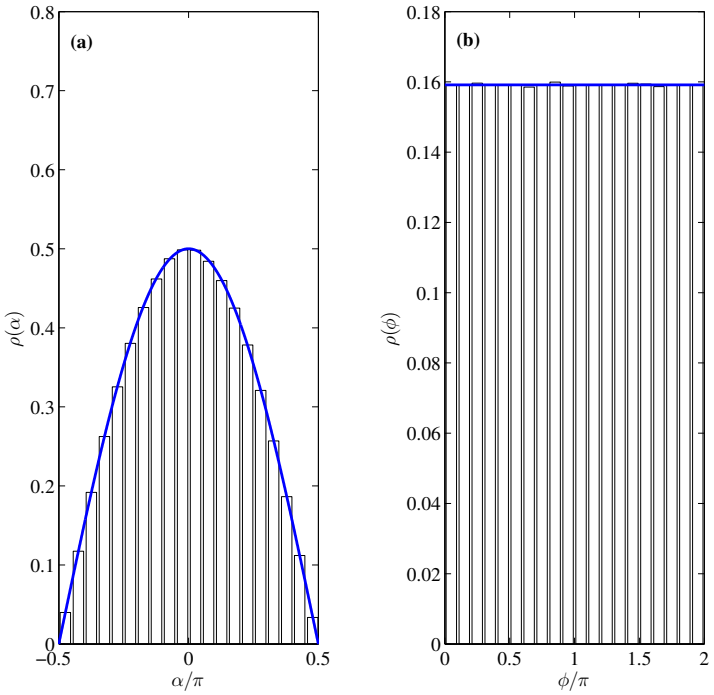

Figure 4.2.: The Probability Distribution Functions (PDFs) of the (a) incidence angle a and (b) azimuthal angle ϕ. The theoretical predictions for the corresponding PDFs are also plotted (solid line).

In Figures 4.3 and 4.4 the rms particle velocity $\tilde{V}$ is shown, as a function of the number of collisions n, for the case of randomized oscillation phase and for the case where the scatterers are oscillating in a randomly chosen direction, i.e. $\theta \in [0, \pi)$. All the simulations are performed on the basis of an ensemble consisting of 10^4 particles, with an initial distribution for the magnitude of the particle velocities $\rho(|V|, 0) = \delta(|V| - V_0)$, $V_0 = \frac{100}{215}$, $\epsilon = \frac{1}{215}$ and $R = \frac{100}{215}$. These parameter values lead, in the static case, to a Lorentz gas with finite horizon and real space normal diffusion [13]. For the sake of comparison the same figures show the corresponding results obtained using the *static* as

μ	**Random Axis**	**Random Phase**
Exact	$1.1880 \pm 2 \times 10^{-4}$	$1.997 \pm 4 \times 10^{-4}$
Hopping	$1.1151 \pm 3 \times 10^{-4}$	$1.8884 \pm 5 \times 10^{-4}$
Static	$0.6088 \pm 2 \times 10^{-4}$	$1.0009 \pm 7 \times 10^{-4}$

Table 4.1.: The values of the fitting parameter μ for the two system setups, i.e. with randomized direction of oscillation and randomized oscillation phase.

well as the *hopping* maps. Additionally, the curves obtained by fitting with the equation $\sqrt{\mu \cdot \epsilon^2 n + V_0^2}$, with μ being the fitting parameter, are also shown. The results of the fit are summarized in Table 4.1.

In Figures 4.3 and 4.4 it is evident that the *static* approximation fails to describe the evolution of the particle root mean square velocity. Specifically, a comparison between the values of μ in Table 4.1, obtained by fitting the results yielded by the iteration of the exact and the *static* maps indicates that the asymptotic increase ($n \gg 1$) of the square of particle velocity $\langle \delta V^2 \rangle$ is underestimated by a factor of two, both in the random phase as well as in the random oscillation axis setup. On the other hand, the *hopping* approximation, clearly provides a much more accurate description of the diffusion process (the small discrepancy between the results given by the exact and the *hopping* approximation is attributed to initial state effects, and becomes smaller the higher the initial velocity of the particles). Given that the fundamental difference between the *static* and the exact map is the motion of the disk in configuration space, the observed differences must be attributed to the disk displacement on collisions. The motion of the disk not only leads to additional fluctuations of the time of free flight as in the case of the stochastic FUM, but also affects the other variables that are intimately connected with the energy transfer between scatterer and projectile during a collision, namely the incident angle a and the azimuthal angle ϕ. The fluctuations caused by the scatterer displacement with respect to a and ϕ are again systematic, leading to an increased acceleration.

As already mentioned, the specific way the Lorentz gas is randomized affects the acceleration of the particles. Evidently, the numerical results obtained by the iteration of the exact map, Eq. (4.2), presented in Figs. 4.3 and 4.4 show that phase randomization leads to a more rapid acceleration compared to the acceleration observed in the setup with randomized direction of oscillation. The reduced acceleration in the case of randomizing the axis of oscillation is due to the autocorrelation of the phase. Indeed, as the particle velocity increases the time of free flight decreases, which correlates the oscillation phase of the nth collisions to the previous, $(n-1)$th, collision. This is demon-

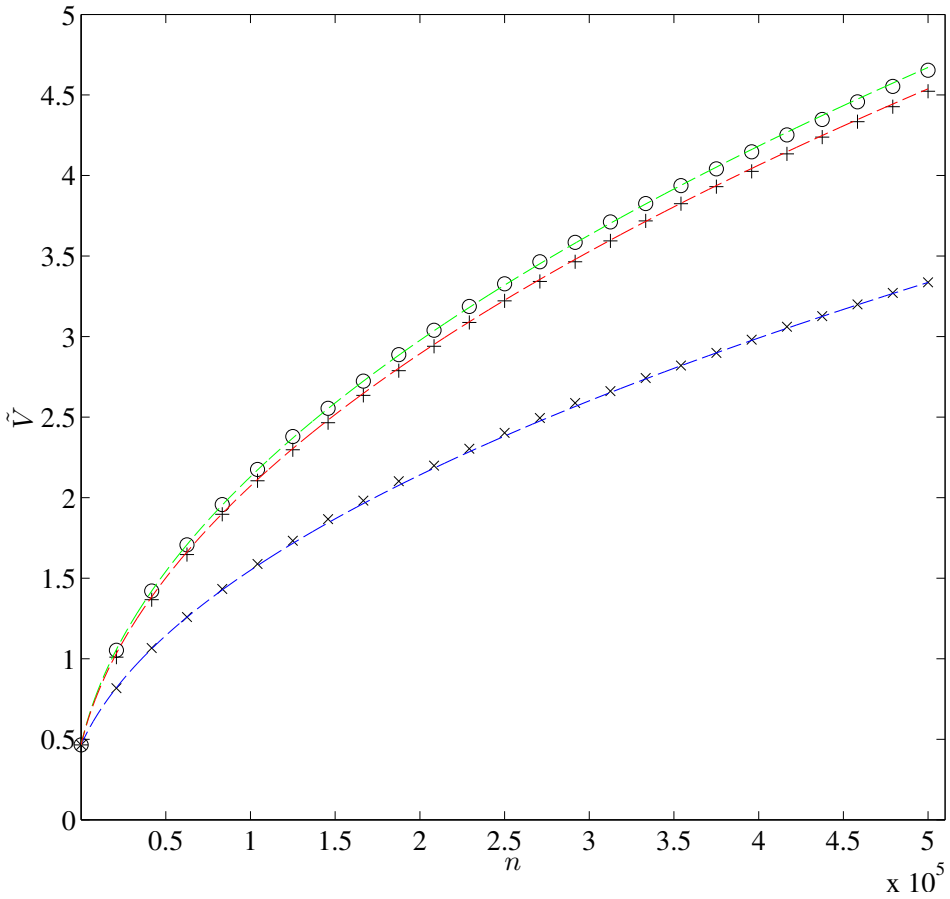

Figure 4.3.: Numerical results for the root mean square particle velocity $\tilde{V}$ as a function of the number of collisions n obtained by the iteration of the exact map, Eq. (4.2) ($\circ$) (with $\epsilon = \frac{1}{215}$ and $V_0 = \frac{100}{215}$) for the driven Lorentz gas consisting of scatterers oscillating horizontally, with the oscillation phase shifted randomly when an incident particle leaves the elementary cell of the lattice. Corresponding results obtained utilizing the *hopping* ($+$) and *static* ($\times$) approximative maps are also presented . The curves obtained by fitting with the model $\sqrt{\mu \cdot \epsilon^2 n + V_0^2}$ are also plotted (dashed lines).

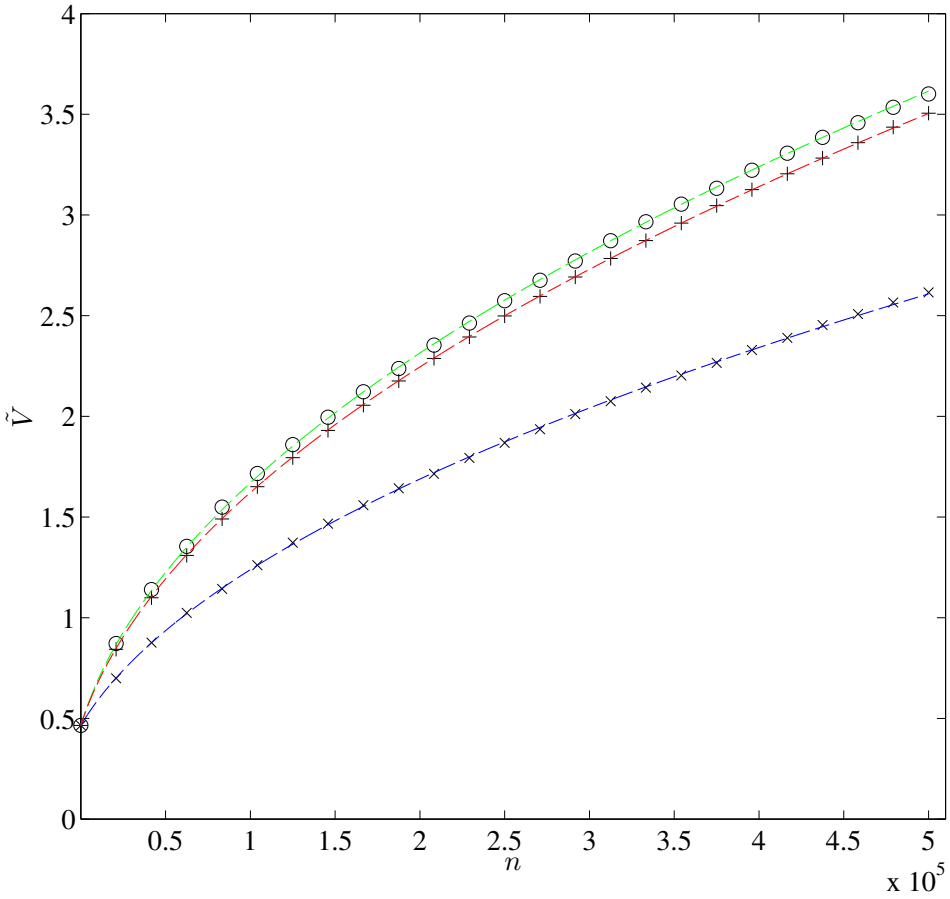

Figure 4.4.: Numerical results for the root mean square particle velocity, $\tilde{V}$, as a function of the number of collisions n obtained by the iteration of the exact map ($\circ$) (with $\epsilon = \frac{1}{215}$ and $V_0 = \frac{100}{215}$) for the setup with scatterers oscillating in a randomly chosen direction. Corresponding results obtained utilizing the *hopping* ($+$) and *static* ($\times$) approximative maps are also presented. The curves acquired by fitting with the model $\sqrt{\mu \cdot \epsilon^2 n + V_0^2}$ are also plotted (dashed lines).

strated in Fig. 4.5, where numerical results of the autocorrelation function of the phase of oscillation $C(n)$ versus the number of collisions n are presented. It can be seen that the autocorrelation of the phase persists for more than 50 collisions.

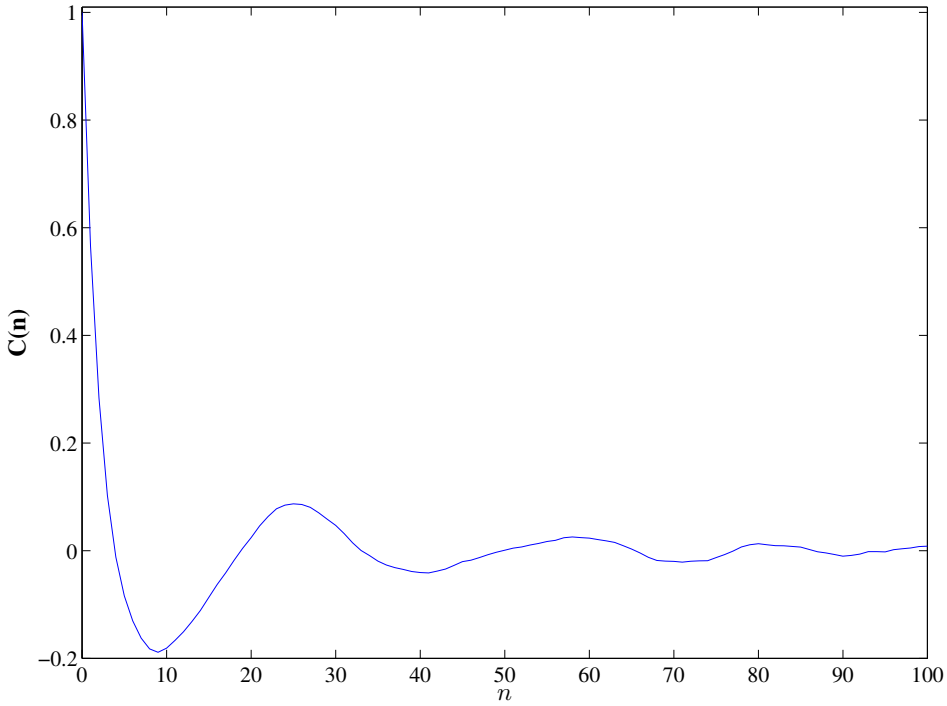

Figure 4.5.: Numerical results for the phase autocorrelation function $C(n)$ versus the number of collisions n for the Lorentz gas consisting of scatterers oscillating in a randomly chosen direction.

4.3. Analytical results within the hopping approximation

In order to account for the dynamically induced correlations caused by the motion of the disks, a similar analysis to that conducted for the FUM should be performed using the corresponding *hopping* approximation, Eq. (4.5). For the sake of simplicity, we assume that the phase of oscillation upon collision is completely uncorrelated, even in a single time step, $(\Delta n) = 1$. Consequently, our results apply only to the setup with randomized oscillation phase (and fixed oscillation axis). An analysis of the case of synchronized oscillations of the scatterers.

Obviously, the disk displacement causes a shift of the values of the incident angle a, the azimuthal angle ϕ and the length of the free path l traveled by the incident particle

on its collision course to a disk. This leads to a shift of the time of free flight $\delta t = \frac{l}{|V|}$. Therefore, assuming that the respective values of the variables on the nth collision, were the disk to be fixed on its equilibrium position, are a_n, ϕ_n and l_n, Eqs. (4.6) and (4.8) can be rewritten as:

$$\begin{aligned} \delta|V_n|^2 &= -4u_{\perp,n}V_{n-1}\cos(a_n+\delta a_n)+4u_{\perp,n}^2 && (4.11)\\ u_{\perp,n} &= -\epsilon\cos(t_{n-1}+\frac{l_n+\delta l_n}{V_n}+\eta_n)\cos(\phi_n+\delta\phi_n), && (4.12)\end{aligned}$$

where δa_n, $\delta\phi_n$ and δl_n denote the change to the values of the respective variables caused by the displacement of the scatterer on the nth collision. From geometrical considerations δa_n, $\delta\phi_n$ and δl_n can be expressed as a function of a_n, ϕ_n, l_n

$$\begin{aligned} \delta l_n &= R\big[\cos(\phi_n)-\cos(\phi_n+\delta\phi_n)-\frac{\epsilon}{R}\sin(t_{n-1}+\eta_n)\big]\times \\ &\quad \sec(a_n+\phi_n)\big] && (4.13)\\ \sin(a_n+\delta a_n) &= \sin(a_n)-\frac{\epsilon}{R}\sin(t_{n-1}+\eta_n)\sin(a_n+\phi_n) && (4.14)\\ \delta\phi_n &= -\delta a_n. && (4.15)\end{aligned}$$

On the supposition of small oscillations the change δa_n, $\delta\phi_n$, δl_n caused by disk displacement to the angle variables and to the free particle path is small, i.e. δa_n, $\delta\phi_n$, $\delta l_n \ll 1$. Therefore, we can expand the left-hand side (l.h.s.) of Eq. (4.14) to the leading order of δa_n to obtain an explicit equation for δa_n.

$$\delta a_n = -\frac{\epsilon}{R}\sec(a_n)\sin(t_{n-1}+\eta_n)\sin(a_n+\phi_n). \quad (4.16)$$

After the substitution of Eqs. (4.13), (4.15) and (4.16) to Eq. (4.11) and integration over η, ϕ and a (for details see Appendix C), assuming that they follow the PDFs defined by Eqs (4.9) and (4.10), we obtain a formula for the mean particle energy gain upon a collision, which reads:

$$\delta V_n^2 = \epsilon^2\cos\left(\frac{\langle l\rangle}{V_n}\right)+\epsilon^2, \quad (4.17)$$

where $\langle l\rangle$ stands for the mean free path on the supposition of fixed scatterers at their corresponding equilibrium positions. In the limit of high particle velocities $\cos\left(\frac{\langle l\rangle}{V_n}\right)$ tends to unity. Thus, the following asymptotic value of δV^2 is obtained:

$$\delta V_n^2 \simeq 2\epsilon^2. \quad (4.18)$$

It follows that the rms particle velocity is:

$$\sqrt{\langle V_n^2 \rangle} = \sqrt{\sum_{j=1}^{n} \langle \delta |V|_j^2 \rangle + V_0^2} = \sqrt{2\epsilon^2 n + V_0^2}. \tag{4.19}$$

In Fig. 4.6 the analytical result given by Eq. (4.19) is shown together with numerical results obtained by the iteration of the exact map, Eq. (4.2), for the setup with randomized oscillation phase. Obviously, numerical and analytical results are in agreement, which proves that the small additional fluctuations both in the time of free flight and in the angle variables, a and ϕ due to the displacement of the scatterer, do not cancel out; on the contrary, they act systematically and account for the increased acceleration observed in the exact dynamics.

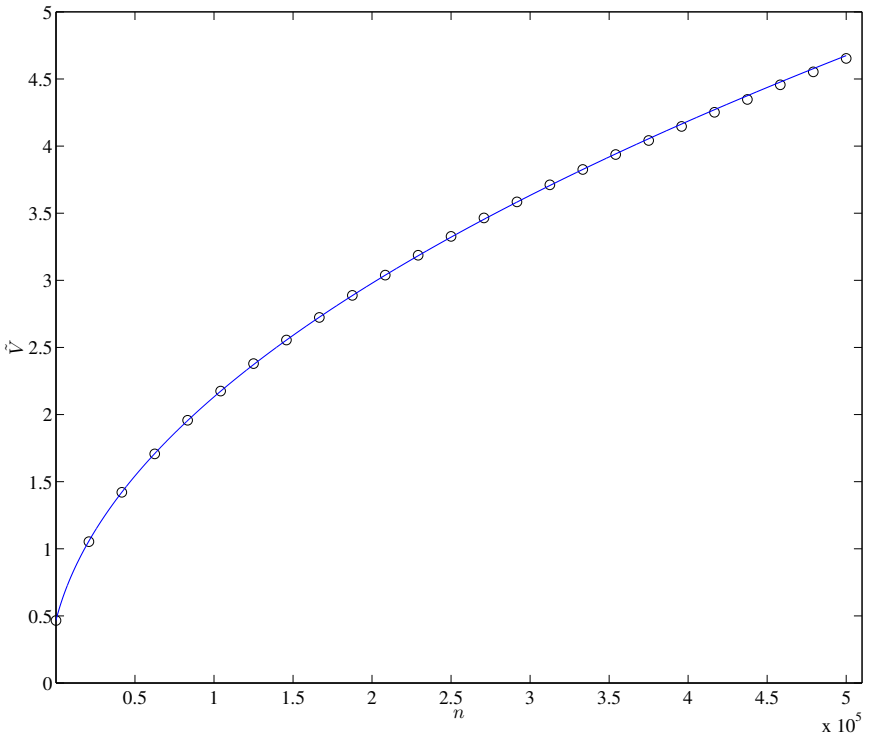

Figure 4.6.: Root mean square particle velocity, $\tilde{V}$, as a function of the number of collisions n obtained by the iteration of the exact map ($\circ$) (with $\epsilon = \frac{1}{215}$ and $V_0 = \frac{100}{215}$) for the case of scatterers with randomized phase of oscillation. For the sake of comparison the analytical result of Eq. (4.19) is also shown (solid line).

In order to obtain the value of the correction factor $R_h(n)$ for the Lorentz gas setup with randomized phase of oscillation, the mean increase of the square of particle velocity δV^2 must be also calculated within the framework of the *static* approximation. This can

easily be done by averaging Eq. (4.8) over a, ϕ and η to obtain, $\delta V_n^2 = \epsilon^2$. Therefore,

$$R_h(n) = \frac{(\langle V^2\rangle - \langle V_0^2\rangle)_{exact}}{(\langle V^2\rangle - \langle V_0^2\rangle)_{SWA}} = \frac{\sum_{i=1}^{n}\langle \delta V_i^2\rangle_{exact}}{\sum_{i=1}^{n}\langle \delta V_i^2\rangle_{static}} \simeq 2 \tag{4.20}$$

It is worth noting that the value of $R_h(n)$, for the harmonically driven Lorentz gas with randomized phase of oscillation coincides with that obtained for the harmonically driven FUM 2.2.1.

Let us now direct our attention to the PDF of the magnitude of the particle velocity and number of collisions n, $\rho\left(|V|, n\right)$. The study of a square periodic Lorentz gas consisting of "breathing" circular scatterers, i.e. with oscillating boundary of the scatterer in the radial direction, in Ref. [71], conducted by means of the *static* approximation concluded that $\rho(|V|, n)$ is a sum of spreading Gaussians. Furthermore, general arguments presented in Ref. [86], where a random time-dependent Lorentz gas has been investigated, also suggest that $\rho(|V|, n)$ is a Gaussian. However, the numerical results presented in Fig. 4.7, which correspond to two snapshots for $n = 5\times10^4$ and $n = 5\times10^5$, obtained through the iteration of the exact map, point to the direction of $\rho(|V|, n)$ being a Maxwell-Boltzmann like distribution, corresponding to a **three dimensional** system. Obviously, $\rho(|V|, n)$ can be analytically obtained through the solution of the Fokker-Planck equation, (3.6). To do so the transport coefficients defined by Eqs. (3.8) must be calculated. Assuming that $\Delta n = 1$ the transport coefficients coincide with the $\langle \delta|V_n|\rangle$ and $\langle (\delta|V_n|)^2\rangle$. From Eq. (4.8) it follows:

$$|V_n| = |V_{n-1}|\sqrt{1 - 4\,\frac{u_{\perp,n}}{V_{n-1}}\cos(a_n + \delta a_n) + 4\left(\frac{u_{\perp,n}}{V_{n-1}}\right)^2}. \tag{4.21}$$

Expanding Eq. (4.21) to the leading order of $\frac{u_{\perp,n}}{V_n}$ we get:

$$\delta|V_n| = \frac{2(u_{\perp,n})^2\sin^2(a + \delta a_n)}{V_{n-1}} - 2u_{\perp,n}\cos(a). \tag{4.22}$$

Taking similar steps to those discussed in Appendix A we obtain

$$\langle \delta|V|\rangle = \frac{2\epsilon^2}{3V} \tag{4.23}$$

$$\langle (\delta|V|)^2\rangle = \frac{2(V-2)\epsilon^2}{3V}. \tag{4.24}$$

Given that for $n \gg 1$ the majority of the particles have velocities $V \gg 1$ we can keep

the dominant term in Eq. (4.24) thus,

$$\langle(\delta|V_n|)^2\rangle \simeq \frac{2\epsilon^2}{3}. \tag{4.25}$$

The specific values of the coefficients together with reflective boundary conditions at $V = 0$ lead to the following solution of the Fokker-Planck equation:

$$\begin{aligned} \rho(|V|, n) =& \sqrt{\frac{2}{\pi}} \frac{1}{\sigma^3} |V|^2 e^{|V|^2/(2\sigma^2)} \\ \sigma =& \sqrt{\frac{2\epsilon^2 n + V_0^2}{3}}. \end{aligned} \tag{4.26}$$

In Fig. 4.7 the analytical result for the PDF, Eq. (4.26), is also plotted for the sake of comparison. Clearly, the analytics provides an accurate description for the PDF $\rho(|V|, n)$ for $n \gg 1$. It must be noted, that the velocity distribution of the V_x, V_y components is symmetric, which implies that their is no drift velocity in the phase randomized driven Lorentz gas. This holds also for the case of the Lorentz gas with randomized direction of oscillation.

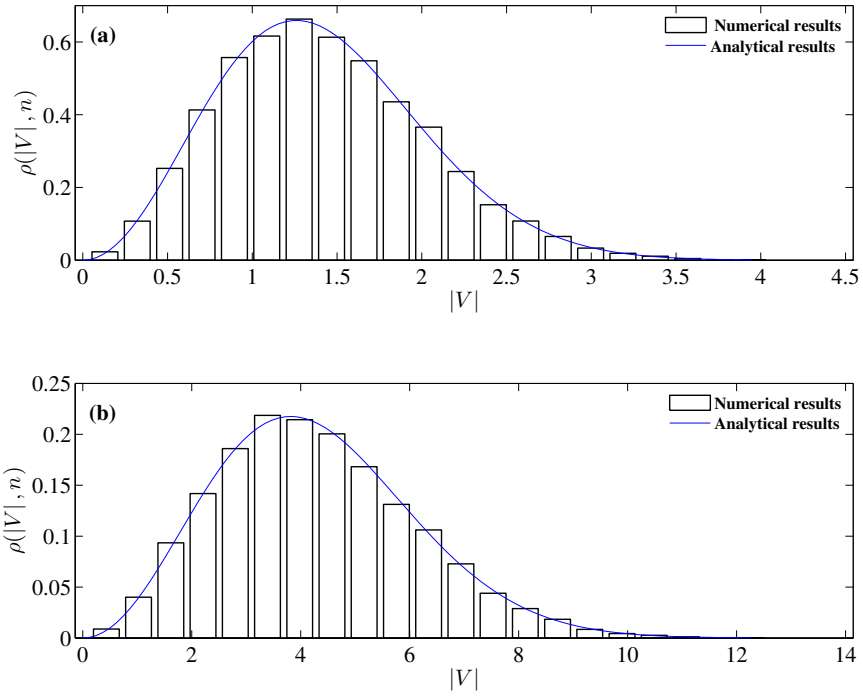

Figure 4.7.: Numerically computed PDF for the magnitude of the particle velocity using an ensemble of 10^4 trajectories and following the exact dynamics for: (a) $n = 5 \times 10^4$ and (b) $n = 5 \times 10^5$ with $\epsilon = \frac{1}{215}$ and $\|V_0\| = \frac{100}{215}$. In each case the analytical result provided by Eq. (4.26) is also shown (solid line).

5. Steady states in the open Lorentz channel

In this chapter, we study the static and driven Lorentz gas in a channel geometry with finite length. We show that non-trivial non-equilibrium steady states exist, even if the energy shell is broken due to external driving. At the same time, we also present results for the steady states developing in the static Lorentz channel, in a fundamentally different geometry than the one considered in the literature [87]; the infinite horizon geometry. Finally, we show how a semi-analytical description of the system's transmission coefficient can be achieved by means of the random walk theory.

5.1. The system

We consider an ensemble of non-interacting point particles which propagate inside a one-dimensional chain composed of N identical two-dimensional cells arranged horizontally. The channel is constructed by superimposing two square lattices of circular scatterers, which have the same lattice spacing w, and radii a and b, respectively. The lattices are positioned such that there is a b disk at the canter of each unit cell of the a lattice. The system is finite in both the x and y direction. In the x direction it extents from 0 to L imposing absorbing boundary conditions. Finally, two hard flat boundaries are placed at $\pm\sqrt{3}w/2$, confining the motion of the particles in the y direction. Particles are injected with a steady flow from the left end and escape the system when reaching either ends of the channel –absorbing boundary conditions. Therefore, the channel is a finite strip of a triangular periodic Lorentz gas and for this reason it is dubbed *Lorentz channel* [87–89]. Finally it is noted that the a lattice is fixed in space, while the centers of the disks comprising the b lattice can oscillate harmonically. In order to eliminate irrelevant parameters, length and time is measured in units of $1/\omega$ and w, respectively.

In the case of the static Lorentz channel, that is when the central disks are also held fixed in their equilibrium position, two different geometries are distinguished in general, depending on the length of the maximum free flight of a particle:

1. Infinite horizon: If $\sqrt{3}/2 - a \leq b$ then particles can travel throughout the channel without ever colliding with any of the circular scatterers. Obviously, these trajectories are regular and the corresponding Lyapunov exponent is zero.

2. Finite horizon: The violation of the geometrical condition stated above, assures that the maximum free flight is bounded from above, leading to a system which is fully hyperbolic.

The two different geometries can be seen in Fig. 5.1. This classification cannot be

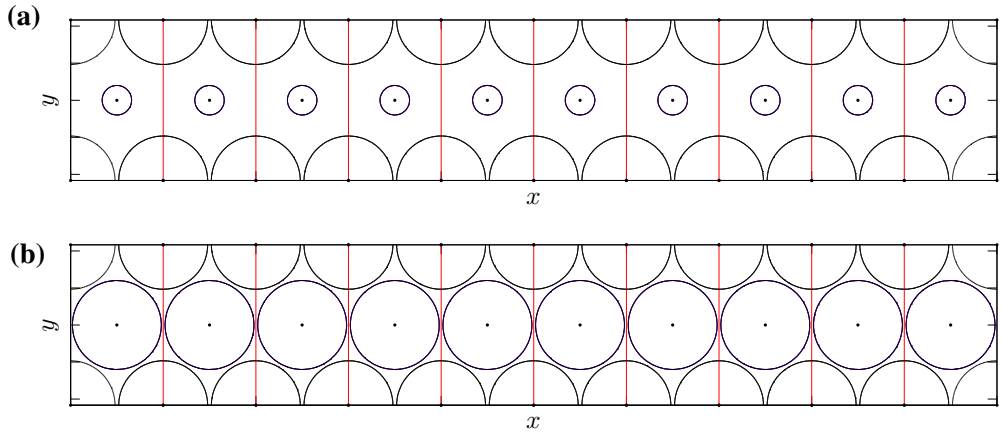

Figure 5.1.: The two different geometries of the Lorentz channel. The oscillating central scatterers are depicted in their equilibrium positions for the sake of clarity. The borders between each unitary cell are denoted with red solid lines.

applied in a straightforward manner to the time-dependent Lorentz channel. If the driving is turned on, then the existence of ballistic corridors depends not only on the geometrical characteristics of the channel, but also on dynamical parameters, such as the amplitude of oscillation, the angle, the distribution of the initial phases, etc. To bridge the gap, we introduce the concept of billiards with *dynamically infinite horizon* (DIH), corresponding to driven billiards which retain characteristics of the static ones with infinite horizon geometry, such as the algebraic decay of the dirstribution of lengths travelled between collisions. This classification of the driven system will be fully justified in the following chapter.

5.2. Steady states

One of the most striking features of the system investigated is that it reaches a steady state, independently of the oscillation parameters, the length of the device and the flux

of the incoming particles as well as their energy. However, the specificities of the steady state reached do depend on the energy of the incoming beam, the dynamical parameters and the geometry of the channel. The numerical experiments done point to the direction that the steady state does not depend on the flux. In order to investigate the impact of the various parameters on the formation of the steady states we vary each parameter separately.

5.2.1. Amplitude

In this section the impact of the amplitude of oscillation on the properties of the system is discussed. In the numerical simulations done, all other parameters except the amplitude are held fixed. Namely, the angle of oscillation θ as well as the frequency ω and the probability density function of the magnitude of velocities of the incoming particles is a delta-Dirac function $\delta(|V| - 0.34)$ (in units of ωw), such that the energy of the beam is comparable to the maximum kinetic energy of the oscillating disks.

The steady state is reached when the net incoming flux of particles —the flux of injected particles minus the flux of the reflected— and the flux of the transmitted particles reaches a constant value. The flux—number of particles per unit time—for three different values of $A = \{0, 0.113, 0.34\}$ is shown in Fig 5.2. The numerical results clearly show that the equilibrium, in terms of particles in the system, is reached both in the static [top panel] and in the time-dependent system [medium and bottom panel]. Furthermore, when the time-dependence is turned on, energy is pumped into the system. Consequently, the mean speed of the particles is increased [see Fig 5.5] and the time needed to be either transmitted or reflected is reduced. This leads to a decrease of the time needed for the system to reach equilibrium.

Given that the flux of the reflected and the transmitted particles reaches a constant value, the total number of particles in the system remains constant. The numerical study we conducted shows that also the distribution of the particles inside the device when the fluxes have reached their maximum values also becomes time-independent. This is exemplified in Fig. 5.3 and 5.4, where the number of particles at $t = \{3, 298, 31, 257 \times 10^3, 10^5\}$—black, red, blue, green line—is shown as a function of the unit-cell number. As can be seen, the static as well as the driven Lorentz channel the system reaches a steady state in the configuration space, i.e. the distribution of the particles inside the device. The linear decay of the number of particles per cell in the static case [Fig. 5.3] and the algebraic decay in the driven Lorentz channel [Fig. 5.4] stems from the fact that particles can travel arbitrarily long without colliding with the scatterers. In other words, this behaviour is attributed to the ballistic corridors—static system—or the

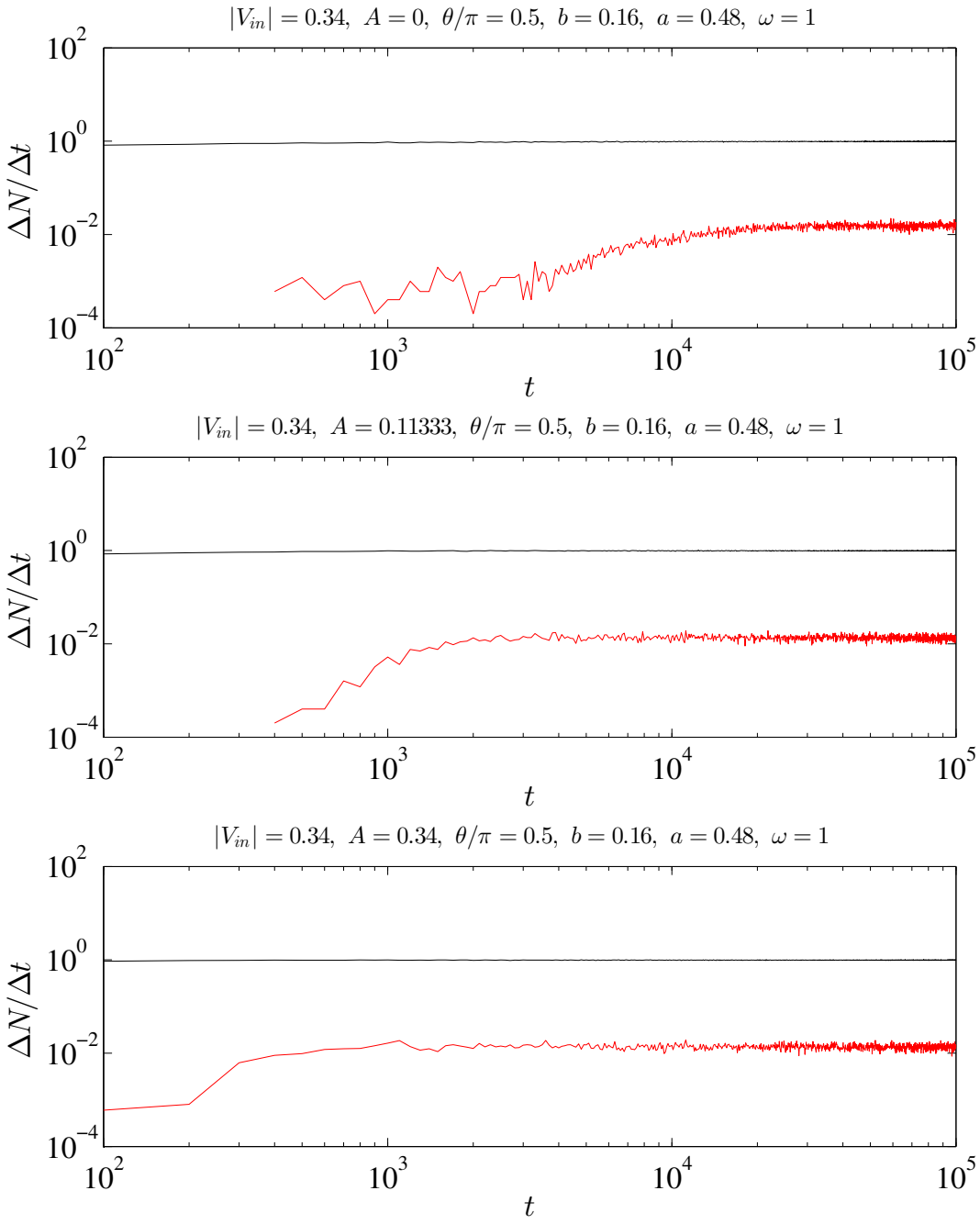

Figure 5.2.: Flux of the reflected—black line— and transmitted particles—red line—for three different values of the amplitude of oscillation, $A = \{0, 0.113, 0.34\}$ –top, middle and bottom panel, respectively.

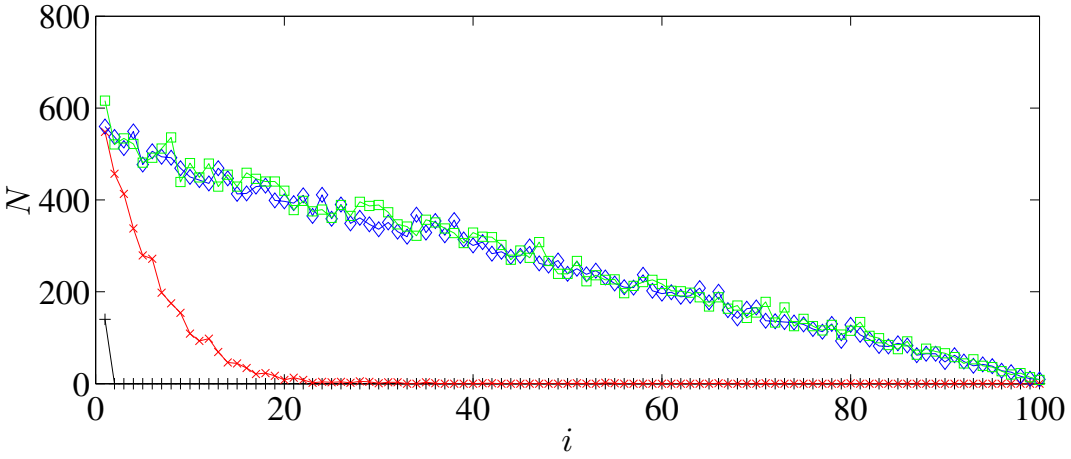

Figure 5.3.: The number of particles per cell at four different times in the static Lorentz channel, i.e. $A = 0$, at $t = \{298, 31.257 \times 10^3, 10^5\}$—black, red, blue, green lines, respectively.

dynamical ballistic corridors—driven system—which leads to a non-exponential decay of the probability a particle to maintain its direction of motion while it is tranmitted from cell to cell within the device. This has a dramatic impact on the character of the steady states appearing in the (dynamically) infinite horizon geometry and will be extensively discussed in the following chapter.

The main difference between the static and the time-dependent Lorentz channel is that the energy is not conserved. Due to the phenomenon of Fermi-acceleration the mean speed of the particles in the system grows. However, as we observe in Fig. 5.5, wherein the histogram of absolute particle velocities at $t = \{3, 298, 3.126 \times 10^4, 10^5\}$ is plotted, the distribution of velocities becomes time-independent, which proves that a steady-state is reached in the momentum space also.

This, can also be verified in Fig. 5.6. In this figure, we have plotted the first and the second moment of the probability distribution function (PDF) of particle absolute velocities as a function of time. Due to Fermi acceleration, the mean absolute velocity and square velocity of the particles grow until the steady state is reached. In Fig. 5.6 we also see that, approximately, the ensemble mean of particle absolute velocities scales linearly with A, i.e. if the amplitude of oscillation is tripled, then, approximately, also the mean value of absolute velocities is tripled.

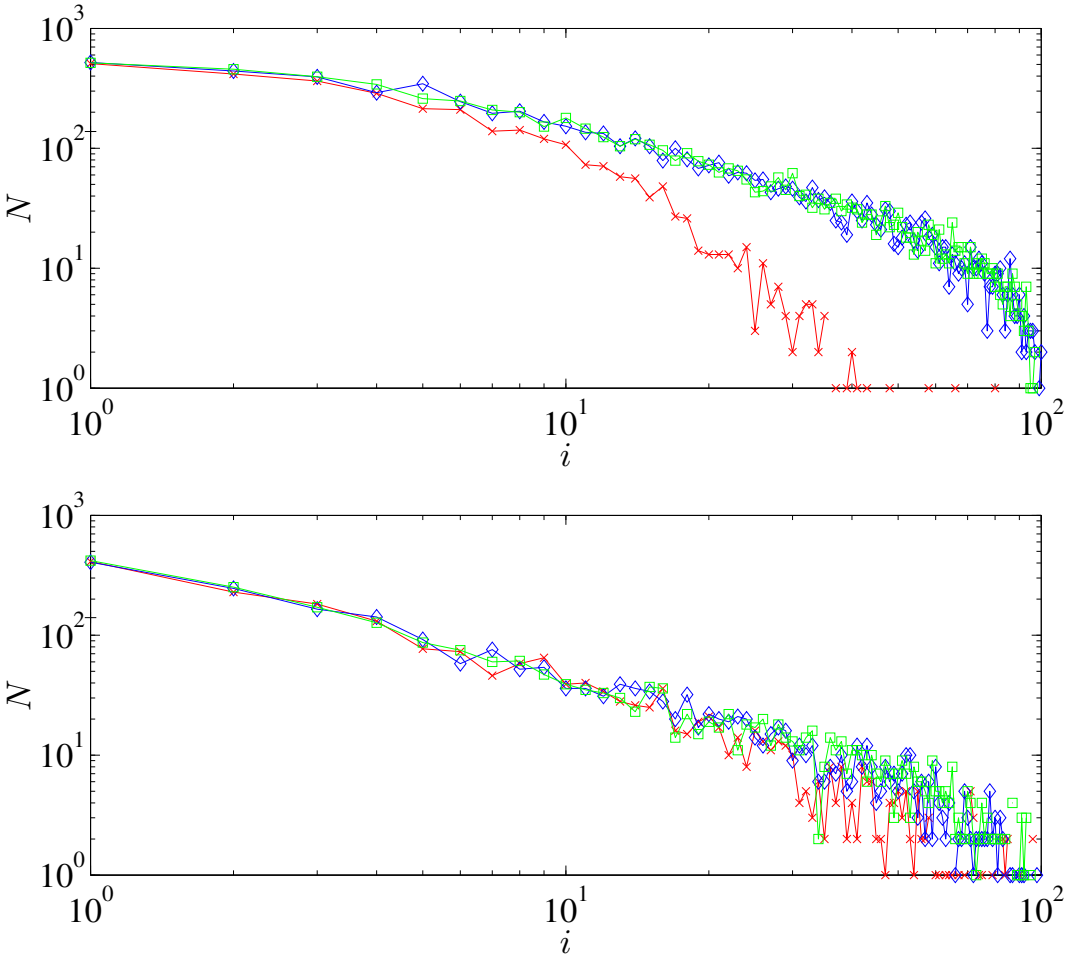

Figure 5.4.: The number of particles per cell at three different times for three different values of the amplitude of oscillation $A \simeq \{0.113, 0.227\}$, at $t = \{298, 31.257 \times 10^3, 10^5\}$—black, red, blue, green lines, respectively.

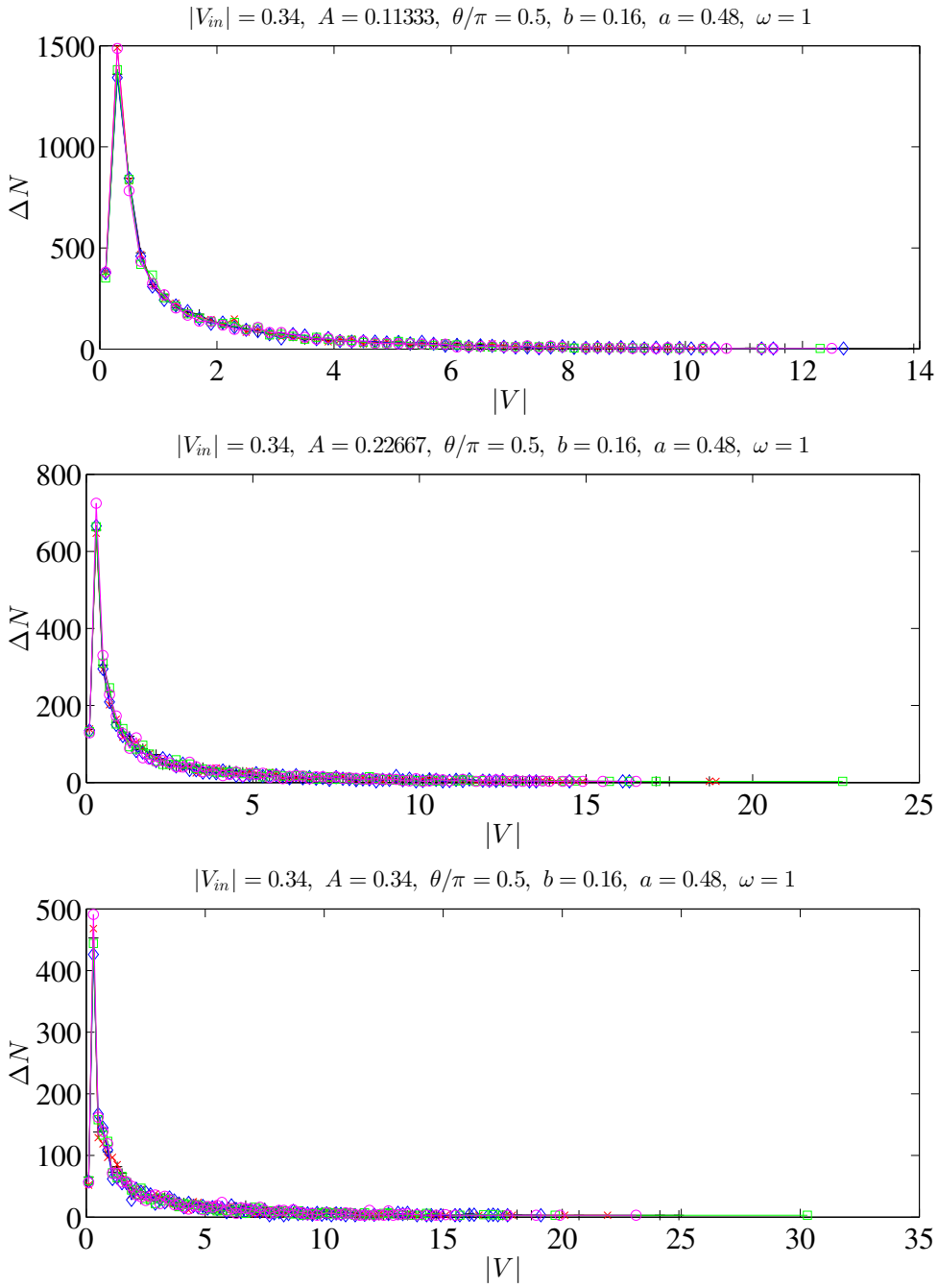

Figure 5.5.: Histogram of the absolute particle velocities for three different values of the amplitude of oscillation, $A \simeq \{0.113, 0.227, 0.34\}$ at $t = \{5.6, 6.7, 7.8, 8.9, 10\} \times 10^4$—black, red, blue, green and magenta line, respectively. The histograms exemplify that a steady state is also reached in the momentum space.

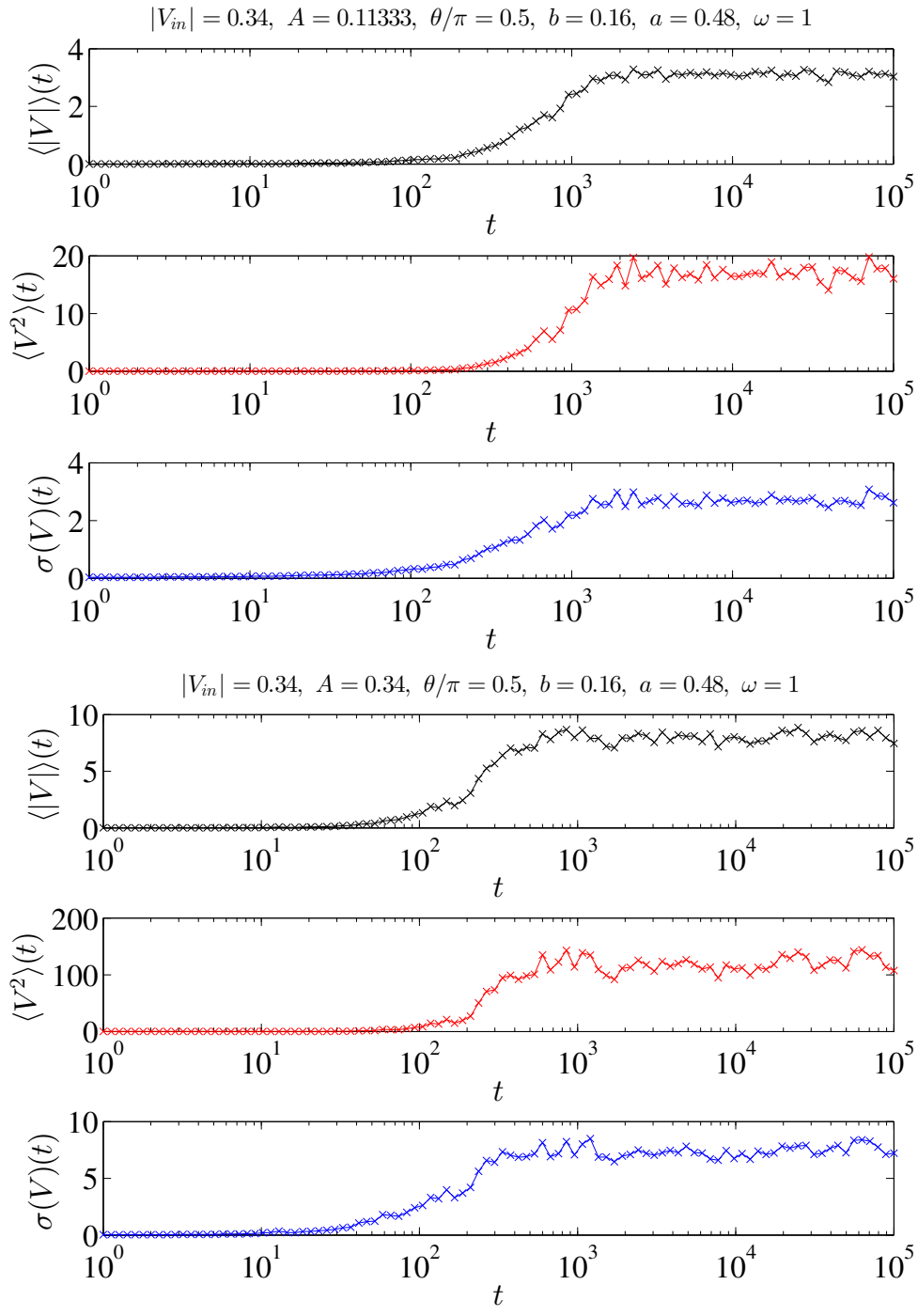

Figure 5.6.: The first and second moment of absolute particle velocities, as well as the standard deviation, as a function of time, for two different values of the amplitude of oscillation, $A \simeq \{0.113, 0.34\}$.

5.2.2. Angle of oscillation

Due to the fact that as the angle of oscillation increases —considering all the other oscillation parameters fixed— the blocking of particles by the moving disks becomes more effective, the occupation probability of the particles in the device decays more rapidly. In other words, particles tend to be more localized towards the injection point, as can be seen in Fig. 5.7

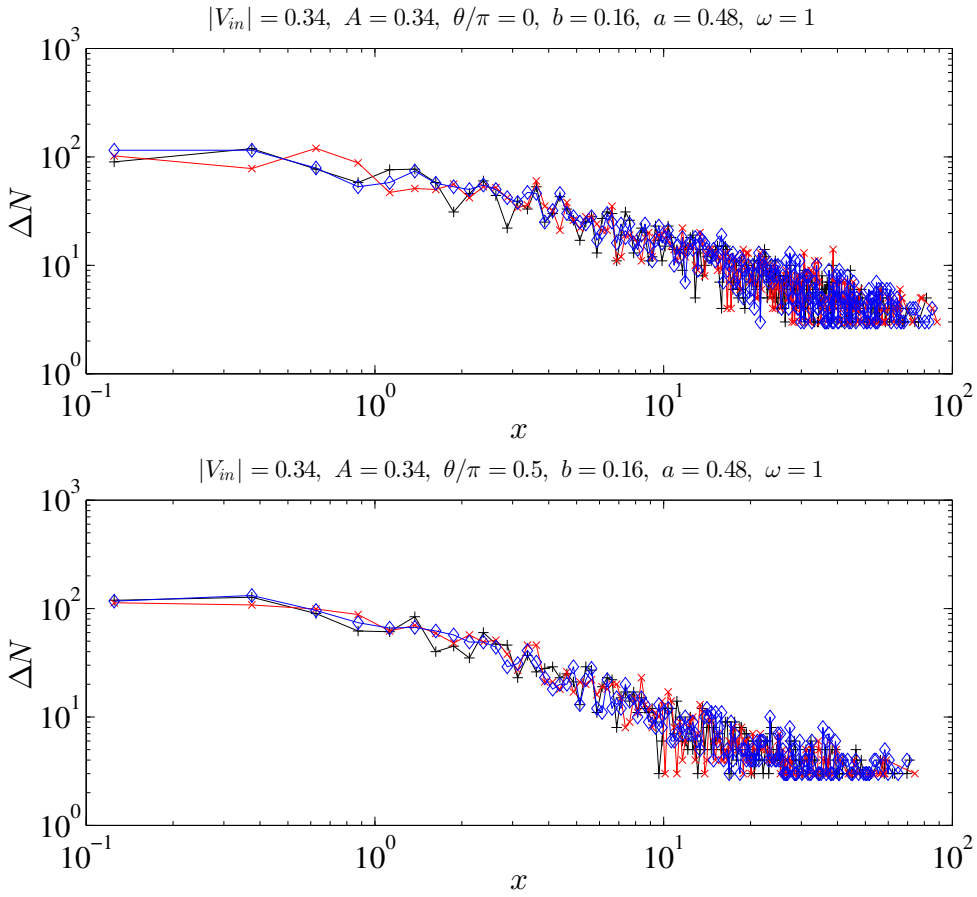

Figure 5.7.: The historgram of particle positions at $t = \{10^3, 4.5 \times 10^4, 10^5\}$ [black, red, and green line] for $\theta/\pi = \{0, 0.5\}$.

At the same time, due to the increase of the probability of the propagating particles to collide with the oscillating scatterers, the "pumping" of energy becomes more effective as the direction of oscillation becomes more inclined to the flow. For this reason the energy content of the particles is increased as the oscillation angle increases. This fact is demonstrated in Fig. 5.8.

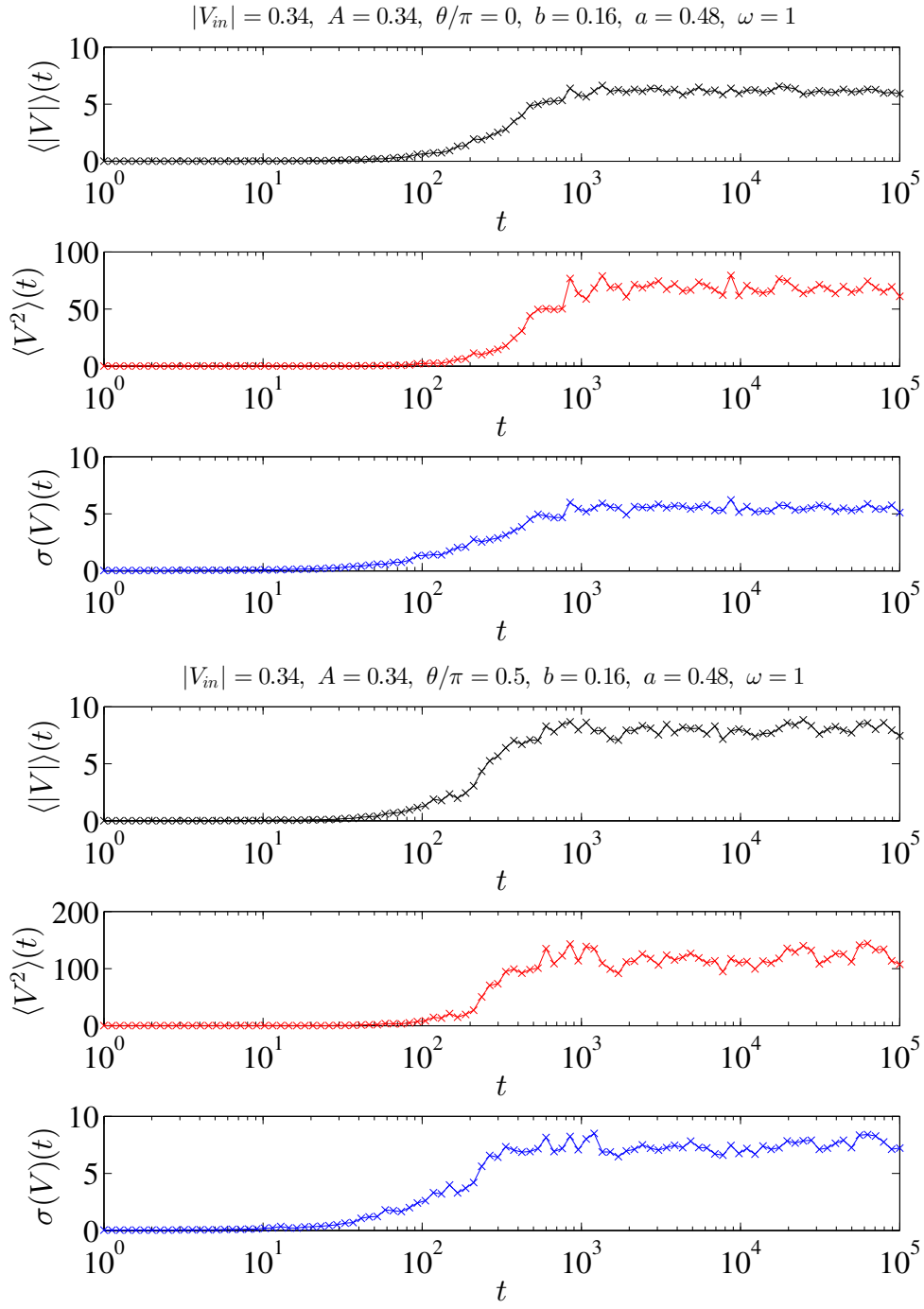

Figure 5.8.: The first and second moment of absolute particle velocities, as well as the standard deviation as a function of time, for two different values of the angle of oscillation, $\theta/\pi = \{0, 0.5\}$.

5.2.3. Energy of the incoming particles

The main impact of the variation of the energy of the incoming particles is on the probability of a particle being transmitted. In this sense, the numerical evidence suggest that the higher the energy of the incoming particles, the more transparent the device becomes. This results into a slower decay of the distribution of particles over the extent of the device as shown in Fig. 5.9. Appartently, a steady state is reached, irrespecitive

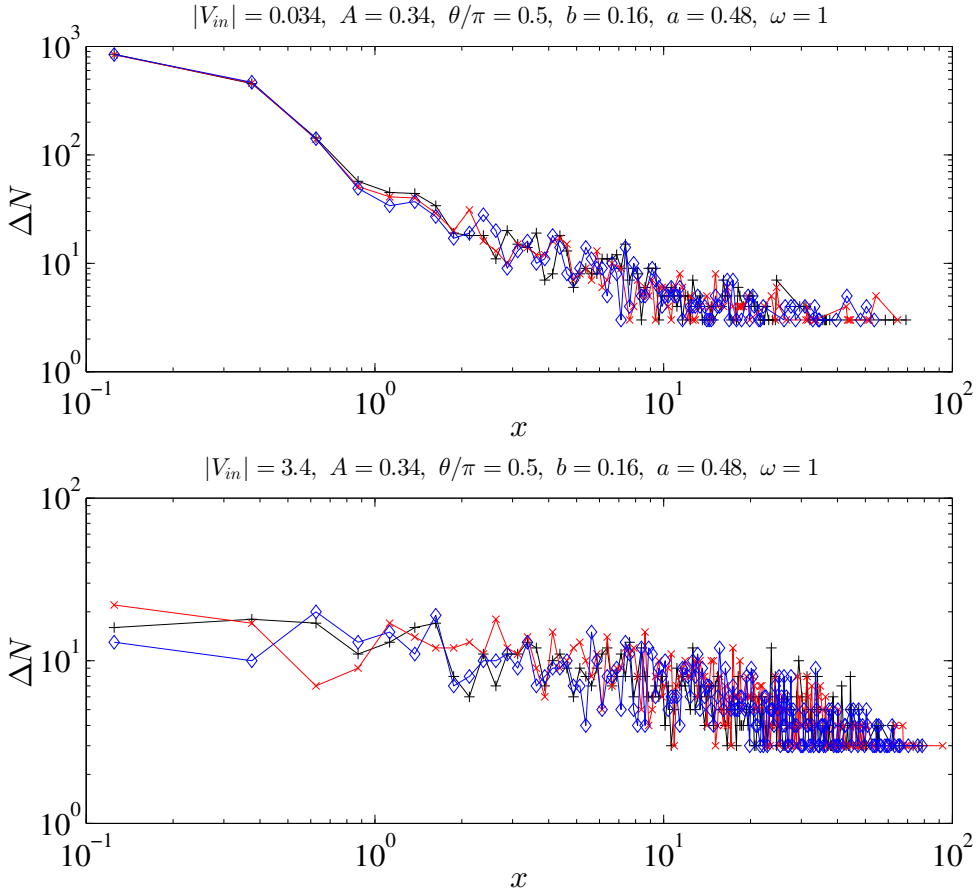

Figure 5.9.: The historgram of particle positions at $t = \{10^3, 4.5 \times 10^4, 10^5\}$ [black, red, and green line] for $V_{in} = \{0.034, 3.4\}$.

of the energy content of the incoming particles.

5.3. The characteristics of the system's output

Two properties of the beam of the transmitted particles are of great interest: The energy content and the directionality. As we can observe in Fig. 5.10, the transmitted particles are aligned towards the x direction even in the case of the static Lorentz channel [top panel] and the driven [bottom panel]. Therefore, the directionality of the output beam is attributed mainly to the geometrical properties of the device.

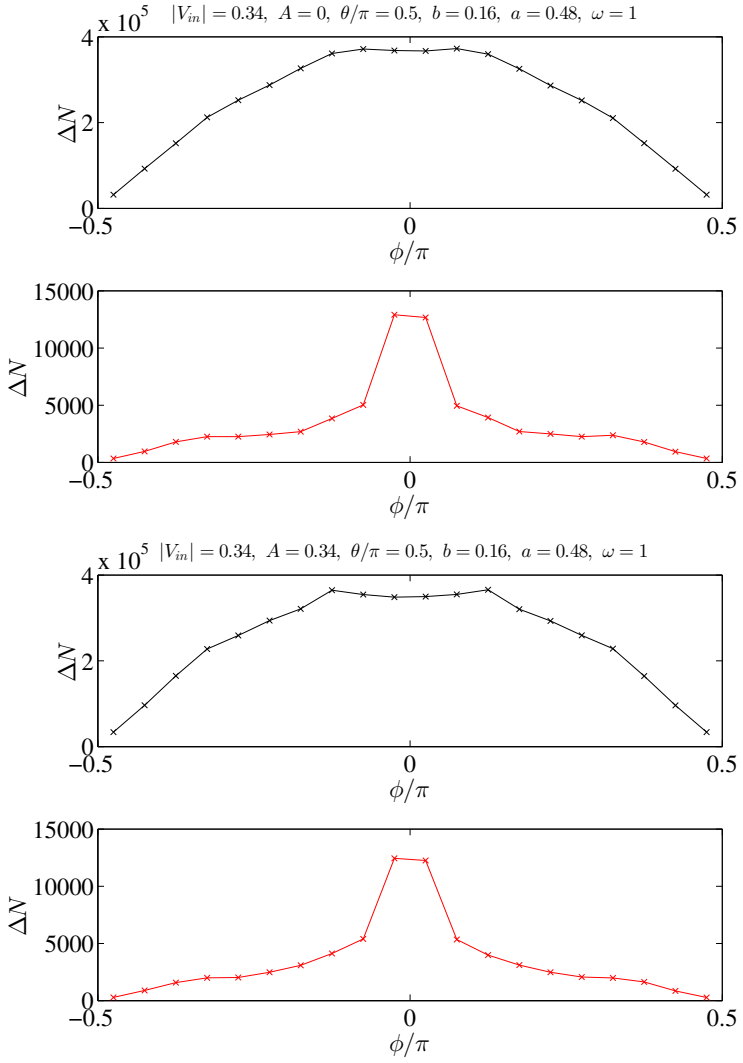

Figure 5.10.: Histogram of the direction angle upon exit from the left (reflected particles) and the right (transmitted particles) for four different values of the amplitude of oscillation $A = \{0, 0.282, 0.563, 0.845\}$

However, in the case of the time-dependent Lorentz channel, there exists a strong correlation between the energy of the particles and their parallelization towards the x axis, as observed in Fig. 5.11. This, in conjuction with the fact that transmission

coefficient of the device can be manipulated by the variation of the parameters of the driving time-law, as we will be shown in the following paragraph, opens-up the prospect of the preparation of a focused particle beam, with specific energy and intensity.

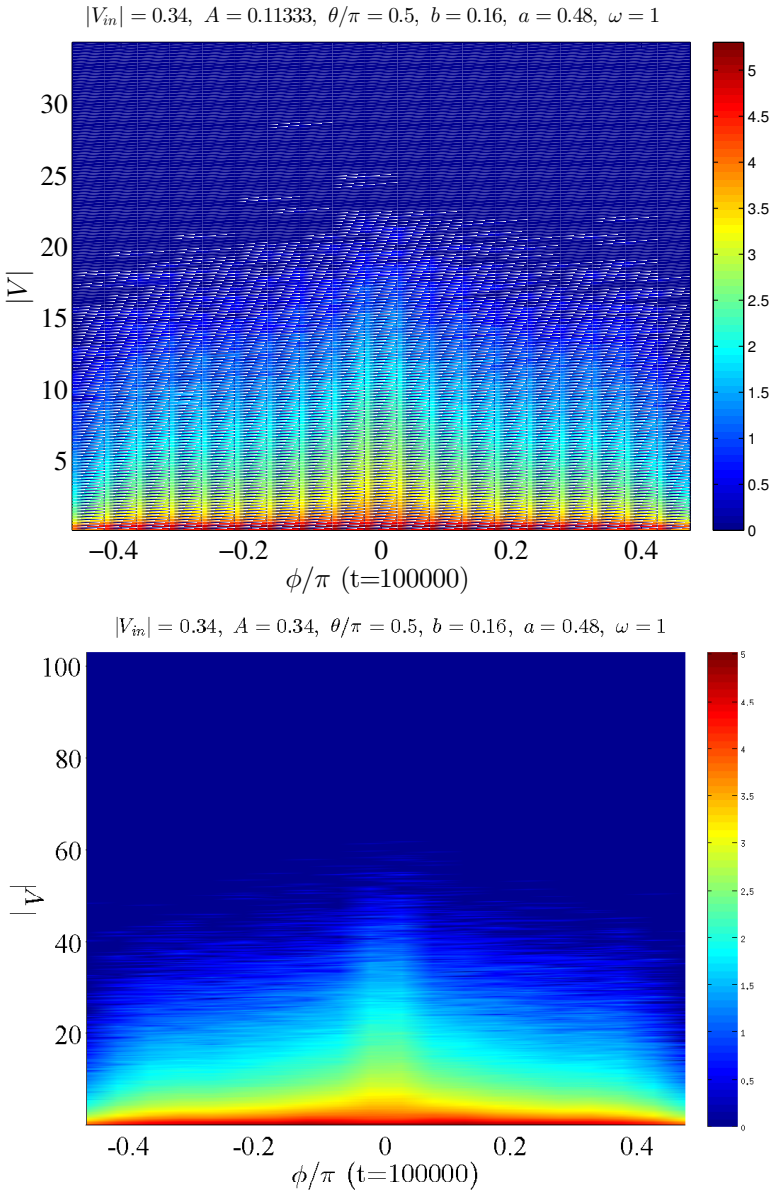

Figure 5.11.: Histogram of the direction angle and the magnitude of particle velocities upon exit from either end of the channel, for two different values of the amplitude of oscillation $A = \{0.282, 0.845\}$

5.4. Transmission coefficient

Due to the strong chaotic properties of the Lorentz gas in a finite horizon geometry, the transport properties can essentialy be described by means of a simple, that is uncorrelated, random walk [12, 13, 90, 91]. The infinite horizon however, due to the presence of ballistic corridors as explained in §5.1, the first moment of the distribution function of free lengths traveled between collisions diverges, and the description via a simple random walk is not possible. However, the transport properties can be investigated within the framework of Lévy flights [92] as shown in Ref. [91].

Despite the slow decay of the autocorrelation function of particle velocities with (dynamically) infinite horizon, we show that a quite accurate description of the transmission (reflection) coefficient can be achieved by means of a simple description offered by the simplest random walk model with finite memory, i.e. one-step memory. We stress however, that the success of this simple description is only pertinent to time-independent properties. In other words, a time-resolved description of the statistical properties of the DIH Lorentz channel cannot be given by means of a finite-memory stochastic process.

In the following we view the motion of the particles propagating in the Lorentz channel as the motion of independent random walkers moving on a linear chain. Each cell of the Lorentz channel will be mapped to the sites of this chain. We will further assume that the particles when interacting with a cell and are moving towards the right, they have a constant probability $p_{RR} = p$ of being transmitted and $p_{RL} = 1 - p$ to be reflected. On the other hand, when a particle is traveling towards the left, it has probability $p_{LL} = q$ to be transmitted and $1 - q$ to be reflected. In the context of the random walk theory, the process is thus equivalent to a discrete biased correlated (nearest neighbor) random walk (BCRW). The BCRW corresponds to a Markov chain of order $m = 1$, with the following transition probability matrix

$$\left(\begin{array}{c|cc} & \text{R} & \text{L} \\ \hline \text{R} & \text{p} & \text{1-p} \\ \text{L} & \text{1-q} & \text{q} \end{array}\right) \tag{5.1}$$

Our theoretical results within the random walk models are obtained employing a quantity known in the theory of stochastic processes as splitting probability. The latter is the probability a random walker reaching a specified site for the first time, without ever touching another specified boundary. This quantity can be analytically calculated in the context of the BCRW as a function of the transition probabilities [Eq. 5.1] and the length of the device, provided that the respective probabilities are space-independent [93].

However, as seen in Fig. 5.12 this is not the case in the open Lorentz channel, due to finite size effects. To resolve this complication, we have empirically found that the best description given by means of the BCRW is to use the mean value of each transition probability obtained numerically over the first 2/3ds of the channel—relative to the side of the device where particles are injected. The analytical solution for the splitting

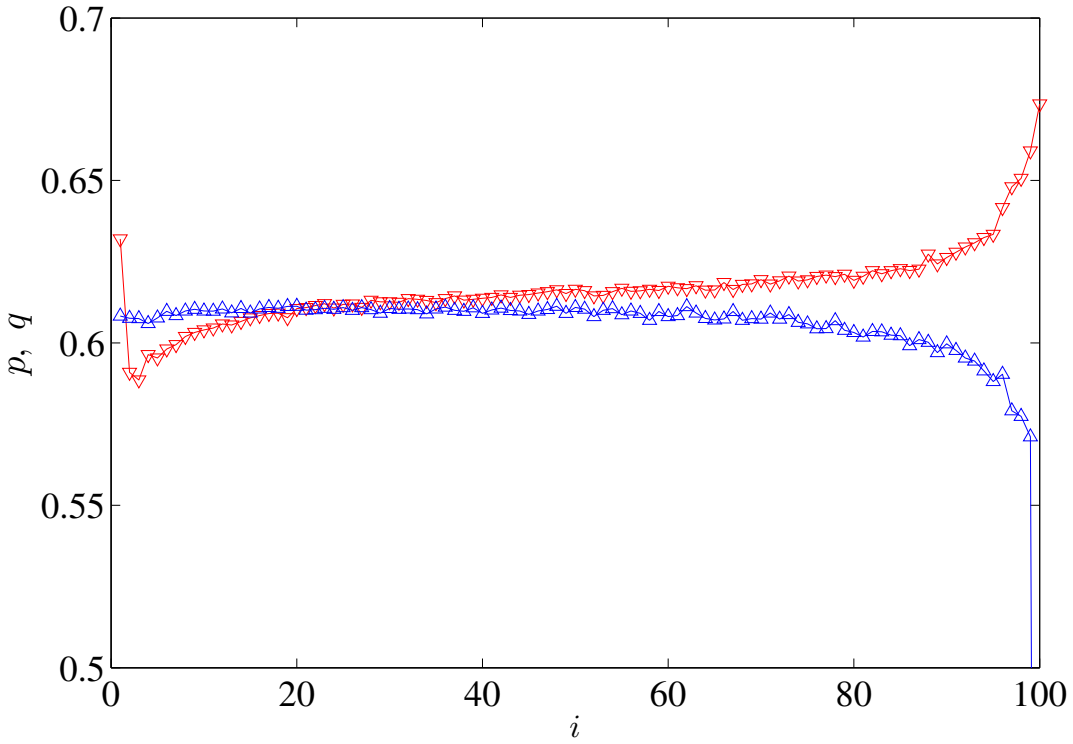

Figure 5.12.: The probability p (q) shown with red (blue) lines for particle to move towards the right (left), if at the previous step moved towards the right (left), as a function of the site number i.

probability of a random walker performing a BCRW with the transition probability matrix given by Eq. 5.1 is [93],

$$T = 1 - \frac{\mathrm{c1}(1-p)\left(\lambda^{k-1}-1\right) + \mathrm{c2}\left((1-p)\lambda^{k-1}-(1-q)\right)}{(1-p)\lambda^{k-1}+q-1}, \tag{5.2}$$

where $\lambda = q/p$ and $k = N+1$, N denoting the total number of sites (unit cells) of the device and c_1, $c_2 = 1-c_1$, the probability of the walker to move right(left) at the first step. We further compare the results of the BCRW with the corresponding obtained by a biased random walk (BRW)—with no memory—and the exact numerical results obtained by the simulation of the system dynamics. To obtain the transmission coefficient within the BRW, we again use a site-independent probability of moving right

or left by averaging over the numerically calculated corresponding probabilities per site. In this case, we have empirically found that the best description is attained, if we average over the first 5/9ths of the channel.

As we can see in Figs. 5.13-5.15. the BCRW succeeds remarkably well in predicting the transmission coefficient of the device, despite the fact that the geometry considered leads to a DIH. A cruder approximation can also be achieved using a BRW.

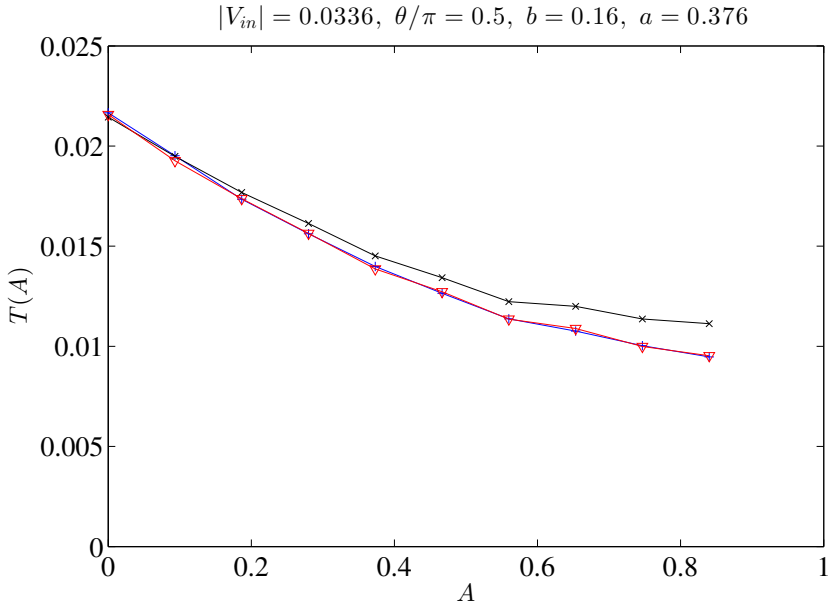

Figure 5.13.: The transmission coefficient T of the device as a function of the amplitude of oscillation A. The results obtained by the exact simulation, the BCRW and the BRW are shown with blue upright crosses, red downright triangles and black diagonal crosses, respectively. The parameters of the system are shown on the top of the figure.

We would also like to draw the attention of the reader to the fact that, as Figs. 5.13, 5.14 suggest, the variation of the driving parameters of the device has a strong impact on the intensity of the outgoing beam. This becomes more intense, if the incoming particles has a low energy content, i.e. the mean initial absolute velocities of the injected particles being much smaller than the maximum velocity of the disks.

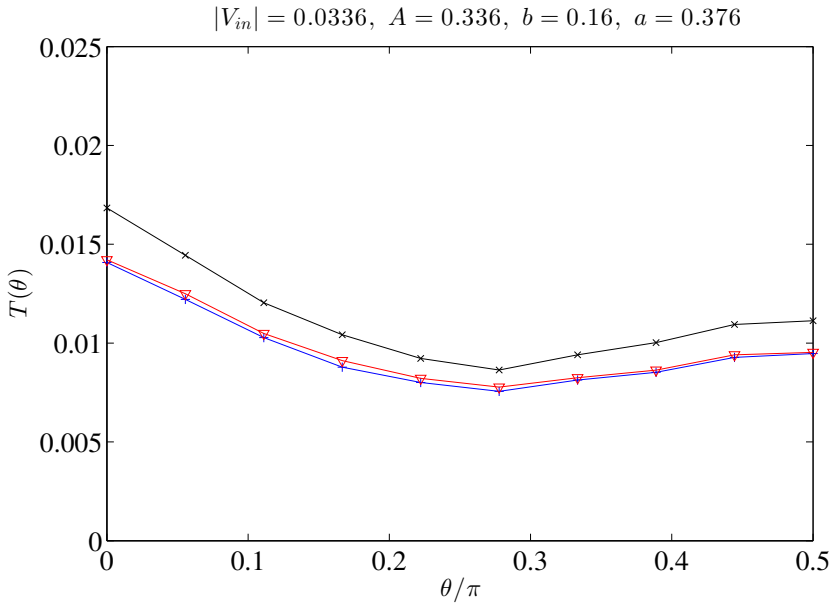

Figure 5.14.: The transmission coefficient T of the device as a function of the angle of oscillation θ. The results obtained by the exact simulation, the BCRW and the BRW are shown with blue upright crosses, red downright triangles and black diagonal crosses, respectively. The parameters of the system are shown on the top of the figure.

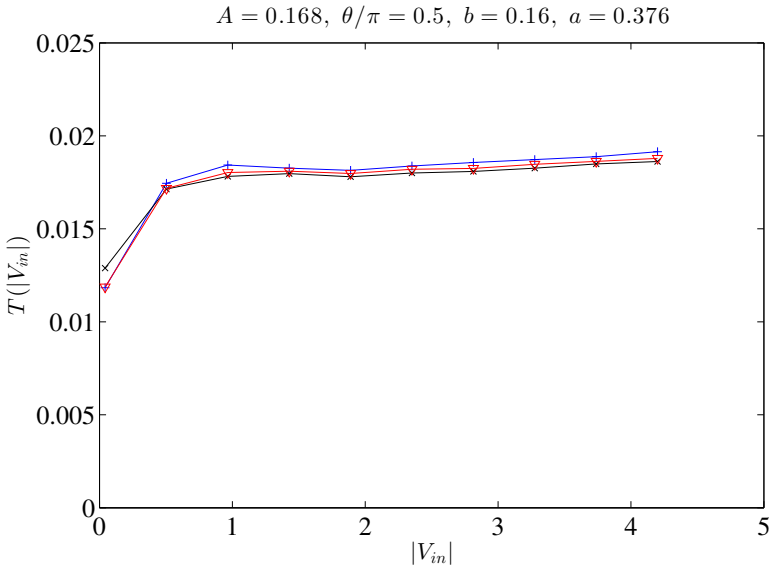

Figure 5.15.: The transmission coefficient T of the device as a function of the magnitude of velocities of the incoming particles V_{in}. The results obtained by the exact simulation, the BRW and the BCRW are shown with blue upright crosses, red downright triangles and black diagonal crosses, respectively. The parameters of the system are shown on the top of the figure.

6. Aspects of self-organized criticality in the infinite Lorentz channel

In the following, the concept of the dynamically infinite horizon (DIH) in driven billiards, briefly discussed in the previous chapter, is elucidated and substantiated. The study of the infinite driven Lorentz channel (LC) setups with DIH, as well as of the static system with infinite horizon (IH), reveals that long-range correlations between the propagating particles emerge. We conclude that the origin of these interparticle long-range correlations is the intermittent dynamics associated with the existence of ballistic corridors in the single particle phase space, constituting the (D)IH. Finally, in the context of the driven LC, we show that Fermi acceleration makes possible the synchronization of the particle motion with the periodic appearance of the ballistic corridors, leading to a DIH, irrespective of the initial conditions considered. The particle ensemble then acquires characteristics of self-organization as the weight of the phase space regions leading to critical behaviour increases with time. In this sense, the driven LC is reminiscent of self-organized critical systems.

6.1. Description of the system

We consider the dynamical system described in §5.1 in the limit of infinite length, in order to supress finite-size effects. As in the case of the open driven LC, the central disks of the device with radii b are allowed to oscillate with amplitude A and angular frequency ω. Without loss of generality, provided that the flat segments between the static discs are small enough to prohibit bouncing orbits in the y direction [1], we choose the radii of the static semi-circles $a/w = 0.48$, where w is the lattice constant. In the following distance and time is measured in units of w and $1/\omega$, respectively. Our study is focused in the parameter regime within which all possible paths parallel to the x-axis,

[1] This would lead to intermittent dynamics within a unit cell, which is irrelevant for the subsequent discussion.

through which a particle can perform arbitrarily long free flight, are periodically blocked by the motion of the driven scatterers. Consequently, the manifestation of arbitrarily long jumps of the propagating particles in these parameter regime becomes non-trivial.

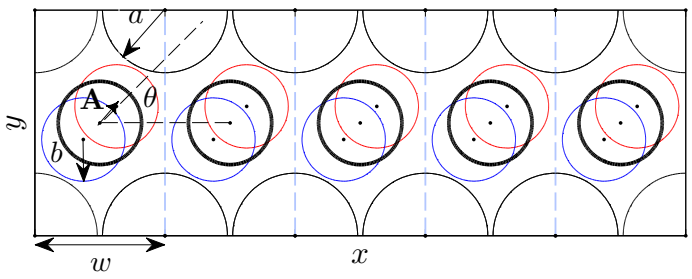

Figure 6.1.: Schematic of the billiard geometry. The central scatterers of radius b are driven harmonically, while the scatterers with radius a remain fixed. **A** and θ are the amplitude and angle of oscillation, respectively. The system is infinite in the x direction, while in the y direction two hard flat boundaries are placed at $\pm\sqrt{3}w/2$, confining the motion of the particles in this direction.The oscillating disks are depicted in their equilibrium positions (black circles) together with the turning point positions (blue and red circles).

6.2. Statistical properties

Inspired by the success of the random walk model in predicting the transmission coefficient of the open LC, presented in §5.4, we use the same coarse-grained description of the dynamics in the driven LC, so that the system can be mapped to a one-dimensional chain. This is achieved by integrating out the motion of the particle inside a unit cell [marked by dashed blue vertical lines in Fig. 6.1] (intra-cell dynamics). Therefore, the focus is solely on the inter-cell properties of particles' motion. At this level the key quantity characterizing the dynamics of the particle is the probability $P(N)$ of travelling N cells between events which lead to a change in the direction of motion. If the horizon is finite, i.e. $\sqrt{3}/2 - a \leq b$, then the system exhibits normal diffusion which can be quite accurately approximated by a simple random walk, with a nearest neighbour jump probability $p = 1/2$. In this case, $P(N)$ decays exponentially, i.e. $P(N) \propto 2^{-N}$. On the contrary, if ballistic corridors open up, the probability of long free flights between

collisions is greatly enhanced, resulting in an algebraic decay, $P(N) \propto N^{-3}$ [91, 94].

In Fig. 6.2(a) we present numerical results for $P(N)$ in the driven LC obtained by the simulation of an ensemble, initially distributed along a semi-circle close to a static scatterer with uniform direction angles ϕ with respect to the x-axis. We stress that the radii of the central disks are chosen minimal for the time-independent LC to possess a FH.

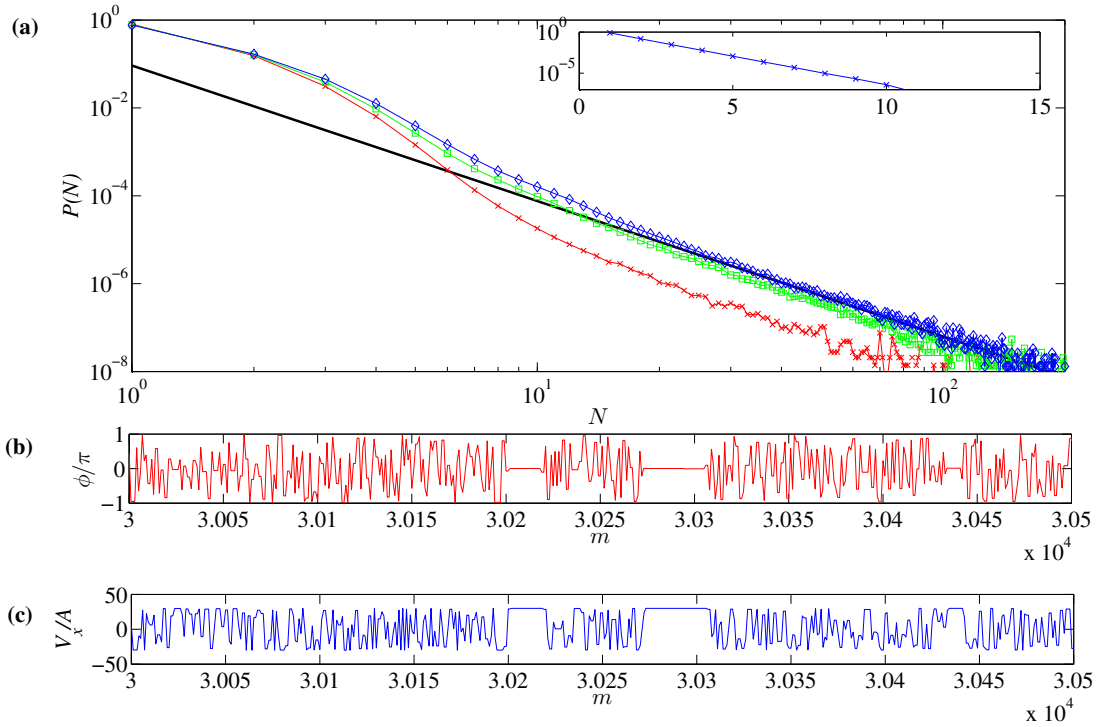

Figure 6.2.: (a) The probability $P(N)$ of crossing N cells without changing direction of motion with $b = \sqrt{3}/2 - a \approx 0.386$, $|\mathbf{A}| = 1/2 - b$ and $\theta = 0$ [inset], $\theta \approx 0.11$ [red diagonal crosses], $\theta \approx 0.28$ [green open squares] and $\theta = 0.5$ [blue diamonds]. The magnitude of the initial particle velocities is fixed to $|\mathbf{V}_0| = A/10$. (b) The angle of the corresponding total velocity with the x-axis) ϕ and (c) the velocity component V_x versus the discretized time variable m.

For $\theta = 0$, in which case a particle cannot cross a cell without performing a collision, the numerical findings corroborate the exponential decay. On the contrary, for $\theta \neq 0$, which is the condition for the existence of dynamically open ballistic corridors, $P(N)$ shows a power-law tail. However, for small N, $P(N)$ is still exponential, due to the dominance of diffusive transport. The value of N for which the crossover from exponential to power-law behaviour takes place depends on θ, while the slope of the power-law tail is θ-independent. Fitting $P(N)$ with the model $P(N) = \alpha N^{\beta}$ [solid black line in Fig. (2.10a)] yields $\beta \approx -3$. Therefore, long unidirectional motion in the driven LC

shares the same behaviour for $N \gg 1$ with the free flights in the static LC with IH. This

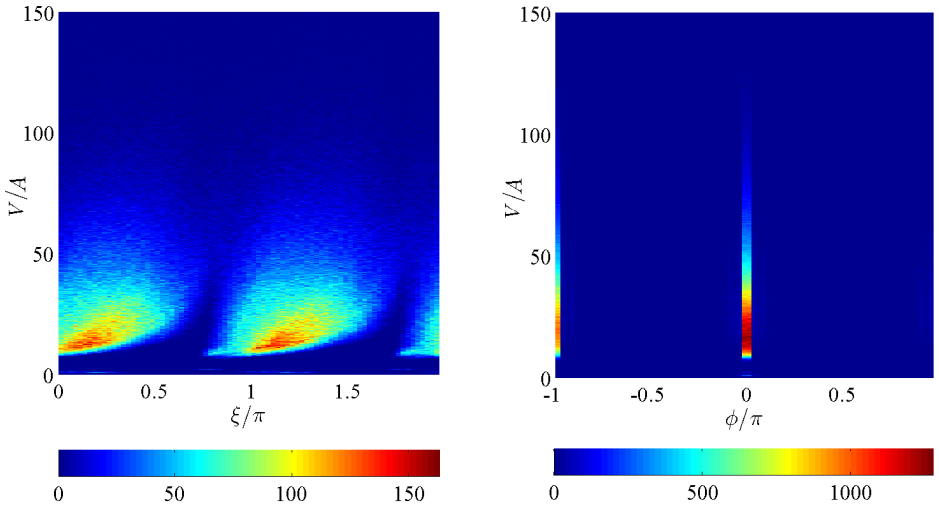

Figure 6.3.: (a) The 2-D histogram of (V, ξ) pairs leading to collisionless ballistic flights crossing from 10 to 40 cells ($V = |\mathbf{V}|$ is the velocity magnitude of a trajectory and ξ is the oscillation phase of the central disk). (b) As in (a) using (V, ϕ) pairs

fact forces us to conclude that, for $\theta \neq 0$, the particles synchronize with the oscillation of the central disks, such that long collisionless flights become possible. A detailed trajectory analysis verifies this, showing that the direction and the speed of the propagating particles must attain specific values determined by the disk oscillation in order to perform these long unidirectional collisionless flights as shown in Fig. 6.3(b),(c). Moreover we observe that the corresponding cell to cell motion is intermittent. This is illustrated in Fig. 6.2(b), (c), where the direction angle ϕ of a particle and the x-component of the velocity are shown as a function of the coarse-grained time variable m, which increases by one, either upon collision with the billiard's boundaries, or upon crossing the border between neighbouring cells. Trajectories exhibit phases of chaotic motion, where the direction angle fluctuates rapidly, interrupted by regular (ballistic) motion. From a dynamical point of view, this corresponds to a transition from the hyperbolic areas, owing to the convex geometry of the billiard's boundary, to areas close to the regular part of the phase space, corresponding to long free flights. The regular part of the phase space exists in the high energy regime for certain combinations of the phase of oscillation ξ of the moving disks and the direction of the velocities of the particles quantified by ϕ (see Fig. 6.3(a), (b)).

An interesting analogy can be drawn between the driven LC and the well-known sandpile model [95] (for a review see Ref. [96]). Out of equilibrium the redistribution of grains in the sandpile model can be described by a diffusion equation [97, 98]. However,

when the sandpile reaches equilibrium the diffusion coefficient diverges and grains are redistributed with avalanches, the probability of the number of sites participating in such events obeying a power-law. In the driven LC the inter-cell motion of the particles can be described by a random walk, if the absolute value of the particle velocities is smaller than a cutoff value, dependent on the details of the LC, such that they cannot cross a cell without performing a collision with the moving disks. In a finite time however, due to Fermi acceleration, a subset of the ensemble of the particles propagating through the device will visit the areas of the phase space corresponding to fast ballistic motion. Consequently the particle dynamics will become intermittent and the simple random walk picture breaks down. The long (Lèvy) flights without collisions lead to the divergence of the diffusion coefficient. Similar to the time-independent LC with infinite horizon [91], in both cases the second moment of the jump probability is infinite. A manifestation of the Lèvy type statistics is the appearance of the power-law tail of $P(N)$, reminiscent to the appearance of avalanches in the sandpile SOC model. For the driven LC criticality is established through the dynamical formation of ballistic corridors implying the synchronized particle-disk motion, which depends on the geometrical details of the set-up and the characteristics of the time-law of the driving. If Fermi acceleration is operational, then the critical state increasingly gains measure (this can be seen in Fig. 2.10(c)), without the need of a fine-tuning of the external parameters. To be able to study the robustness of the critical state under the variation of system parameters, we construct a complexity measure C, which is the product of two terms [99]: the first term is the quadratic distance of $P(N)$ from the exponential behaviour expected for a fully hyperbolic system; the second term quantifies the amount of information —in the Shannon sense— stored in the system, not necessarily related to complex behaviour:

$$\begin{aligned} C &= -\lim_{M\to\infty}\sum_{N=1}^{M}\left[\log\left(P(N)\right)-\log\left(\frac{2^{-N}}{1-2^{-M}}\right)\right]^2\times \\ &\quad \sum_{N=1}^{M}\frac{P(N)\log(P(N))}{\log(M)}. \end{aligned} \tag{6.1}$$

To obtain a normalized complexity measure $\tilde{C}$, C is divided by its maximum value in each case. By construction $\tilde{C}$ is positive definite, maximizes when the probability of the occurrence of long collisionless flights becomes maximum and tends to zero when the motion of particles in the systems is completely chaotic.

In Fig. 6.4, we present contour plots of the measure $\tilde{C}$ as a function of the radii b of the oscillating disks and the angle of oscillation θ. In Fig. 6.4(a), the oscillation of the central disks is synchronous, whereas in Fig. 6.4(b) the initial phases of the oscillating disks

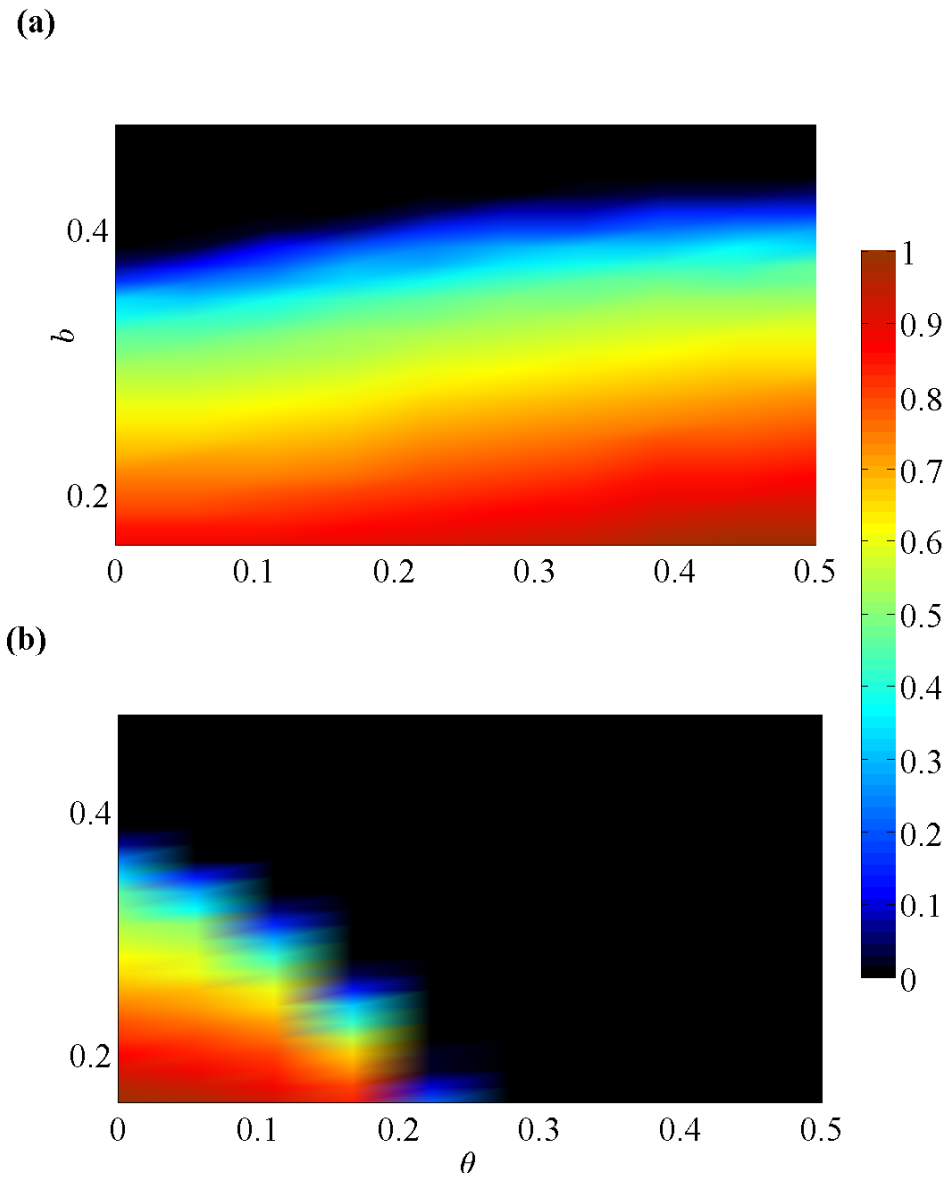

Figure 6.4.: Contour plot of $\tilde{C}$ for 25 different values of b and 10 values of θ. The black area corresponds to the non-critical state (exponential $P(N)$). (a) Synchronous oscillations of the central disks, (b) uniformly distributed random initial phases. We use $|\mathbf{A}| = 1/2 - b$.

are randomly chosen in the interval $[0, 2\pi)$. As seen in Fig. 6.4(a), the system always reaches the critical state, independently of the initial energy of the ensemble, unless the parameters of oscillation and the radius b are such that ballistic corridors remain closed for all times. On the contrary, when the initial phases are randomly chosen dynamically open ballistic corridors cannot appear. Therefore, in this case ballistic corridors exist only in the static sense, i.e. corridors remain continuously open despite the motion of the central disks. Thus, from geometrical considerations, the "phase boundary" is $\sqrt{3} - 2a - (1 - 2b)\sin\theta - 2b = 0$.

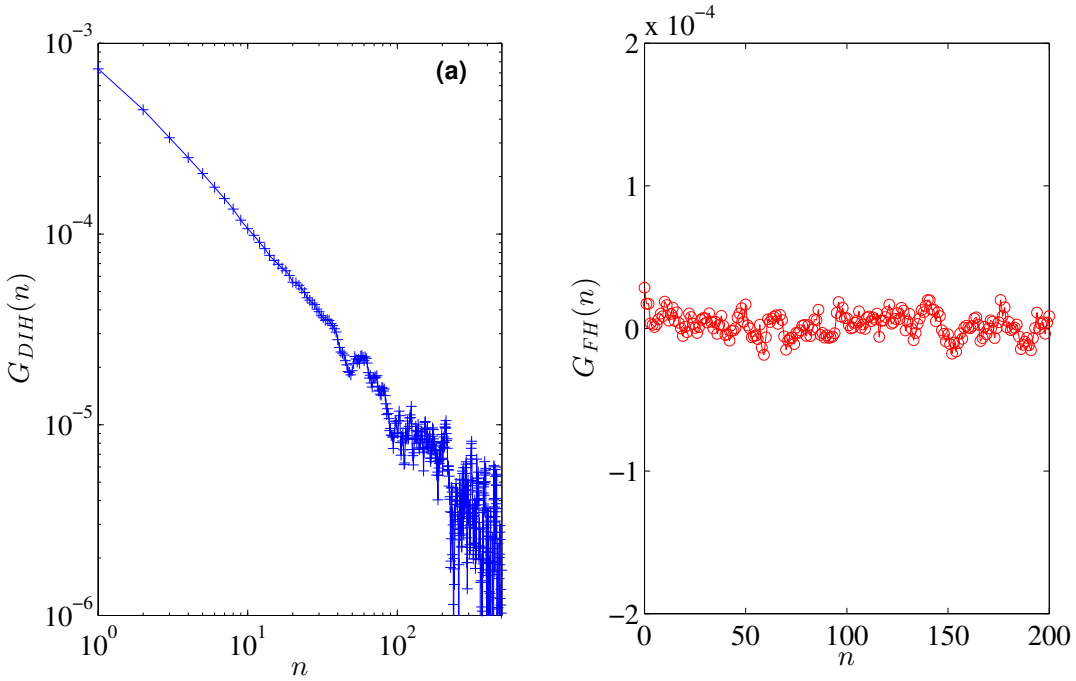

Figure 6.5.: (a) Cross-correlation function G_{DIH} of independent trajectories in a DIH setup, for $b = 0.16$. (b) $G_{\mathrm{FH}}(n)$ for a FH set-up with $b = a = 0.48$.

The landmark of criticality is the existence of power-law cross-correlations between the members of a statistical ensemble. However, in the LC a direct computation of the cross-correlations on the basis of the microscopic dynamics is futile, due to the chaotic background induced by the strong hyperbolicity of the system. To overcome this obstacle, we perform a symbolic dynamics analysis by introducing a coarse-graining. Specifically, we partition the phase space into two subsets: The part close to $(\phi \mod \pi) \leq \delta\phi$, $\delta\phi \ll 1$, leading to a cell crossing without a collision, which we call laminar small phi (LSP) region, and its complement, the chaotic region. In this fashion we construct trajectories assigning, in each cell crossing, a binary symbol s which takes the value 0 if the trajectory crosses the cell without having performed any collision in the preceding cell and the value 1 otherwise. In Fig. 6.5(a) we present the mean value of the correlation

function $G(m) = \left(\frac{1}{N_s}\right) \langle \sum_{n=1}^{N_s} (s_{i,n} - \langle s_i \rangle)(s_{j,n+m} - \langle s_j \rangle)/(\sigma_{s_i}\sigma_{s_j}) \rangle$, obtained by averaging over 1.99×10^4 pairs of sequences i, j starting from different initial conditions, containing $N_s = 5 \times 10^6$ symbols each. Here $\sigma_{s_{i,j}}$ denotes the standard deviation of the i, jth trajectory, whereas $\langle s_{i,j} \rangle$ stands for the corresponding mean value of the sequence. We observe that when the driven LC has a DIH (critical state) the cross-correlation function $G_{DIH}(n)$ decays algebraically. On the contrary, when the system is away from criticality (FH), the cross-correlation function G_{FH}, as shown in Fig. 6.5(b), fluctuates around zero. Given that the particles propagating through the LC are non-interacting, the question arises as to how critical cross-correlation can emerge. It can be rigorously shown that intermittency leads to power-law cross-correlations, if the first moment of the distribution of laminar lengths, i.e. the time spent in the laminar region, diverges. In the LC, this condition is not met in a straightforward manner, as the probability of N unidirectional steps—notice that these steps in general involve collisions—decays as N^{-3}, and consequently the first moment is finite. To clarify this apparent contradiction we calculate the conditional probability $P(N|N_c)$ of remaining N time-steps in the LSP phase (i.e. without collisions) after having spent exactly N_c time-steps in the chaotic region before being injected in the LSP region. The results for various values of N_c are displayed in Fig. 6.6(a-b). One can clearly see in Fig 6.6(b), that for $N_c = 3$ (red crosses) $P(N|3)$ decays as N^{-3} which is the expected behaviour. In fact the results are almost identical for any $N_c > 2$. For $N_c = 2$ (blue triangles) $P(N|2)$ follows N^{-2} for small N and turns to N^{-3} for large N [see also Fig. 6.6(a)]. Finally for $N_c = 1$ (black crosses) $P(N|1)$ decays as N^{-2} and the corresponding mean time spent in the LSP region diverges inducing cross-correlations among the propagating particles. The microscopic origin of this behaviour is the connection of certain unstable periodic orbits with the fixed points in the laminar region, thereby rendering very possible highly aligned flights towards the x-axis after shorter ballistic jumps. An example of such a trajectory is given in Fig. 6.6(c). We see that the particle after performing quite a few collisions close to unstable periodic orbits, it finally enters the LSP suffering a single collision in the chaotic region prior to its entrance (the point where the blue line ends and the red one begins).

6.3. Final remarks

In conclusion, we have shown, using symbolic dynamics defined by an appropriate phase space partitioning, that strong intermittency (or sporadicity) [100] induces power-law (critical) cross-correlations between non-interacting particles propagating in the LC. The

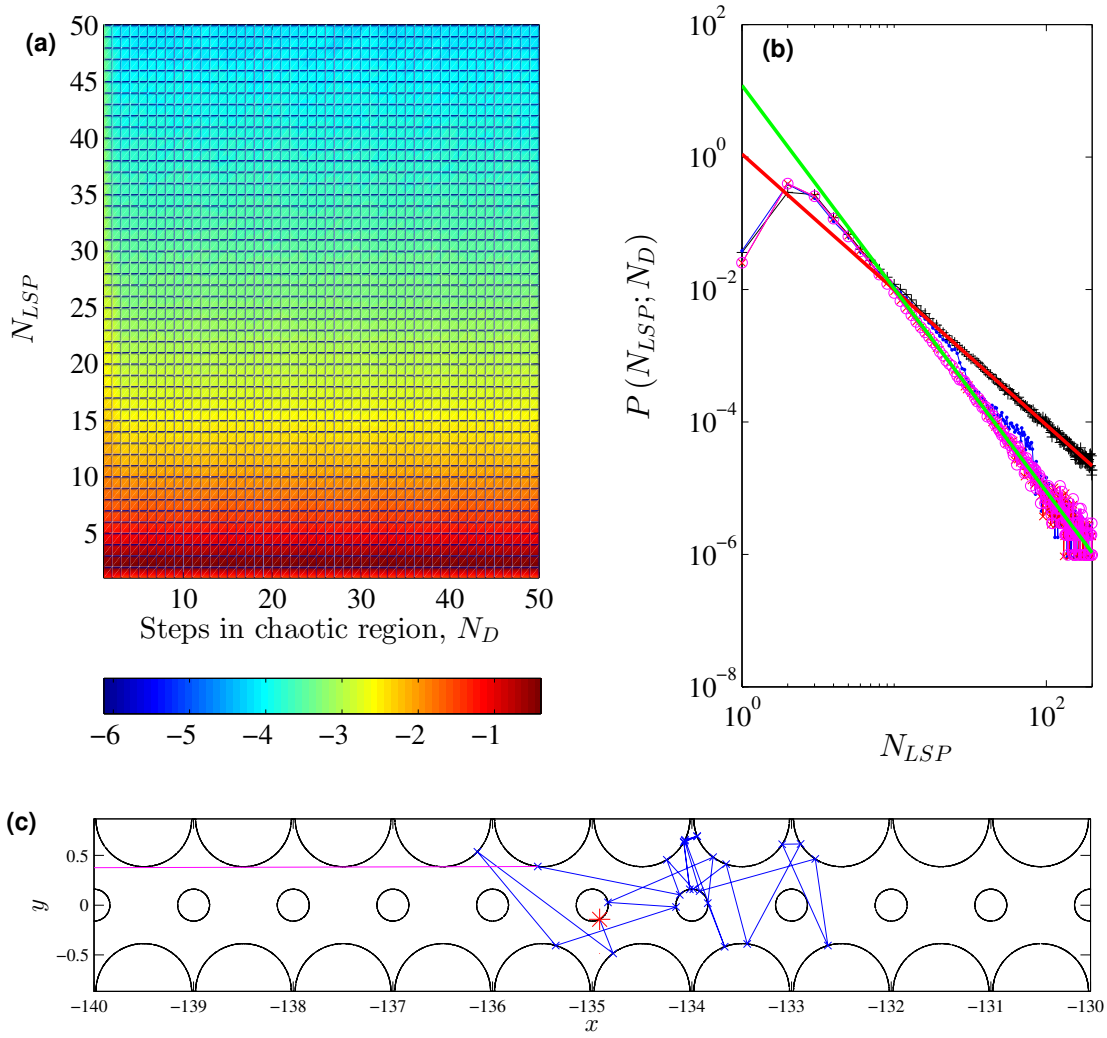

Figure 6.6.: (a) The contour plot of the conditional probability $P(N|N_c)$ for various values of N_c and (b) for $N_c = 1$ (black crosses), $N_c = 2$ (blue triangles) and $N_c = 3$ (red crosses). The red (green) line has slope -2 (-3) in log-log scale. In panel (c) a typical trajectory suffering a single collision in the cell it enters the LSP—where the blue line ends and the red begins—where it performs a very long free flight. The initial position is denoted with a red asterisk.

interrelation of intermittent dynamics and critical behaviour has already been pointed out in Ref. [101], in the framework of the 3D Ising model. However, herein the mechanism leading to power-law cross-correlations is reduced to its basic ingredients, due to the absence of any inter-particle interaction in the considered ensemble. This goes one step beyond the model of self-driven particles [102, 103], where inter-particle interactions are substituted by certain rules, leading to correlations. In this sense, our work sheds new light on the emergence of power-law correlations and criticality in dynamical systems in general.

7. Concluding remarks

In this final chapter, we summarize the main results presented in the thesis and draw some final conclusions.

Our study of the FUM led to the development of a novel simplifying approximation, dubbed the hopping wall approximation (HWA), for the study of time-dependent billiards. We showed that the HWA succeeds into reproducing very accurately the results obtained using the exact dynamical equations, while at the same time is computantionally efficient, and even more, it allows an analytical treatment of Fermi acceleration. The use of the HWA in the FUM and the driven Lorentz channel, revealed that the scatterer displacement, which is routinely neglected in the literature, produces a systematic effect in the acceleration process, even if the movement of scatterers is randomized. Specifically, the displacement of the scatterer leads to an increased acceleration compared to that observed when employing the standard approximation used up to this date in the literature. The increase in the acceleration observed in the FUM is related to small additional fluctuations of the time of free flight of the particles caused by the displacement of the disk. These fluctuations act *systematically* and lead to more energy gain or less energy loss in each collisional event. In the case of the driven Lorentz gas it was shown that a similar mechanism is at work, leading again to an increase in particle acceleration. Specifically, the displacement of the disks upon collision not only affects the time of the free flight of the particles, but it also alters the incident angle a and the azimuthal angle ϕ in such a way that leads again to more energy transfer from the disk to the particle and less energy loss.

We then turned our attention to the methods used until now, for the investigation of Fermi acceleration —in the class of time-dependent billiards in which it develops. In this context, the evolution of the density of particle velocities is determined by the application of the Fokker-Planck equation. However, its derivation is always based on assumptions and approximations that rarely can be justified. Moreover, its prediction power is limited in the long-term statistics of the system and no information is given for the transient behaviour. Even more, its use in the SFUM, which is the first system

that was successfully investigated with the use of the FPE, is completely redundant, as the CLT yields the same results in a far more straightforward manner.

As a means for resolving these issues, we proposed a consistent methodology, which obviates unclear assumptions and even more, can give an accurate description of the transient evolution of particle velocities. The cornerstone of this methodology is the use of the Chapman-Kolmogorov equation. The fundamental difference in comparison with the traditional approach using the FPE, is that no assumption for the continuity of the stochastic process describing Fermi acceleration needs not to be made. Another advantage of the proposed approach is that all collision events can be taken into account, which cannot be done in the construction of the FPE, and even when possible, it can lead to less accurate results. The method was successfully applied to the standard simplified FUM and the exact model, showing how the effect of the motion of the wall in the configuration space can be included in the description of Fermi acceleration through the CKE.

The investigation of the distribution functions of particle velocities in the FUM revealed that irrespective of the specific driving of the billiard (sawtooth or harmonic) the same profile is obtained for $n \gg 1$, resembling a 2D Maxwell-Boltzmann distribution. Moreover, we have shown that the application of the generalization of the *hopping* approximation leads to a similar profile for the PDF in the case of higher dimensional billiards, such as the phase randomized harmonically driven Lorentz Gas, in which case it was shown that the PDF of the particle velocities is again Maxwell-Boltzmann-like (only in this case corresponding to a higher dimensional system). Another interesting aspect of this finding is that, though in the randomized FUM and in the driven Lorentz gas no steady state of the distribution of the particle velocities exists, in all circumstances, i.e. independently of the specific billiard and driving, all the corresponding PDFs converge to a similar profile.

The numerical study of the open Lorentz channel, provided convincing evidence for the existence of non-trivial non-equilibrium steady states, independently of the dynamical or geometrical system parameters. Furthermore, we provided a minimal random walk model, which despite its simplicity, succeeds in describing the most prominent transport coefficient, i.e. the transmission coefficient of the device. Moreover, we introduced a new classification scheme for time-dependent billiards in general.

Finally, the study of the Lorentz channel in the thermodynamic limit revealed that power-law (critical) correlations emerge between the propagating particles. The key property leading to criticality is intermittency, which, combined with ergodicity, generates power-law cross-correlations. Intermittency implies the mixing of ordered with chaotic parts of trajectories at all time-scales, while ergodicity is responsible for trans-

ferring trajectory properties to the statistical ensemble. In this sense, these results shed new light on the emergence of power-law correlations and criticality in dynamical systems in general. Finally, in the driven Lorentz channel with dynamically infinite horizon, we demonstrated a novel role of Fermi acceleration as an effective driving force steering an ensemble of propagating particles towards the critical state, inducing this way characteristics of self-organization.

Appendices

A. Solution of the FPE in the sawtooth driven FUM

The evolution of the PDF can be described as a diffusion process in momentum space. Therefore, the PDF can be obtained by solving the Fokker-Planck equation,

$$\frac{\partial}{\partial n}\rho\left(|V|,n\right)=-\frac{\partial}{\partial V}\left[B\rho\left(|V|,n\right)\right]+\frac{1}{2}\frac{\partial^2}{\partial V^2}\left[D\rho\left(|V|,n\right)\right] \tag{A.1}$$

where the transport coefficients B, D are,

$$B(V) = \left(\frac{1}{\Delta n}\right)\int \Delta|V|P\; d(\Delta|V|) \tag{A.2a}$$

$$D(V) = \left(\frac{1}{\Delta n}\right)\int (\Delta|V|)^2P\; d(\Delta|V|) \tag{A.2b}$$

In Eqs. (A.2) P is the probability of a particle possessing the velocity $|V|$ if it had the velocity $|V|-\Delta|V|$, Δn collisions earlier. Assuming that $\Delta n = 1$, Eqs. (A.2) become $B(V)=\langle\delta|V|\rangle$ and $D(V)=\langle(\delta|V|)^2\rangle$, where $\langle\delta|V|\rangle$ is the mean increment of the magnitude of the particle velocity during one mapping period, i.e. in the course of one collision. From Eq. (2.1) it follows that $|V_{n+1}|=|V_n|\pm 2u_n$, depending on the wall (left or right) with which a particle collides. Thus,

$$\Delta|V|=\pm 2u_n \tag{A.3}$$

The evolution of the PDF in a randomized billiard, as discussed in Sec. II E, can be determined by the Fokker-Planck (F-P) equation. Therefore, to determine $\langle\frac{1}{|V|}\rangle$ as a function of the number of collisions, n, we must first obtain the PDF by solving the F-P equation,

$$\frac{\partial}{\partial n}\rho\left(|V|,n\right)=-\frac{\partial}{\partial V}\left[B\rho\left(|V|,n\right)\right]+\frac{1}{2}\frac{\partial^2}{\partial V^2}\left[D\rho\left(|V|,n\right)\right] \tag{A.4}$$

where the transport coefficients B, D are,

$$B(V) = \left(\frac{1}{\Delta n}\right)\int \Delta|V|P\ d(\Delta|V|) \tag{A.5a}$$

$$D(V) = \left(\frac{1}{\Delta n}\right)\int (\Delta|V|)^2 P\ d(\Delta|V|) \tag{A.5b}$$

Assuming $\Delta n = 1$ the coefficients B, D coincide with the mean particle velocity increment $\delta|V|\rangle$ and the square of the particle velocity increment $\langle(\delta|V|)^2\rangle$, respectively, whereas, $\delta|V|$ is given by Eq. (A.3). Therefore, to determine the F-P coefficients, the average of the wall velocity, $\langle\langle u_n\rangle\rangle$ and $\langle\langle u_n^2\rangle\rangle$ over the oscillation phase must be calculated. Following the steps thoroughly discussed in Sec. II D, one finds:

$$B = \langle\delta|V|\rangle = 2\frac{u_0^2}{|V|}\left(\frac{1}{a} + \frac{4}{b-a} + \frac{1}{1-b}\right) \tag{A.6a}$$

$$D = \langle(\delta|V|)^2\rangle = 4u_0^2\Bigg[\left(\frac{1}{a} + \frac{4}{b-a} + \frac{1}{1-b}\right) + \frac{u_0}{|V|}\left(\frac{1}{a^2} - \frac{8}{(b-a)^2} + \frac{1}{(1-b)^2}\right)\Bigg] \tag{A.6b}$$

Assuming the amplitude of wall velocity is small, $u_0 = \frac{A}{T} \ll 1$ and at the limit of high particle velocities $V \gg 1$ the first term on the r.h.s. of Eq. (A.6b) dominates and the coefficient $D(|V|)$ becomes asymptotically equal to:

$$D \simeq 4u_0^2\left(\frac{1}{a} + \frac{4}{b-a} + \frac{1}{1-b}\right) \tag{A.7}$$

Assuming reflective boundary conditions at $|V| = 0$ the solution of Eq. (A.4) is:

$$\rho(|V|, n) = \frac{|V|}{\sigma^2}e^{-|V|^2/(2\sigma^2)} \tag{A.8}$$

where

$$\sigma = \sqrt{4u_0^2\left(\frac{1}{a} + \frac{4}{b-a} + \frac{1}{1-b}\right)n + \frac{|V_0|^2}{2}}$$

Thus, $\langle\frac{1}{|V_n|}\rangle$ as a function of the number of collisions, n, reads:

$$\langle\frac{1}{|V_n|}\rangle = \sqrt{\frac{\pi}{2}}\frac{1}{\sigma} \tag{A.9}$$

B. Calculation of the variance of particle speeds in the FUM

In order to estimate the variance, one uses the separation of the collision events into the sets C_1 and C_2 described in detail in Chapter 2 [§2.3.2, Eq. (2.34)]. Substituting $|V_n| = -V_n$ in Eqs. (2.36) and raising to the square we obtain

$$[(\delta V_n)_1]^2 = 4u_n^2 \tag{B.1a}$$

$$[(\delta V_n)_2]^2 = 4\left(V_{n-1}^2 + u_n^2 + 2u_n V_{n-1}\right) \tag{B.1b}$$

where $[(\delta V_n)_i]^2$ $(i = 1, 2)$ stands for the square change of the particle velocity upon the nth collision, which belongs to the set C_i $(i = 1, 2)$. The ensemble mean value of $(\delta V_n)^2$ can be obtained as the weighed sum of the square of the ensemble mean change of particle velocities calculated within each set C_1 and C_2.

$$\langle(\delta V_n)^2\rangle = w_1(n)\langle[(\delta V_n)_1]^2\rangle + w_2(n)\langle[(\delta V_n)_2]^2\rangle \tag{B.2}$$

where $w_i(n)$ $(i = 1, 2)$ stands for the statistical weight of the collisions which belong to the set C_i $(i = 1, 2)$.

Let $p_1(\xi, n)$, $p_2(\xi, n))$ and $p(\xi, n)$ denote the PDFs of the phase $\xi = t+\eta$ upon the nth collision event, which belongs to the set of events C_1, C_2 and $C \equiv C_1 \cup C_2$, respectively. Averaging over the phase ξ upon collision yields

$$\langle\langle[(\delta V_n)_1]^2\rangle\rangle = 4\int_0^{2\pi} p_1(\xi, n)u_n^2 d\xi \tag{B.3a}$$

$$\langle\langle[(\delta V_n)_2]^2\rangle\rangle = 4\Big(\langle\langle V_{n-1}^2\rangle\rangle_2 + \int_0^{2\pi} p_2(\xi, n)u_n^2 d\xi + 2\langle\langle V_{n-1}\rangle\rangle_2 \int_0^{2\pi} p_2(\xi, n)u_n d\xi\Big) \tag{B.3b}$$

In Eqs. (B.3), the notation $\langle\langle\ \rangle\rangle$ denotes phase averaging. The ensemble mean square change of particle velocities within each set C_i $(i = 1, 2)$ is obtained after integrating

Eqs. (B.3) over the corresponding PDFs of particle velocities $\rho_i(V,n)$ $(i=1,2)$;

$$\langle[(\delta V_n)_1]^2\rangle = 4\int_0^{2\pi} p_1(\xi,n)u_n^2 d\xi \tag{B.4a}$$

$$\langle[(\delta V_n)_2]^2\rangle = 4\Big(\langle V_{n-1}^2\rangle_2 + \int_0^{2\pi} p_2(\xi,n)u_n^2 d\xi + 2\langle V_{n-1}\rangle_2 \int_0^{2\pi} p_2(\xi,n)u_n d\xi\Big) \tag{B.4b}$$

The substitution of Eqs. (B.4) in Eq. (B.2) gives

$$\langle(\delta V_n)^2\rangle = 4\int_0^{2\pi} \left(w_1(n)p_1(\xi,n) + w_2(n)p_2(\xi,n)\right) u_n^2 d\xi + 4w_2(n)\left(\langle V_{n-1}^2\rangle_2 + 2\langle V_{n-1}\rangle_2 \int_0^{2\pi} p_2(\xi,n)u_n d\xi\right) \tag{B.5}$$

By virtue of Eq. (2.44), the first term on the RHS of Eq. (B.5) is equivalent to $\int_0^{2\pi} p(\xi,n)u_n^2 d\xi$, where $p(\xi,n)$ is the phase upon all types of collisions. As discussed in Sec. III B, $p(\xi,n)$ is a uniform distribution in the interval $[0,2\pi)$ and moreover is independent of the number of collisions n. Therefore the first term on the RHS of Eq. (B.5) yields

$$4\int_0^{2\pi} \left(w_1(n)p_1(\xi,n) + w_2(n)p_2(\xi,n)\right) u_n^2 d\xi = 2\epsilon^2 \tag{B.6}$$

Furthermore, there is an upper limit in the value of the velocity or square velocity average with respect to the set C_2 in Eq. (B.5), since the magnitude of velocity in this set is always less or equal to 2ϵ. Therefore the expansion of $\langle V_{n-1}\rangle_2$ and $\langle V_{n-1}^2\rangle_2$ with respect to n must involve only terms of the form $\frac{1}{n^\beta}$ with $\beta \geq 0$. In addition, the statistical weight of the rare collision events $w_2(n)$, after a sufficiently large number of collisions n, so that Fermi acceleration is fully developed in the system, is a decreasing function of n, irrespective of the initial distribution of particle velocities. Thus, $\langle(\delta V_n)^2\rangle$ to the leading order is:

$$\langle(\delta V_n)^2\rangle = 2\epsilon^2 \tag{B.7}$$

C. Estimation of the mean particle energy increase the driven LG

Assuming that the amplitude of oscillation A is small compared to the radii of the scatterers R the change caused by disk displacement to the angle variables δa_n, $\delta\phi_n$ and to the free particle path δl_n is small, i.e. δa_n, $\delta\phi_n$, $\delta l_n \ll 1$. Therefore, after the substitution of Eqs. (4.13) and (4.15) in Eq. (4.11) we expand the r.h.s. of the resulting

equation to the leading order of δa_n, to obtain:

$$\begin{aligned}
\delta V_n^2 =& \frac{8\cos^2(\phi_n)\cos\left(\frac{l_n}{V_{n-1}}+\eta_n+t_{n-1}\right)\sec(a_n+\phi_n)\sin\left(\eta_n+t_{n-1}\right)\sin\left(\frac{l_n}{V_{n-1}}+\eta_n+t_{n-1}\right)\epsilon^3}{V_{n-1}} \\
&+ 4\cos^2(\phi_n)\cos^2\left(\frac{l_n}{V_{n-1}}+\eta_n+t_{n-1}\right)\epsilon^2 \\
&+ 4\cos(a_n)\cos(\phi_n)\sec(a_n+\phi_n)\sin\left(\eta_n+t_{n-1}\right)\sin\left(\frac{l_n}{V_{n-1}}+\eta_n+t_{n-1}\right)\epsilon^2 \\
&+ 4V_{n-1}\cos(a_n)\cos(\phi_n)\cos\left(\frac{l_n}{V_{n-1}}+\eta_n+t_{n-1}\right)\epsilon \\
&+ \delta a_n\Bigg[\frac{16\cos(\phi_n)\cos\left(\frac{l_n}{V_{n-1}}+\eta_n+t_{n-1}\right)\sec(a_n+\phi_n)\sin(\phi_n)\sin\left(\eta_n+t_{n-1}\right)}{V_{n-1}} \\
&\times\sin\left(\frac{l_n}{V_{n-1}}+\eta_n+t_{n-1}\right)\epsilon^3 + 8\cos(\phi_n)\cos^2\left(\frac{l_n}{V_{n-1}}+\eta_n+t_{n-1}\right)\sin(\phi_n)\epsilon^2 \\
&+ \frac{8R\cos^2(\phi_n)\cos\left(\frac{l_n}{V_{n-1}}+\eta_n+t_{n-1}\right)\sec(a_n+\phi_n)\sin(\phi_n)\sin\left(\frac{l_n}{V_{n-1}}+\eta_n+t_{n-1}\right)\epsilon^2}{V_{n-1}} \\
&- 4\cos(\phi_n)\sec(a_n+\phi_n)\sin(a_n)\sin\left(\eta_n+t_{n-1}\right)\sin\left(\frac{l_n}{V_{n-1}}+\eta_n+t_{n-1}\right)\epsilon^2 \\
&+ 4\cos(a_n)\sec(a_n+\phi_n)\sin(\phi_n)\sin\left(\eta_n+t_{n-1}\right)\sin\left(\frac{l_n}{V_{n-1}}+\eta_n+t_{n-1}\right)\epsilon^2 \\
&- 4V_{n-1}\cos(\phi_n)\cos\left(\frac{l_n}{V_{n-1}}+\eta_n+t_{n-1}\right)\sin(a_n)\epsilon + 4V_{n-1}\cos(a_n) \\
&\times\cos\left(\frac{l_n}{V_{n-1}}+\eta_n+t_{n-1}\right)\sin(\phi_n)\epsilon \\
&+ 4R\cos(a_n)\cos(\phi_n)\sec(a_n+\phi_n)\sin(\phi_n)\sin\left(\frac{l_n}{V_{n-1}}+\eta_n+t_{n-1}\right)\epsilon\Bigg]
\end{aligned} \tag{C.1}$$

The substitution of Eq. (4.16) into Eq. (C.1) followed by integration over η_n yields:

$$\begin{aligned}
\langle\langle\delta V_n^2\rangle\rangle =& 2\epsilon^2\cos^2(\phi_n) + 2\epsilon^2\cos\left(\frac{l_n}{V_{n-1}}\right)\cos(a_n)\cos(\phi_n)\sec(a_n+\phi_n) \\
&+ \frac{2V_{n-1}\epsilon^2\sin\left(\frac{l_n}{V_{n-1}}\right)\sin(\phi_n)\sin(a_n+\phi_n)}{R} \\
&- \frac{2V_{n-1}\epsilon^2\cos(\phi_n)\sin\left(\frac{l_n}{V_{n-1}}\right)\sin(a_n+\phi_n)\tan(a_n)}{R} \\
&- \epsilon^2\cos\left(\frac{l_n}{V_{n-1}}\right)\sin(2\phi_n)\tan(a_n+\phi_n)
\end{aligned} \tag{C.2}$$

The length of the free path l_n traveled by a particle between any two successive collisions, assuming the disk with which it experiences its nth collision to be fixed at its equilibrium position, is itself a function of the angle variables a_n and ϕ_n as well as the respective ones upon the previous collision, a_{n-1} and ϕ_{n-1}. Moreover, l_n also depends on the phase of oscillation at its previous, $(n-1)$th, collision due to the displacement of the disk at the previous step. However, as explained in §2.2.2, it is the displacement of the scatterer at its nth collision that affects the energy transfer on the same collision. In other words, the variation of l_n does not systematically affect the energy gain of a particle during a collision. Therefore, to facilitate analytical treatment in Eq. (C.2) we substitute l_n with its mean value $\langle l \rangle$. The final step is to obtain the mean value of δV_n^2 with respect to a_n and ϕ_n using the PDFs given by Eqs (4.9) and (4.10). The integration yields:

$$\delta\langle V_n^2 \rangle = \epsilon^2 \left[\cos\left(\frac{\langle l \rangle}{V_{n-1}} \right) + 1 \right] \tag{C.3}$$

Bibliography

[1] P. Gaspard. *Chaos, scattering and statistical mechanics*. Cambridge University Press Cambridge, 1998.

[2] J.R. Dorfman. *An introduction to chaos in nonequilibrium statistical mechanics*, volume 14. Cambridge Univ Pr, 1999.

[3] R. Klages. *Microscopic chaos, fractals and transport in nonequilibrium statistical mechanics*, volume 24. World Scientific Pub Co Inc, 2007.

[4] G. Gallavotti, W.L. Reiter, and J. Yngvason. *Boltzmann's legacy*. Amer Mathematical Society, 2008.

[5] P. Castiglione, M. Falcioni, A. Lesne, and A. Vulpiani. *Chaos and coarse graining in statistical mechanics*. Cambridge University Press, 2008.

[6] G. M. Zaslavsky. Chaos, fractional kinetics, and anomalous transport. *Physics Reports*, 371(6):461–580, 2002.

[7] O. Penrose. Foundations of statistical mechanics. *Reports on Progress in Physics*, 42:1937, 1979.

[8] D. Ruelle. Smooth dynamics and new theoretical ideas in nonequilibrium statistical mechanics. *Journal of Statistical Physics*, 95(1):393–468, 1999.

[9] L. A. Bunimovich and H. Spohn. Viscosity for a periodic two disk fluid: an existence proof. *Communications in mathematical physics*, 176(3):661–680, 1996.

[10] H. A. Lorentz. Motion of electrons in metals. In *Proc. Amsterdam Acad*, volume 438, pages 588–684, 1905.

[11] L. A. Bunimovich. On the ergodic properties of nowhere dispersing billiards. *Communications in Mathematical Physics*, 65:295–312, 1979. 10.1007/BF01197884.

[12] L. A. Bunimovich and Ya. G. Sinai. Markov Partitions for dispersed billiards. *Communications in Mathematical Physics*, 78:247–280, 1980. 10.1007/BF01942372.

[13] Jonathan Machta and Robert Zwanzig. Diffusion in a Periodic Lorentz Gas. *Physical Review Letters*, 50(25):1959–1962, June 1983.

[14] P. Gaspard and G. Nicolis. Transport properties, Lyapunov exponents, and entropy per unit time. *Phys. Rev. Lett.*, 65(14):1693–1696, 1990.

[15] P. Gaspard and F. Baras. Chaotic scattering and diffusion in the Lorentz gas. *Phys. Rev. E*, 51(6):5332, 1995.

[16] R. Klages and C. Dellago. Density-dependent diffusion in the periodic Lorentz gas. *Journal of Statistical Physics*, 101(1):145–159, 2000.

[17] Domokos Szász and Tamás Varjú. Limit Laws and Recurrence for the Planar Lorentz Process with Infinite Horizon. *Journal of Statistical Physics*, 129(1):59–80, July 2007.

[18] Ch. Dellago and H.A. Posch. Field and density dependence of the Lyapunov spectrum for the driven random Lorentz gas. *Physica D: Nonlinear Phenomena*, 112(1–2):241–249, 1998.

[19] C.P. Dettmann, G.P. Morriss, and L. Rondoni. Irreversibility, diffusion and multifractal measures in thermostatted systems. *Chaos, Solitons & Fractals*, 8(5):783–792, 1997.

[20] R. Klages, K. Rateitschak, and G. Nicolis. Thermostating by deterministic scattering: Construction of nonequilibrium steady states. *Phys. Rev. Lett.*, 84(19):4268–4271, 2000.

[21] R. Klages, G. Nicolis, and K. Rateitschak. Thermostating by deterministic scattering: the periodic Lorentz gas. *J. Stat. Phys*, 99:1339–1364, 2000.

[22] H. Van Beijeren and J. R. Dorfman. On thermostats and entropy production. *Physica A: Statistical Mechanics and its Applications*, 279(1):21–29, 2000.

[23] D. Cohen. Driven Chaotic Mesoscopic Systems, Dissipation and Decoherence. In Piotr Garbaczewski and Robert Olkiewicz, editors, *Dynamics of Dissipation*, volume 597 of *Lecture Notes in Physics*, pages 317–350. Springer Berlin / Heidelberg, 2002. 10.1007/3-540-46122-1_14.

[24] C. Jarzynski. Energy diffusion in a chaotic adiabatic billiard gas. *Phys. Rev. E*, 48:4340–4350, Dec 1993.

[25] Doron Cohen and Tsampikos Kottos. Quantum-Mechanical Nonperturbative Response of Driven Chaotic Mesoscopic Systems. *Phys. Rev. Lett.*, 85:4839–4843, Dec 2000.

[26] A. Barnett, D. Cohen, and E. J. Heller. Rate of energy absorption for a driven chaotic cavity. *Journal of Physics A: Mathematical and General*, 34:413, 2001.

[27] P. K. Papachristou, F. K. Diakonos, E. Mavrommatis, and V. Constantoudis. Nonperiodic delay mechanism and fractallike behavior in classical time-dependent scattering. *Phys. Rev. E*, 64:016205, Jun 2001.

[28] P. K. Papachristou, F. K. Diakonos, V. Constantoudis, P. Schmelcher, and L. Benet. Classical scattering from oscillating targets. *Physics Letters A*, 306(2–3):116–126, 2002.

[29] P. K. Papachristou, F. K. Diakonos, V. Constantoudis, P. Schmelcher, and L. Benet. Scattering off two oscillating disks: Dilute chaos. *Phys. Rev. E*, 70:056215, Nov 2004.

[30] E. Fermi. On the Origin of the Cosmic Radiation. *Phys. Rev.*, 75:1169–1174, Apr 1949.

[31] Roger Blandford and David Eichler. Particle acceleration at astrophysical shocks: A theory of cosmic ray origin. *Physics Report*, 154(1):1–75, 1987.

[32] Alessandro Veltri and Vincenzo Carbone. Radiative Intermittent Events during Fermi's Stochastic Acceleration. *Phys. Rev. Lett.*, 92:143901, Apr 2004.

[33] K. Kobayakawa, Y. S. Honda, and T. Samura. Acceleration by oblique shocks at supernova remnants and cosmic ray spectra around the knee region. *Phys. Rev. D*, 66:083004, Oct 2002.

[34] M. A. Malkov. Ion leakage from quasiparallel collisionless shocks: Implications for injection and shock dissipation. *Phys. Rev. E*, 58:4911–4928, Oct 1998.

[35] G. Michalek, M. Ostrowski, and R. Schlickeiser. Cosmic-Ray Momentum Diffusion in Magnetosonic versus Alfvénic Turbulent Field. *Solar Physics*, 184:339–352, 1999. 10.1023/A:1005028205111.

[36] A. V. Milovanov and L. M. Zelenyi. Strange Fermi processes and power-law nonthermal tails from a self-consistent fractional kinetic equation. *Physical Review E*, 64(5):052101, 2001.

[37] F. Saif, I. Bialynicki-Birula, M. Fortunato, and W. P. Schleich. The Fermi accelerator in atom optics. *Arxiv preprint quant-ph/9809040*, 1998.

[38] A. Steane, P. Szriftgiser, P. Desbiolles, and J. Dalibard. Phase modulation of atomic de Broglie waves. *Phys. Rev. Lett.*, 74(25):4972–4975, 1995.

[39] G. Lanzanò, E. De Filippo, D. Mahboub, H. Rothard, S. Aiello, A. Anzalone, S. Cavallaro, A. Elanique, E. Geraci, M. Geraci, F. Giustolisi, A. Pagano, and G. Politi. Fast Electron Production at Intermediate Energies: Evidence for Fermi Shuttle Acceleration and for Deviations from Simple Relativistic Kinematics. *Phys. Rev. Lett.*, 83:4518–4521, Nov 1999.

[40] S. Ulam. Proceedings of the Fourth Berkley Symposium on Mathematics, Statistics, and Probability. California University Press, 1961.

[41] A. J. Lichtenberg and M. A. Lieberman. *Regular and chaotic motion.* 1992.

[42] G. M. Zaslavsky. Long way from the FPU-problem to chaos. *Chaos: An Interdisciplinary Journal of Nonlinear Science*, 15(1):015103, 2005.

[43] Germán A. Luna-Acosta. Regular and chaotic dynamics of the damped Fermi accelerator. *Phys. Rev. A*, 42:7155–7162, Dec 1990.

[44] Edson D. Leonel and R. Egydio de Carvalho. A family of crisis in a dissipative Fermi accelerator model. *Physics Letters A*, 364(6):475–479, 2007.

[45] Edson D. Leonel and P. V. E. McClintock. Dissipative area-preserving one-dimensional Fermi accelerator model. *Phys. Rev. E*, 73:066223, Jun 2006.

[46] Edson D Leonel. Breaking down the Fermi acceleration with inelastic collisions. *Journal of Physics A: Mathematical and Theoretical*, 40(50):F1077, 2007.

[47] Jorge V. José and Robert Cordery. Study of a quantum fermi-acceleration model. *Phys. Rev. Lett.*, 56:290–293, Jan 1986.

[48] William M. Visscher. Class of classically chaotic time-periodic Hamiltonians which lead to separable evolution operators. *Phys. Rev. A*, 36:5031–5045, Nov 1987.

[49] A. J. Makowski and S. T. Dembiński. Exactly solvable models with time-dependent boundary conditions. *Physics Letters A*, 154(5–6):217–220, 1991.

[50] M. Razavy. Time-dependent harmonic oscillator confined in a box. *Phys. Rev. A*, 44:2384–2387, Aug 1991.

[51] Sudhir R. Jain. Fractal-like quasienergy spectrum in the Fermi-Ulam model. *Phys. Rev. Lett.*, 70:3553–3556, Jun 1993.

[52] L. D. Pustylnikov. Stable and oscillating motions in nonautonomous dynamical systems. *Trans. Moscow. Math. Soc*, 2:1–101, 1978.

[53] Denis Gouvêa Ladeira and Jafferson Kamphorst Leal da Silva. Scaling properties of a simplified bouncer model and of Chirikov's standard map. *Journal of Physics A: Mathematical and Theoretical*, 40(38):11467, 2007.

[54] P.J. Holmes. The dynamics of repeated impacts with a sinusoidally vibrating table. *Journal of Sound and Vibration*, 84(2):173–189, 1982.

[55] R. M. Everson. Chaotic dynamics of a bouncing ball. *Physica D: Nonlinear Phenomena*, 19(3):355–383, 1986.

[56] Anita Mehta and J. M. Luck. Novel temporal behavior of a nonlinear dynamical system: The completely inelastic bouncing ball. *Phys. Rev. Lett.*, 65:393–396, Jul 1990.

[57] Edson D. Leonel and André L.P. Livorati. Describing Fermi acceleration with a scaling approach: The Bouncer model revisited. *Physica A: Statistical Mechanics and its Applications*, 387(5–6):1155–1160, 2008.

[58] Z.J. Kowalik, M. Franaszek, P. Pieranski, et al. Self-reanimating chaos in the bouncing-ball system. *Phys. Rev. A*, 37(10):4016, 1988.

[59] Sergio Celaschi and Robert L. Zimmerman. Evolution of a two-parameter chaotic dynamics from universal attractors. *Physics Letters A*, 120(9):447–451, 1987.

[60] Edson D Leonel and P V E McClintock. A crisis in the dissipative Fermi accelerator model. *Journal of Physics A: Mathematical and General*, 38(23):L425, 2005.

[61] G. Casati, B. V. Chirikov, D. L. Shepelyansky, and I. Guarneri. Relevance of classical chaos in quantum mechanics: the hydrogen atom in a monochromatic field. *Physics Reports*, 154(2):77–123, 1987.

[62] M. M. A. Stocklin and T. S. Monteiro. Classical momentum diffusion in double-δ-kicked particles. *Physical Review E*, 74(2):026210, 2006.

[63] P. H. Jones, M. Goonasekera, D. R. Meacher, T. Jonckheere, and T. S. Monteiro. Directed motion for delta-kicked atoms with broken symmetries: Comparison between theory and experiment. *Phys. Rev. Lett..*, 98(7):73002, 2007.

[64] M. A. Lieberman and A. J. Lichtenberg. Stochastic and adiabatic behavior of particles accelerated by periodic forces. *Phys. Rev. A*, 5(4):1852, 1972.

[65] A. J. Lichtenberg, M. A. Lieberman, and R. H. Cohen. Fermi acceleration revisited. *Physica D: Nonlinear Phenomena*, 1(3):291–305, 1980.

[66] Edson D. Leonel, P. V. E. McClintock, and J. Kamphorst Leal da Silva. Fermi-Ulam Accelerator Model under Scaling Analysis. *Phys. Rev. Lett.*, 93:014101, Jun 2004.

[67] Edson D. Leonel, J.Kamphorst Leal da Silva, and Sylvie O. Kamphorst. On the dynamical properties of a Fermi accelerator model. *Physica A: Statistical Mechanics and its Applications*, 331(3–4):435–447, 2004.

[68] Denis Gouvêa Ladeira and Jafferson Kamphorst Leal da Silva. Time-dependent properties of a simplified Fermi-Ulam accelerator model. *Phys. Rev. E*, 73:026201, Feb 2006.

[69] G. M. Zaslavskii and B. V. Chirikov. Fermi acceleration mechanism in the one-dimensional case. In *Soviet Physics Doklady*, volume 9, page 989, 1965.

[70] H. Brahic. Numerical Study of a Simple Dynamical System. I. The Associated Plane Area-Preserving Mapping. *Astronomy and Astrophysics*, 12:98, 1971.

[71] A. Y. Loskutov, A. B. Ryabov, and L. G. Akinshin. Mechanism of Fermi acceleration in dispersing billiards with time-dependent boundaries. *Journal of Experimental and Theoretical Physics*, 89(5):966–974, 1999.

[72] A. Loskutov, A. B. Ryabov, and L. G. Akinshin. Properties of some chaotic billiards with time-dependent boundaries. *Journal of Physics A: Mathematical and General*, 33(44):7973, 2000.

[73] Cesar Manchein and Marcus W. Beims. Dissipation effects in the ratchetlike fermi acceleration, 2009.

[74] Denis G. Ladeira and Edson D. Leonel. Dynamical properties of a dissipative hybrid Fermi-Ulam-bouncer model. *Chaos: An Interdisciplinary Journal of Nonlinear Science*, 17(1):013119, 2007.

[75] Alexander Loskutov and Alexei Ryabov. Particle Dynamics in Time-Dependent Stadium-Like Billiards. *Journal of Statistical Physics*, 108:995–1014, 2002. 10.1023/A:1019735313330.

[76] A. K. Karlis, P. K. Papachristou, F. K. Diakonos, V. Constantoudis, and P. Schmelcher. Hyperacceleration in a stochastic Fermi-Ulam model. *Phys. Rev. Lett.*, 97(19):194102, 2006.

[77] Donald C. Ellison, Stephen P. Reynolds, and Frank C. Jones. First-order Fermi particle acceleration by relativistic shocks. *The Astrophysical Journal*, 360:702, September 1990.

[78] U Jaekel and R Schlickeiser. The Fokker-Planck coefficients of cosmic ray transport in random electromagnetic fields. *Journal of Physics G: Nuclear and Particle Physics*, 18(6):1089–1118, June 1992.

[79] Brian T. Park and Vahe Petrosian. Fokker-Planck Equations of Stochastic Acceleration: A Study of Numerical Methods. *The Astrophysical Journal Supplement Series*, 103:255, March 1996.

[80] Brian T. Park and Vahe Petrosian. Fokker-Planck Equations of Stochastic Acceleration: Green's Functions and Boundary Conditions. *The Astrophysical Journal*, 446:699, June 1995.

[81] Kwok Tsang and K. Ngai. Dynamics of relaxing systems subjected to nonlinear interactions. *Physical Review E*, 56(1):R17–R20, July 1997.

[82] H. Risken. *The Fokker Planck equation, Methods of solution and application 2nd Ed.* Springer Verlag, Berlin, Heidelberg, 1989.

[83] N. G. van Kampen. *Stochastic processes in physics and chemistry.* North Holland, 2007.

[84] C. Goutis and G. Casella. Explaining the saddlepoint approximation. *American Statistician*, pages 216–224, 1999.

[85] C. W. Gardiner. *Handbook of stochastic methods for physics, chemistry and the natural sciences.* Berlin et al., 1985.

[86] Freddy Bouchet, Fabio Cecconi, and Angelo Vulpiani. Minimal Stochastic Model for Fermi's Acceleration. *Phys. Rev. Lett.*, 92:040601, Jan 2004.

[87] Pierre Gaspard. What is the role of chaotic scattering in irreversible processes? *Chaos (Woodbury, N.Y.)*, 3(4):427–442, October 1993.

[88] David P. Sanders. Fine structure of distributions and central limit theorem in diffusive billiards. *Phys. Rev. E*, 71:016220, Jan 2005.

[89] Daniel Alonso, Roberto Artuso, Giulio Casati, and Italo Guarneri. Heat Conductivity and Dynamical Instability. *Physical Review Letters*, 82(9):1859–1862, March 1999.

[90] LA Bunimovich and YG Sinai. Statistical properties of Lorentz gas with periodic configuration of scatterers. *Communications in Mathematical Physics*, 497:479–497, 1981.

[91] Hernán Larralde, François Leyvraz, Gustavo Martínez-Mekler, Raúl Rechtman, and Stefano Ruffo. Transmission and scattering of a Lorentz gas on a slab. *Physical Review E*, 58(4):4254–4260, October 1998.

[92] Jean-Philippe Bouchaud and Antoine Georges. Anomalous diffusion in disordered media: Statistical mechanisms, models and physical applications. *Physics Reports*, 195(4-5):127–293, November 1990.

[93] C Mohan. The gambler's ruin problem with correlation. *Biometrika*, 42(3):486–493, 1955.

[94] Jean-Philippe Bouchaud and Pierre Doussal. Numerical study of aD-dimensional periodic Lorentz gas with universal properties. *Journal of Statistical Physics*, 41(1-2):225–248, October 1985.

[95] Per Bak, Chao Tang, and Kurt Wiesenfeld. Self-organized criticality: An explanation of the 1/f noise. *Physical Review Letters*, 59(4):381–384, July 1987.

[96] Donald L Turcotte. Self-organized criticality. *Reports on Progress in Physics*, 62(10):1377–1429, October 1999.

[97] J. Carlson, J. Chayes, E. Grannan, and G. Swindle. Self-orgainzed criticality and singular diffusion. *Physical Review Letters*, 65(20):2547–2550, November 1990.

[98] Leo P. Kadanoff. Complex Structures from Simple Systems. *Physics Today*, 44(3):9, March 1991.

[99] R. López-Ruiz, H.L. Mancini, and X. Calbet. A statistical measure of complexity. *Physics Letters A*, 209(5-6):321–326, December 1995.

[100] P. Gaspard. Sporadicity: Between Periodic and Chaotic Dynamical Behaviors. *Proceedings of the National Academy of Sciences*, 85(13):4591–4595, July 1988.

[101] Y. Contoyiannis, F. Diakonos, and A. Malakis. Intermittent Dynamics of Critical Fluctuations. *Physical Review Letters*, 89(3), June 2002.

[102] Tamás Vicsek, András Czirók, Eshel Ben-Jacob, Inon Cohen, and Ofer Shochet. Novel Type of Phase Transition in a System of Self-Driven Particles. *Physical Review Letters*, 75(6):1226–1229, August 1995.

[103] Cristián Huepe and Maximino Aldana. Intermittency and Clustering in a System of Self-Driven Particles. *Physical Review Letters*, 92(16), April 2004.